Section I

Research in Progress

August 1971

The Effective Two Nucleon Force from Inelastic Nucleon Scattering

Sam M. Austin

There have been two main approaches to determining an effective interaction suitable for microscopic model analyses of inelastic scattering and charge exchange data. It has been shown[1,2] that "realistic" forces, similar to those often used in bound state calculations, describe the scattering data reasonably well in the 20-60 MeV range. These forces, however, have rather complex radial shapes and are difficult to use in commonly available DWA codes. Further it is difficult to assess the accuracy of the assumptions made in their derivation.

An alternative procedure[3] is to assume a force of a convenient form and to attempt to fix the parameters of the force by comparison with experiment in particularly favorable circumstances. In this report we present preliminary results of a survey of the available information on the effective two-body interaction V assuming V has the form

$$V_{ip}(r)=[V_0+V_{10}\vec{\sigma}_i\cdot\vec{\sigma}_p+V_{01}\vec{\tau}_i\cdot\vec{\tau}_p+V_{11}\vec{\sigma}_i\cdot\vec{\sigma}_p\vec{\tau}_i\cdot\vec{\tau}_p]\frac{e^{-\alpha r}}{\alpha r}.$$

Here the subscripts on the V_{ST} are the transferred spin and isospin while p prefers to the projectile and i to the valence nucleon. The quantity α is the inverse range of the force and was taken to be $1.0F^{-1}$.

Corrections for exchange have been made in a number of cases where only direct processes out were included in the original calculation. Most of the transitions relevant to V_{10}, V_{01}, and V_{11} had an angular momentum (L) transfer of 0 or 1 and these corrections were small.[3] In the case of V_{00} the transitions were L=2,3 and inclusion of exchange enhanced the cross-section by a factor between two and four.[1,4] In the V_{00} case the selection of relevant analyses was rather limited since it was necessary that the wavefunctions adequately describe the collective properties of the states. The results of this survey are given in Figs. 1 to 4 and references to the original analyses are in Table I. (Note $V_{00}\equiv V_0$, $V_{10}\equiv V_\sigma$, $V_{01}\equiv V_\tau$, $V_{11}\equiv V_{\sigma\tau}$). The numbers shown near the points are the mass number A of the target and the L transfer where appropriate (A,L). Also shown on the figures are other estimates of the V_{ST}. The points or lines labelled impulse approximation give the strengths of 1.0F range Yukawas that yield the same cross-section as the impulse approximation pseudopotential of Petrovich, et al.[1] The lines labelled KK, KKD, and HJ are the Yukawas which have the same volume integrals[2] as the long range parts of the Kallio-Kolltveit force (with and without density dependence (D)[5]) and the Hamada-Johnston force, respectively. Finally, the points labelled optical model in Fig. 1 were determined by matching the volume integral of the optical-model-real-potentials of Greenlees, et al.[6] and making a correction[7] for exchange contributions.

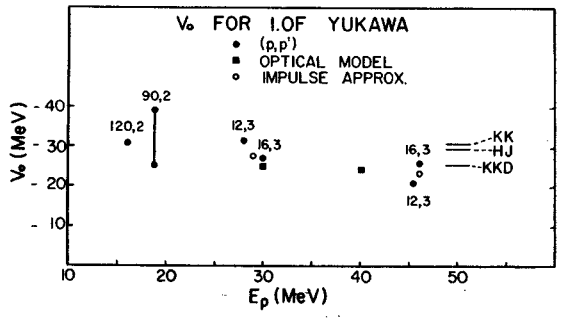

Figure 1

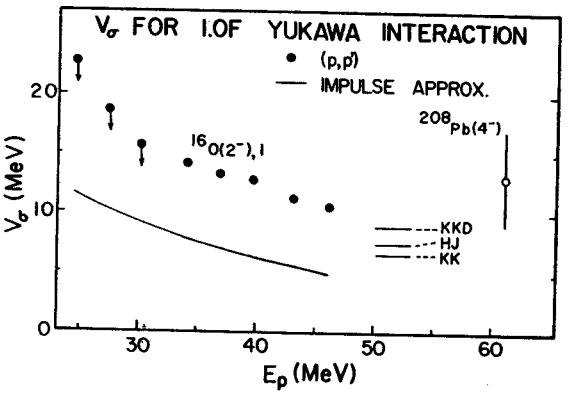

Figure 2

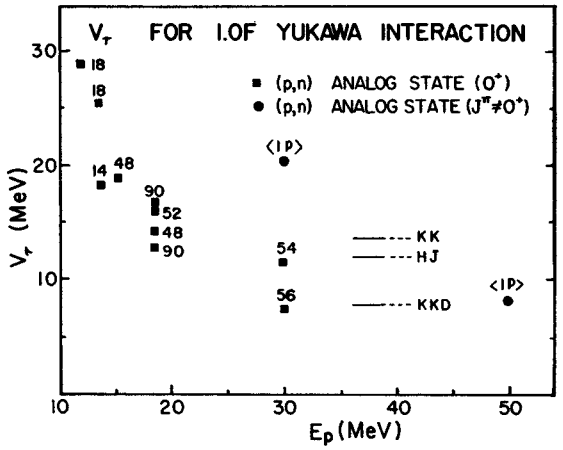

Figure 3

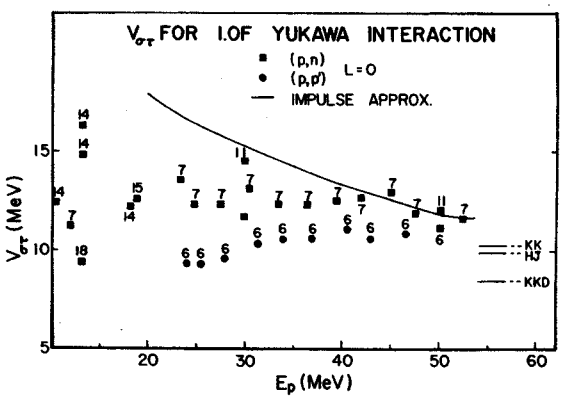

Figure 4

In an empirical procedure such as that described here the main test of the approximation is the consistency of the results. For Ep>20 MeV, the results for V_0 and $V_{\sigma\tau}$ are quite encouraging but data on V_σ and V_τ are quite scanty. This survey is being extended to include the spin orbit and tensor forces.

References

1. F. Petrovich, H. McManus, V.A. Madsen, and J. Atkinson, Phys. Rev. Letters 22, 895(1969).
2. W.G. Love and G.R. Satchler, Nuclear Physics A159, 1(1970).
3. G.R. Satchler, Nuclear Phys. A95, 1(1967).
4. J. Atkinson and V.A. Madsen, Phys. Rev. C1, 1377(1970).
5. A.M. Green, Phys. Letters 24B, 384(1967).
6. G.W. Greenlees, W. Makofske and G.J. Pyle, Phys. Rev. C1, 1145(1970).
7. D. Slanina and H. McManus, Nucl. Phys. A116, 271(1968).
8. S.M. Austin, P.J. Locard, S.N. Bunker, J.M. Cameron, J.R. Richardson, J.W. Verba, and W.T.H. van Oers, Phys. Rev. C3, 1514(1971).
9. A. Scott, N.P. Mathur and G.R. Satchler, to be published.
10. J.D. Anderson, S.D. Bloom, C. Wong, W.F. Hornyak, and V.A. Madsen, Phys. Rev. 177, 1416(1969).
11. C.J. Batty, B.E. Bonner, E. Friedman, C. Tschalär, L.E. Williams, A.S. Clough, and J.B. Hunt, Nuclear Phys. A116, 643(1968).

Table I

Figure	Mass	Ref.	Figure	Mass	Ref.
1($V_{00}\equiv V_0$)	12	1	3($V_{01}\equiv V_\tau$)	14,18	10
	16	8		48	3,10
	90,120 Optical Model	4		52	3
		6,7		54,56	11
				90	3,10
2($V_{10}\equiv V_\sigma$)	^{16}O	8		<1p>	12
			4($V_{11}\equiv V_{\sigma\tau}$)	6,7	12,13,14
	^{208}Pb	9		11	12
				14+	10,15
				15	10
				18	2,10

+Results for $^{14}C(p,n)^{14}N(g.s.)$ were excluded since these are known to be dominated by the tensor part of the effective interaction.

References (con't.)

12. A.S. Clough, C.J. Batty, B.E. Bonner and L.E. Williams, Nucl. Phys. A143, 385(1970). The quantities given are averages of the results of this paper.
13. S.M. Austin, P.J. Locard, W. Benenson, and G.M. Crawley, Phys. Rev. 176, 1227(1968).
14. A.S. Clough, C.J. Batty, B.E. Bonner, C. Tschalär, L.E. Williams, and E. Friedman, Nucl Phys. A137, 222(1969).
15. C. Wong, J.D. Anderson, V.A. Madsen, F.A. Schmittroth, and M.J. Stomp, Phys. Rev. C3, 1904(1971).

Renormalized Operators and Collective Particle-Hole Excitations in ^{40}Ca

M. Dworzecka and H. McManus

ABSTRACT

Collective particle-hole excitations in ^{40}Ca are calculated with Sussex matrix elements in Tamm-Dancoff approximation. Calculations are done both with bare and renormalized operators. Renormalization is accomplished by including core polarization effects by perturbation in both the two-body interaction and transition moments. The results are similar to those obtained in random-phase approximation using realistic forces with core polarization screening.

Considerable success has been achieved by Gillet, et al. Nucl. Phys. 88, 321(1966); 54, 472(1964); 54, 321(1964); 57, 698(1964); in describing negative parity collective excitations in closed shell nuclei by means of a simple particle-hole model with ground state correlations taken into account via the R.P.A. The ground state correlations so treated consist of multiplet excitations within the single particle and hole configurations originally picked for the description of the state (model space), and give, compared with the T.D.A. calculations in the original model space, a large energy shift and an increase in collectivity as measured, for instance, by the BE3 of a 3^- state. However, the calculations used a force whose parameters were fixed by comparing calculation with experiment. Kuo, et al., Phys. Letters 29B, 544(1969), did a similar calculation using realstic forces, i.e. derived from the G-matrix. In this case the force between nucleons near the Fermi surface is altered by another type of correlation, core-polarization. This involves excitations, for instance, of positive parity particle-hole excitations, not included in the ground state correlations in the R.P.A. approxmiation. The results of the calculation were very sensitive to the way the core-polarization effects were taken into account, though some of the variations were due to an incorrect choice of backward going graphs in the R.P.A. Similar calculations were done by Dieperink, Nucl. Phys. A116, 556(1968). This method treats one type of correlation—core-polarization, by perturbation theory, and another, ground state correlations, by a different approximation, the R.P.A. The present calculation compares the results of treating both effects by perturbation theory with the results of using R.P.A. taking the 3^- states of ^{40}Ca as an example. In perturbation theory both the effective interaction and the effective transition operator have to be calculated. The effective interaction is calculated from the diagrams of Fig. 2. V is the bare force, in this case Sussex matrix elements, $V_{2p-2h}=V_{ph}+V_{pp}+V_{hh}$ the lowest order core-polarization contributions involving energy denominators 2h . V_{GSC} gives the effect on the interaction of ground state correlations, via 3p-3h intermediate states and hence should not be used in R.P.A. calculations. The effective operator is given by the diagram of Fig. 3. t_{DIR} being the bare operator if all correlations are neglected and t_{cp} the addition to the bare operator from correlations. In the present case, the whole effect of t_{cp} comes from ground state correlations, so it corresponds to the effect of the Y parts of the vectors in R.P.A. For the perturbation calculation, vectors were calculated in the usual T.D.A. with an effective force and the transition operators BE3 calculated from these vectors with a corresponding effective operator. Thus if the bare force V was used, neglecting all correlations, then the bare operator t_{DIR} was used for calculating BE3. If ground state correlations were included then $V=V+V_{GSC}$, and $t=t_{DIR}+t_{cp}$. The corresponding R.P.A. calculation used V in both A and B matrices. If core polarization was included $V=V+V_{2p2h}+V_{GSC}$, then $t=t_{DIR}+t_{cp}$ and the corresponding R.P.A. calculation used $V=V+V_{2p2h}$ in the A matrix and V=V in the B matrix. The results for the lowest 3^- state of ^{40}Ca are shown in Table. 1.

Table 1

	TDA			Corresponding RPA	
Interaction	Transition Operator	E(MeV)	BE3(WU)*	E	BE3
None					
Pure $f_{7/2}d_{3/2}^{-1}$	t_{DIR}	7.1	0.72	*1WU=	$665fm^6$
V	"	6.14	9.0	-	-
$V+V_{2p2h}$	"	6.34	6.75	-	-
$V+V_{GSC}$	$t_{DIR}+t_{cp}$	5.43	16.5	4.74	23.4
$V+V_{2p2h}+V_{GSC}$	"	5.68	14.2	5.16	19.6

The main configuration $f_{7/2}d_{3/2}^{-1}$ lies originally at 7.1 MeV, and has a small BE3 of 0.72 W.U. Switching on the interaction (Col. 2) immediately creates a moderately collective state lowering the energy to 6.14 MeV and increasing the BE3 to 9.0 W.U. The overall effect of correlations is to decrease the energy further to 5.68 MeV and increase the transition rate to 14.2 W.U., most of the effect coming from ground state correlations, essentially similar to the R.P.A. results.

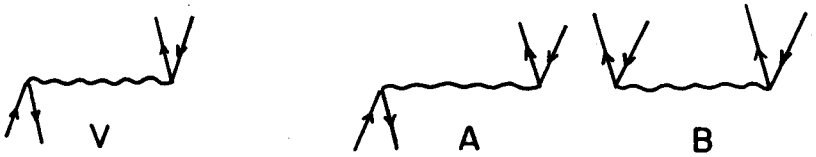

Fig.1

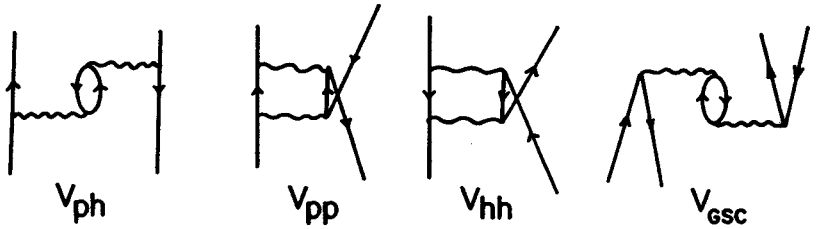

Fig.2

Fig.3

Electron and Proton Inelastic Scattering from ^{40}Ca and ^{208}Pb

G.R. Hammerstein and F. Petrovich

The differential cross-section for inelastic electron-nucleus scattering can be written

$$\frac{d\sigma}{d\Omega}=\sigma_m\left\{|F_{LONG}(q)|^2+\frac{1}{2}(1+2\tan\frac{2\theta}{2})|F_{TRANS}(q)|^2\right\}$$

where σ_m is the Mott cross-section and F_{LONG} and F_{TRANS} are the longitudinal and transverse form factors.

For normal parity excitations the longitudinal form factor provides the dominant contribution except at very large angles, so the transverse form factor usually is neglected.

In Born approximation F_{LONG} as a function of linear momentum transfer, q, for the excitation of a nucleus with charge Z and a spin zero ground state to a final state of angular momentum J is

$$F_{LONG}(q)=\frac{1}{Z}[(4\pi)(2J+1)]^{1/2}\int_o^\infty j_J(qr)\rho_J(r)r^2dr$$

where j_J is a spherical Bessel function. The relevant nuclear information is contained in the radial charge transition density ρ_J.

Since the electromagnetic interaction is well understood, reliable charge transition densities can be extracted from empirical form factors.

Similarly, the physical information required for a distorted wave approximation calculation of inelastic proton-nucleus scattering is contained in form factors

$$F^{LSJ}(r)=\sum_{x=p,n}\int_o^\infty v_{px}^{SL}(r,r_o)F_x^{LSJ}(r_o)r_o^2dr_o$$

where L, S, and J are the orbital, spin, and total angular momenta transferred in the interaction and x refers to the protons or the neutrons. v^{SL} is the Lth multipole coefficient of the proton-target nucleon interaction; the functions F_{LSJ} are transition densities, which contain the nuclear structure information.

For normal parity transitions the two functions F_p^{J0J} and F_n^{J0J} are important. F_p^{J0J} is essentially the same as the function ρ_J, which can be inferred from an electron scattering experiment; thus only F_n^{J0J} remains to be determined.

For T=0 excitations in N=Z nuclei neutrons and protons play symmetric roles, so in these cases we can set $F_p^{J0J}=F_n^{J0J}$. Since

$$v_{T=0}=v_{pp}+v_{pn}$$

we are left with the single form factor

$$F^{J0J}=2\int_o^\infty v_{T=0}^{0J}(r,r_o)F_p^{J0J}(r_o)r_o^2dr_o$$

Confrontation with experiment of an angular distribution calculated using this form factor essentially tests the quality of our choice of the nonspin-flip, isoscalar part of the projectile-nucleus interaction.

In the case of the 3^-, T=0 excitation at 3.73 MeV in ^{40}Ca, we took the charge transition density to be of the form

$$\rho(r)=N\frac{d}{dr}[1+\exp(\frac{r-R}{c})]^{-1}$$

and adjusted N, R, and C to obtain the form factor shown and compared with experiment in Fig. 1. The calculation was done in Born approximation employing finite proton size and local wave number corrections. Using this transition density in the manner discussed above, we calculated the angular distribution for proton scattering in the same transition, assuming a projectile-nucleus interaction which was the long range part of the Kallio-Kolltveit (KK) potential. The possibility of exchange of the projectile with one of the target nucleons was taken into account in an approximate way. The result is compared with experiment in Fig. 2.

Heisenberg and Sick recently extracted a charge transition density from inelastic electron scattering on the 3^- excitation at 2.63 MeV in ^{208}Pb.

While for lead the connection between charge and matter transition densities is not as clear as in the ^{40}Ca case, we nonetheless expect, in the spirit of the collective model, that neutrons and protons play rather similar roles in a strong vibrational excitation. Therefore we set $F_n^{J0J}=\frac{N}{Z}F_p^{J0J}$ and obtain a proton scattering from factor

$$F^{J0J}(r)=\frac{A}{Z}\int_o^\infty[v_{T=0}^{0J}(r,r_o)-\frac{N-Z}{A}v_{T=1}^{0J}(r,r_o)]F_p^{J0J}(r_o)r_o^2dr_o$$

We neglected the second term in brackets both because of the $\frac{N-Z}{A}$ term and because for the KK force the isovector term is smaller than the isoscalar by a factor of three. The angular distribution of scattered protons predicted using this form factor with the same force and treatment of exchange as in the ^{40}Ca case is shown as the solid line and compared with experiment in Fig. 4.

We also calculated transition densities and a proton scattering angular distribution for the same 3^- state using a wave function obtained by Kuo in a preliminary random phase approximation calculation which included 47 1$\hbar\omega$ particle-hole excitations but no higher excitations. The matter transition density is shown as the dashed curve in Fig. 3 and the angular distribution is the dashed curve in Fig. 4.

The similarity of the two angular distributions for lead—despite the differences in transition density for points in the nuclear interior—suggest that proton inelastic scattering is sensitive primarily to structural features which lie near the nuclear surface.

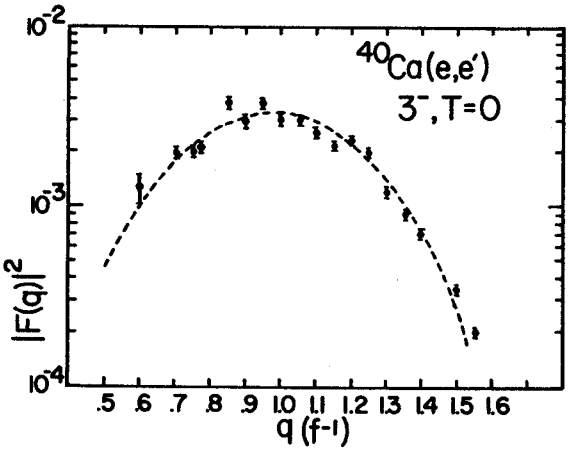

Figure 1

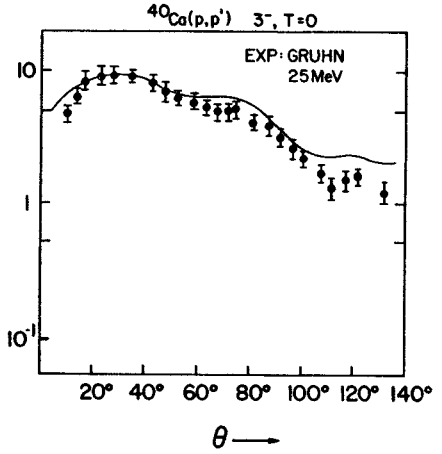

Figure 2

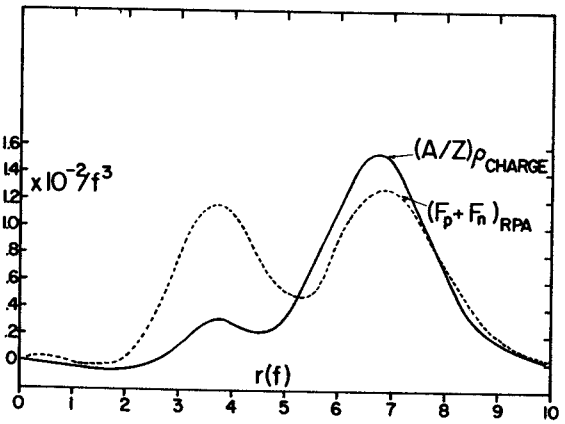

Figure 3

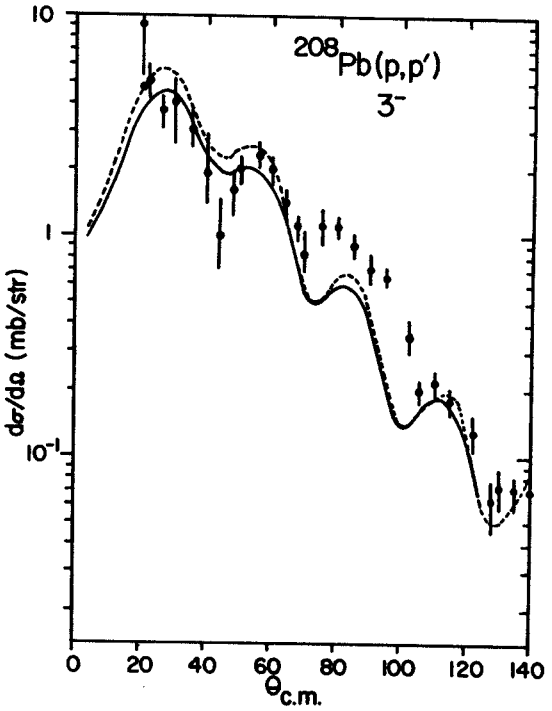

Figure 4

An Eikonal Approximation for Electron-Nucleus Scattering

G.R. Hammerstein

An important problem in any theoretical description of electron-nucleus scattering is treatment of the electron wave's distortion in the nuclear Coulomb field.

The familiar Born (plane wave) approximation gives a fairly accurate account of the gross features of cross-sections. But while experimental cross-sections display marked diffraction minima, the Born approximation predicts absolute zeros and these are shifted to too large values of linear momentum transfer. Thus we need to employ a calculational method which takes into account Coulomb distortion if we are to be able to study details of nuclear structure.

A method which has been used extensively describes the electron wave through numerical, partial wave solutions of the Dirac equation. Since this method is highly accurate, it probably will not be superceded in last-step analysis of nuclear data. Nonetheless, it suffers from two drawbacks: it is time consuming and, more importantly, when it is employed everything happens inside the computer. Direct connections are difficult to see between details of proposed nuclear models and details of the resultant cross-sections.

It is of interest then to devise a calculational method which takes Coulomb distortion into account but retains the perspicuity of the Born approximation.

A number of years ago Yennie, Boos, and Ravenhall proposed an eikonal approximation for elastic electron-nucleus scattering. While their quoted results agreed well with partial wave calculations, the wave function they obtained was such a complicated object that their procedure was hardly to be preferred to the exact numerical method.

The method described here employs the YBR eikonal treatment of the wave function, but with a constant spinor and a minimum of analytic approximations. The result is almost identical in form to the Born approximation. It should be of interest primarily in the treatment of longitudinal inelastic scattering and can be employed in a straightforward way in the case of transverse excitations as well, but we will describe here the formally simpler case of elastic scattering.

The S-matrix element for elastic electron scattering can be written in position space as

$$S_{FI}=\delta_{FI}-ie\int d^4X\phi_F(X)\gamma^\mu\psi_I(X)A^\mu(X)$$

where ψ_I solves the Dirac equation

$$(i\gamma^\mu\partial^\mu-m)\psi_I=e\gamma^\mu A^\mu\psi_I.$$

The function A^μ is the nulcear four-potential and ϕ_F is a Dirac plane wave.

We neglect the electron mass compared to the incident energy and suppose that only distortions due to the Coulomb field are important $A_\mu\to V$. The basic assumption is that ψ can be represented as

$$\psi = U \exp(-iEt)\exp(iS)$$

where U is a constant spinor and S depends only on the spatial coordinates. Then the Dirac equation becomes

$$(-\vec{\gamma}\cdot\vec{\nabla}S+\gamma^0(E-V))\psi(x)=0.$$

Solutions exist only if the Hamilton-Jacoby equation

$$(E-V)^2=(\vec{\nabla}S)^2$$

is satisfied.

The appropriate boundry condition is that ψ reduce to a logarithmically distorted plane wave at large distances. Then

$$S(\vec{x})=S(o)+\vec{k}\cdot\vec{x}-\int_0^{\vec{x}}V(\vec{x})dr$$

where k is the incident wave number, dr is an increment along the classical trajectory, and S(o) is the phase at the origin. Since dr depends on V, the remaining integral is quite complicated. We assume that it can be written as a series in powers of the fine structure constant:

$$S(\vec{x})=S(o)+\vec{k}\cdot\vec{x}+S_1(\vec{x})+S_2(\vec{x})+....$$

Substituting this series in the above Hamilton-Jacoby equation and requiring that $S_i(o)=0$, we find that

$$S_1(\vec{x})=-\int_0^z V(\vec{x})dz+\int_0^\infty[V(z)-V(\vec{x})]dz$$

$$S_2(\vec{x})=-(1/2k)\int_{-\infty}^z(\partial S_1/\partial y)^2dz$$

and so on, where dz is along the path through the origin and dy is in a direction perpendicular to that path.

Then

$$\psi(X)=U\exp(-iEt)\exp(S(o)+\vec{k}\cdot\vec{x}+S_1(\vec{x})+...)$$

is the desired wave function.

Inserting this function in the S-matrix expression for Coulomb scattering and forming a cross-section in the standard fashion, we obtain

$$\frac{d\sigma}{d\Omega}=4e^2k^2\cos^2(\theta/2)\left|\int d^3_{\vec{x}}V(\vec{x})\exp(iS)\exp(-i\vec{k}_F\cdot\vec{x})\right|^2$$

which differs from the Born approximation solely in the presence of exp(iS) instead of a plane wave.

The actual performance of calculations has proved to be fraught with numerical difficulties. Nonetheless preliminary calculations have been encouraging in that they indicate the desired contributions by the correction terms. The trouble seems to lie with the rather roundabout treatment of the underlying Born approximation.

Concerning Calculation of Strong Absorption Parameter in the Strong Cut Regge Absorption Model

David Perry

Preliminary Remarks: Two body high energy processes ab cd show a definite preference for small momentum transfers, and the early attempts to incorporate this forward peaked behavior into calculations of differential cross-sections for inelastic reactions revolved around Born terms, i.e., single particle exchanges which produce a certain amount of peaking due to the presence of the propagator of the exchanged particle.

$$\Rightarrow T_{ab\to cd} \sim V_{ace} \frac{1}{T-M_e^2} V_{deb}$$

The π since it is the particle of small s+mass, would give the greatest peaking and could be exchanged in many reactions, e.g. $\pi p \to \rho p$. Even for this reaction the forward peaking was not enough, but density matrix arguments suggested that the basic mechanism was correct.

To induce sharper peaking than afforded by the Born term alone, absorptive corrections (among others) were introduced. This correction accounts for the loss of flux from ab, cd into inelastic channels—flux not available for the exchange reaction we are considering. The procedure is to partial wave analyze the Born term in an eikonal sense $B_{fi}(t) \to B_{fi}(b)$, write $A_{fi}(b) = B_{fi}(b) I(b)$ where I(b) is a factor obtained from elastic scattering account for loss of flux and resum the series to obtain $A_{fi}(t)$. I(b) is obtained from the forward elastic peak, $I(b) = 1 - Cc^{-\gamma b^2}$ which supresses lower partial waves and so pronounces the forward peak. If we write $A(b) = B(b) - ce^{-\gamma b^2} B(b)$ on resuming the series we have $A(t) = B(t) - A(t)$ and we can call the first term Born and the second, cut.

Strong Regge Cut Absorption Model

While the above procedure worked pretty well for exchanges, it was clearly wrong (in both energy and angular dependance) for exchanges like ρ, present in reactions like $\pi^- p \to \pi^0 n$. Great improvement came with (for both s and t) the introduction of a Reggeized version of the exchange particles which treatments $J_{exch} = \alpha(t)$. Absorption corrections are again introduced the same way $A_{fi}(b) = B_{fi}(b) I(b)$ but now B(b) represents a reggeon exchange. If $I(b) = 1 - Cc^{-\gamma b^2}$, then $A(t) = R(t) - A(t)$ and it was found by U.M. group that one can fit the dip present at t -.6 $BeV^{-\gamma}$ if one uses instead $A(t) = R(t) - \lambda \delta A(t)$ with $\lambda \sim 2$. This is the strong cut regge absorption model. Amplitudes are now a sum of two terms pole + cut or Born + absorption correction, the second is (mostly) negative with respect to lst, and varies more slowly with angle. The effect of λ is tomove the dips in.

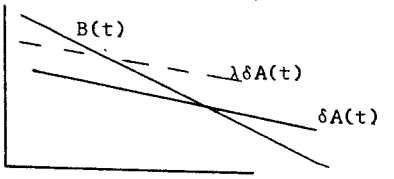

This mechanism has been found to fit many other quantum exchange reactions well.

Calculations: My attempts have been to see if so large a cut enhancement factor, λ, could emerge naturally from a calculation. The initial approach taken was to see if it could be due to the coherent action of inelastic states (the reason originally given by the U.M. group).

For the reaction pn→np for the part that goes by π exchange this amounts to calculation of graphs of the type

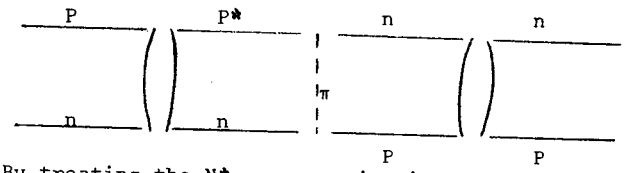

By treating the N* as a quasi-spinor particle of effective coupling $g(\pi NN^*)$, and relating g^* to the decay, one can calculate a scaling factor—and we found $\lambda_\pi \leq 1.4$. The calculation is extremely crude but one at least obtains an estimate. It agrees roughly with previous calculations by Ravenhall for $\pi^- p \to \pi^0 n$ who found $\lambda(e) \leq 1.2$. Because of the small values emerging from calculations of this sort we decided to look elsewhere. One attempt was to try improvements in I(b) where I(b) is now assumed to fit large t elastic data as well. A number of forms were used some theoretical, some phenomological, some just guessed at. The result is that at small t the n=0 amplitudes (zero net flip amplitudes) can have $\lambda \sim 1.4$, 1.5 but that $n \neq 0$ amplitudes do not change much or can even be renormalized downward. At larger t they will all rise and take on a curvature induced by I(b). A look at the data shows that this cannot be correct.

Another attempt was to look at reactions through a quark model, and one can calculate things using the Glauber formalism developed for the scattering of composite systems (mostly nuclei).

Single scattering of quarks by other quarks when summed over all constituents supplies a Born term; double scattering supplies a cut. The quark-quark amplitudes must then be related back to $A_{ab\to cd}$.

It was found that no enhancement is possible in this model, if you stay with quark-quark amplitudes.

Other mechanisms considered and rejected were polynomial t dependence of the residue functions, and possible spin-flip contribution in the elastic amplitude.

Conclude: So large an enhancement factor is pretty difficult to obtain. Entirely different mechanisms are now being pursued.

The Structure of the Lighter N=82 Nuclei

B.H. Wildenthal and D.C. Larson

Recent advances in experimental techniques have made possible the quantitative study of the lighter mass nuclei having 82 neutrons.[1-4] Spectra have been obtained for ^{133}Sb, ^{134}Te, and ^{135}I; these nuclei correspond respectively to one, two and three protons outside the Z=50, N=82 doubly-magic ^{132}Sn core. The properties of these systems are interesting because their presumed structural simplicity permits a relatively unambiguous delineation of the various facets involved in nuclear structure phenomena. The nuclei around ^{208}Pb have been extensively studied in this same spirit in order to extract such quantities as effective charges and effective g-factors. Next to the ^{208}Pb neighborhood, the N=82 region may well exhibit the best "closed shell" behavior available to us. In addition the N=82 nuclei provide what the lead region does not, namely a long string of nuclei (14 have been studied at present) built by adding protons to the doubly-magic core. Thus for N=82 we will have the opportunity to pursue the consequences of our deductions based on the simple, "few" nucleon systems through a series of "many" nucleon systems.

Actually, of course, because of the accidents of nuclear stability, the situation has been inverted in the N=82 region. The naturally stable, many-proton, systems have been extensively studied both experimentally and theoretically for some time, and the few-proton nuclei have just become available for study within the last year or so. In this note we present theoretical predictions for the structure of the Z=(50+1,2,3, and 4), N=82 nuclei and compare these results to the presently available experimental data.

Our predictions for ^{133}Sb, ^{134}Te, and ^{135}I are based on previous shell-model calculations for heavier N=82 nuclei.[5] These calculations employ an MSDI residual interaction[6,7] and a model space comprised of all $0g_{7/2}$-$1d_{5/2}$ configurations plus all configurations formed by exciting one particle from the $0g_{7/2}$-$1d_{5/2}$ subspace to either a $2s_{1/2}$ or $1d_{3/2}$ orbit. In our initial work[5] we chose values for the SDI strength and for the single-particle-energy (SPE) splittings which optimized agreement between model and experimental excitation energies for all known positive-parity N=82 states in A=136-145 inclusive. Subsequently, because the model space is most appropriate for the lighter N=82 nuclei, we readjusted the SDI strength and the SPE splittings to optimize agreement only for A=136-140. The significant change which resulted from the new approach was an increase, from 0.48 MeV to 0.88 MeV, of the $0g_{7/2}$-$1d_{5/2}$ SPE splitting.

We have used these A=136-140 parameters, and the same model space assumptions, to calculate the structure of the one, two, three, and four proton systems. The predicted and experimentally observed energies are given in Table 1. The agreement is satisfactory. Several other data are available on these nuclei which bear on the wave functions of these states. In Table II we present some predictions from our wave functions for purposes of comparison to experiment.

The ^{133}Sb nucleus does not offer much material for discussion from our point of view, of course. The single gamma-ray (E_γ=0.963 MeV) attributed to this system presumably corresponds to the "single-proton" $1d_{5/2}$ to $0g_{7/2}$ transition. Any additional energy levels below the $0h_{11/2}$, $1d_{3/2}$, and $2s_{1/s}$ single-proton states at ≃3 MeV excitation would signal the breaking of the assumed model core and problems for our approach.

In addition to the level energies of ^{134}Te, the lifetime of the 1691 keV to 1576 keV transition has been measured[2,3] and the transition interpreted as a $J^\pi=6^+$ to 4^+ electric quadrupole decay. The B(E2) extracted from the 162 ns lifetime of this decay is 85 e^2F^4. The calculated B(E2) for the transition between the lowest 6^+ and 4^+ state in our ^{134}Te model spectrum (under the assumptions of harmonic oscillator single-particle wave functions ($\hbar\omega$=41 $A^{-1/3}$) and a proton charge of 1e) is 39 e^2F^4. This implies an effective charge for protons in this region of E_p(eff)=1.47e. Our model wave functions for each of the lowest 0^+, 2^+, 4^+, and 6^+ states are dominated (≃80%) by the $(g_{7/2})^2$ configuration. However, the difference between the effective proton charge derived from a pure $g_{7/2}$ assumption for these states and our present value is 1.74e vs 1.47e.

The structure of the low-lying levels of ^{135}I have been studied both by gamma-ray decay and by proton pickup[8] from ^{136}Xe. The ^{136}Xe(d,^{3}He)^{135}I reaction populates the 0.604 and 0.871 MeV states with ℓ=2 transfer. Systematics argue against interpreting the higher energy state as being fed by $1d_{3/2}$ pickup, yet study of the heavier N=82 nuclei gives no evidence for any but the lowest $5/2^+$ state being populated in such a pickup reaction. The experimental and calculated S-factors are presented in Table II and it can be seen that our theory predicts this phenomenon with quantitative accuracy. Its occurance depends upon the drawing close of the $[(g_{7/2})^2_{J=0}(d_{5/2})]_{J=5/2}$ state and the $[(g_{7/2})^3]_{J=5/2}$ state so that their amplitudes mix. In the BCS language we would speak of the $1d_{5/2}$ one-quasiparticle state mixing with the $0g_{7/2}$ three-quasiparticle J=5/2 state. That is, in the three proton system we witness the transition from the "super-conducting" type of nuclear structure characteristic of the heavier N=82 systems to a more typical "shell-model" structure. Of course, our present shell-model treatment encompasses both types of structure simultaneously, the changes in overt behavior

just arising from the different numbers of active particles.

Although ^{136}Xe, the 4-proton system, is a stable isotope, rather little is experimentally known about the structure of its low-lying states either. One feature that has been recently discovered[4] is an isomeric gamma-ray transition that appears to be a 6^+ to 4^+ E(2) transition analogous to that discussed for ^{134}Te. The strength of this transition in ^{136}Xe is 0.6 e^2F^4, as opposed to the value of 85 e^2F^4 in ^{134}Te. Our predicted B(E2), using the effective proton charge of 1.47e, is 3.5 e^2F^4. This marked reduction in strength in going from the 2 proton to the 4 proton system arises in the model because of a selection rule forbidding E2 transitions between components having the same seniority and a half-full j-shell.

References

1. G.B. Holm, S. Borg, and B. Rydberg, Conference on the Properties of Nuclei Far from the Region of Beta-Stability, Leysin, Switzerland.
2. W. John, F.W. Guy, and J.J. Wesolowski, Phys. Rev. C2, 1451(1970).
3. S. Borg, P. Carlé, L.E. DeGeer, G. Holm, and A. Kerek, Annual Report, Research Institute for Physics, Stockholm, Sweden.
4. L.C. Carraz, J. Blachot, E. Monnand, and A. Moussa, Nucl. Phys. A158, 403(1970).
5. B.H. Wildenthal, Phys. Rev. Letters 22, 1118(1969).
6. R. Arvieu and S.A. Moszkowski, Phys. Rev. 145, 830(1966).
7. P.W.M. Glaudemans, P.J. Brussaard, and B.H. Wildenthal, Nucl. Phys. A102, 593(1967).
8. B.H. Wildenthal, E. Newman, and R.L. Auble, Phys. Rev. C3, 1199(1971).

Table II. Electromagnetic and single-nucleon transition strengths in ^{134}Te, ^{135}I, and ^{136}Xe.

Nucleus	$J^\pi_\nu \to J'^\pi_{\nu'}$	Calc.	Expt.
		B(E2)'s in units of e^2F^4	
^{134}Te	$2^+_1 \to 0^+_1$	81[b]	
	$4^+_1 \to 2^+_1$	81	
	$6^+_1 \to 4^+_1$	39	85
^{136}Xe	$2^+_1 \to 0^+_1$	122	
	$4^+_1 \to 2^+_1$	9	
	$4^+_2 \to 2^+_1$	65	
	$6^+_1 \to 4^+_1$	1.6	0.6
	$6^+_2 \to 4^+_1$	11	
		Single Nucleon S-factors	
^{136}Xe → ^{135}I	$0^+_1 \to 7/2^+_1$	318	274
	$0^+_1 \to 5/2^+_1$	58	34
	$0^+_1 \to 5/2^+_2$	17	12

[b] e_p assumed to be 1.0e.

Table I. Characteristics of Low-Lying Levels of ^{133}Sb, ^{134}Te, ^{135}I, and ^{136}Xe

Nucleus	J^π_ν	$E_{calc.}$	$E_{expt.}$	Model Wave Function (Largest Components)[a]
^{133}Sb	$7/2^+$	0.00	0.00	$1.00g_7$
	$5/2^+$	0.88	0.963	$1.00d_5$
^{134}Te	0^+_1	0.00	0.00	$.90(g_7)^2 + .43(d_5)^2$
	2^+_1	1.39	1.279	$.90(g_7)^2 + .26(g_7d_3) + .22(d_5)^2$
	4^+_1	1.76	1.576	$.93(g_7)^2 - .27(g_7d_5)$
	6^+_1	1.93	1.691	$.93(g_7)^2 - .37(g_7d_5)$
^{135}I	$7/2^+_1$	0.00	0.00	$.90(g_7)^3_{J=7} - .42(g_7)^1(d_5)^2_{J=0}$
	$5/2^+_1$	0.65	0.604	$.84(g_7)^2_{J=0}(d_5)^1_{J=5} - .40(g_7)^3_{J=5} + .27(d_5)^3_{J=5}$
	$5/2^+_2$	0.82	0.871	$.42(g_7)^2_{J=0}(d_5)^1_{J=5} + .80(g_7)^3_{J=5} + .19(d_5)^3_{J=5}$
^{136}Xe	0^+_1	0.00	0.00	$.80(g_7)^{4,0} + .58(g_7)^2_{J=0}(d_5)^2_{J=0} + .16(d_5)^4$
	2^+_1	1.38	1.313	$.80(g_7)^{4,2} + .37(g_7)^2_{J=2}(d_5)^2_{J=0} + .24(g_7)^2_{J=0}(d_5)^2_{J=2}$
	4^+_1	1.76	1.694	$.82(g_7)^{4,2} + .38(g_7)^2_{J=4}(d_5)^2_{J=0} + .26(g_7)^3_{J=7}(d_5)^1_{J=5}$
	6^+_1	1.92	1.892	$.79(g_7)^{4,2} - .44(g_7)^3_{J=7}(d_5)^1_{J=5} - .37(g_7)^2_{J=6}(d_5)^2_{J=0}$
	4^+_2	2.20		$.81(g_7)^{4,4} + .24(g_7)^3_{J=7}(d_5)^1_{J=5} - .21(g_7)^3_{J=9}(d_3)^1_{J=3}$
	6^+_2	2.33		$.80(g_7)^3_{J=7}(d_5)^1_{J=5} + .44(g_7)^{4,2} - .30(g_7)^1_{J=7}(d_5)^3_{J=5}$

[a] Half-integral spins are given as two times their value, i.e. 7/2=7. The additional quantum numbers labeling a few components are the seniorities, e.g. $(g_7)^{4,2}$ refers to the seniority 2, coupling of four 7/2 particles coupled to total angular momentum J.

Proton Induced Spallation of ^{14}N, ^{16}O and the Astrophysical Production of Li, Be, and B

Helmut Laumer, Lolo Panggabean, and Sam M. Austin

The program for measuring the production cross-sections of the light elements Li, Be, B from proton spallation of ^{14}N and ^{16}O has been completed. We have made measurements at proton beam energies from 17 MeV to 42 MeV. The gas cell described elsewhere in this report was an essential part of the measuring apparatus. We found total cross sections by measuring differential cross-sections at a number of angles and integrating the resulting distribution over angle. Particle mass identification was accomplished by a time-of-flight technique in which one simultaneously measures the time-of-flight t and energy E of a particle and forms the product Et^2 which is proportional to the particle mass ($Et^2 = 1/2 MV^2 \times (\frac{\text{distance}}{V})^2 \propto M$). Mass identification is sufficient[1] since for all possible product nuclei only one isobar is stable and all others decay to it on astrophysical time scales.

Particles produced in a gas target were detected in a thin (between 78μ and 150μ) Ortec silicon surface barrier detector placed about 27 cm from the target. A timing signal derived from this energy (E) pulse starts a time-to-amplitude converter (TAC); a second timing signal from the Cyclotron RF system stops the TAC. Linear signals E and TAC are decoded by Northern Scientific-629 ADC's. Using the all purpose code TOOTSIE[2] the Sigma-7 computer calculates the quantities $t = T_o - TAC$ and Et^2 and displays Et^2 vs. E in a two dimensional array (128x128 channels) on a storage oscilloscope. T_o is adjusted so the mass bands displayed can be easily identified. For the proper choice of T_o, $(T_o - TAC) \propto t$, the particle flight time between the reaction site and the detector.

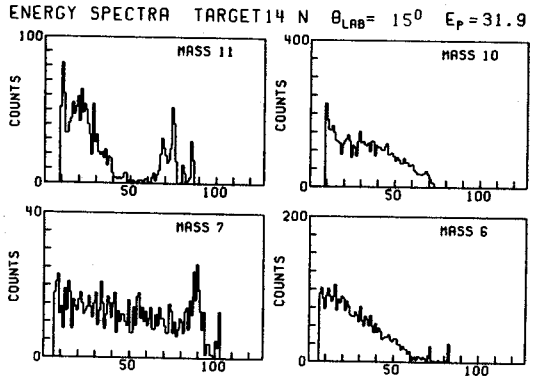

Figure 1

Energy spectra are obtained by defining mass bands on the scope display and storing the energy spectra for each mass. Examples of the energy spectra obtained are shown in Fig. 1. The low energy cutoff evident in these spectra is due to the finite flight time available between consecutive beam bursts; heavy low energy particles from one burst can arrive at the same time as light particles at the same energy from the next burst. The burst spacing is beam energy dependent; it is 53 nsec at 42 MeV and 72 nsec at 22 MeV. For mass 6 the sensitivity of the timing pulse pickoff unit also can limit the low energy particle detection. The low energy portion of the energy spectra are mainly made up of particles from multi-body break up rather than from two-body final states. From phase space arguments[3] one finds that the energy spectrum goes to zero at zero particle energy. In calculating the differential cross-sections a low energy extrapolation of the energy spectra was performed by assuming the channels below the cutoff have the same number of counts as an average of the last few non-zero channels. One half of this contribution to the differential cross-section is assigned as error. This is the major contributor to the error quoted for the total production cross-section.

At beam energies below 26 MeV mass 11 production from $^{14}N+P$ is dominated by the reaction $^{14}N(P,^{11}C^*)^3He$. Since ^{11}C excited above 7.5 MeV particle decays, there is a natural energy cutoff in the spectra at forward angles and no extrapolation need be made.

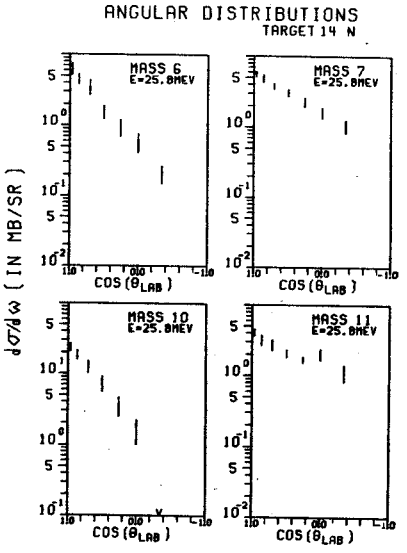

Figure 2

Due to the low energy cutoff there is also always a maximum detection angle beyond which no particles can be detected. As seen from sample angular distributions in Fig. 2, this usually represents a small error contribution in the cross-section integration. Again $^{14}N(P,^{11}C^*)^4He$ is an exception, the contribution of two-body final states at back angles now represents a large uncertainty.

Proton Induced Spallation of ^{20}Ne and the Astrophysical Production of the Lithium Isotopes

L.M. Panggabean, H. Laumer, and Sam M. Austin

It is believed that Li, Be, B (masses 6 through 11) are not part of the products of thermonuclear reactions which is assumed to be the process that generates the different elements in the stars. It has been suggested that another mechanism, spallation by high energy protons, produced these elements. The important targets in this case are ^{12}C, ^{14}N, ^{16}O, ^{20}Ne, ^{24}Mg, ^{28}Si.[1-3]

There have been many data obtained on the production cross-sections of Li, Be, B from most of these targets in the high energy region.[4] However, data on the lower energy region (20-70 Mev) are needed.[4] In this laboratory efford is being made to measure the production cross-sections of Li, Be, B with protons energy ranges from 22 to 42 MeV. Charge particle time-of-flight techniques, which were used in the previous work,[5] have been applied to measure the similar cross-sections from proton spallation of ^{20}Ne.

The reaction Ne+p has been studied at three different energies i.e. 30, 35, 40 MeV. An isotopically enriched (99.95% ^{20}Ne out of a gross composition of 99.5% neon) ^{20}Ne gas target[6] in an ultra thin gas cell is used. A pressure of about 0.052 atm which is, at 15°, equivalent to an 80 $\mu g/cm^2$ target, is used. This enables one to measure down to about 1 MeV particles of mass-6 and 7. The low energy cutoffs for mass 8, 9, and 10 are about 1.5 MeV. A background run has always been taken and total yields have been calculated by subtracting the normalized background counts at each angle.

A two dimensional display (mass versus energy) of the data indicates that masses 6,7,8,9, and 10 can be well separated except for the very low energy region (below 5 MeV). The band of mass 11 is mostly covered by the band of mass 12 and therefore is not extractable. Angular distributions are taken for each bombarding energy. They slowly rise at forward angles. The overall feature of the cross-sections at different energies shows a small dependence on bombarding energy (see Figs. 1 and 2). At the time this report is written data on 30 MeV are being analyzed and not shown on the diagrams. The cross-sections get smaller as the bombarding energy goes down. The preliminary analysis shows that the integrated cross-section at 40 MeV is about 1.97 mb for mass-6, 1.75 mb for mass-7, 0.90 mb for mass-8, .92 mb for mass-9 and 1.92 mb for mass-10. Plans are being made to extrapolate the yields into the zero energy region. The numbers quoted above do not include these regions and hence can be considered as their lower limits.

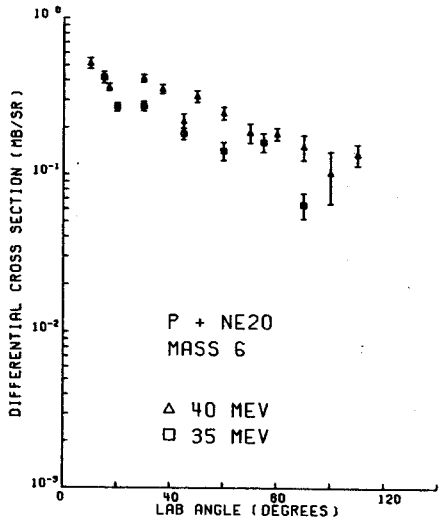

Fig. 1 Comparison between the cross-sections of mass-6 at 40 and 35 MeV.

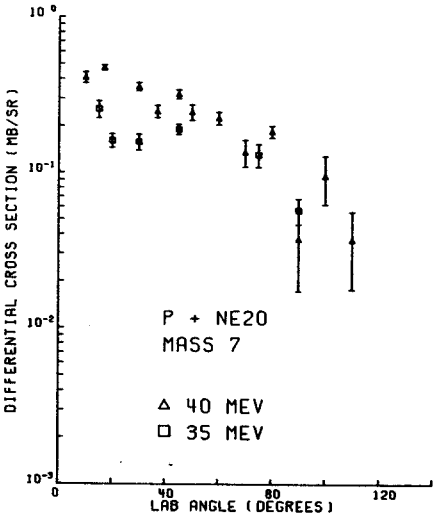

Fig. 2 Comparison between the cross-sections of mass-7 at 40 and 35 MeV.

References

1. D.D. Clayton, Principle of Stellar Evolution and Nucleosynthesis, Ch. V, McGraw-Hill, 1968.
2. R. Bernas et al. Annals of Physics 44, 426(1967).
3. H. Reeves et al. Nature 226, 727(1970).
4. B.S.P. Shen (ed.) High Energy Nuclear Reactions in Astrophysics, Benjamin, 1967.
5. C. Davids et al. PRL 22, 1388(1969).
6. See topic on Ultra-thin Window Gas Cell in this report.

The $^{14}N(p,p')^{14}N$ Reaction at 29.8, 36.6, and 40.0 MeV

S.H. Fox, S.M. Austin and D. Larson

The reaction $^{14}N(p,p')^{14}N^*(Ex=2.31)$ has been of interest to a number of investigators[1-4] The L=0 inelastic scattering matrix element for the $1^+(T=0)$ to $0^+(T=1)$ transition in ^{14}N is nearly proportional to the matrix element for the Gamow-Teller beta decay of ^{12}C which is strongly inhibited. Hence if one assumes only a central effective interaction in microscopic model calculations of the reaction, the normally dominant L=0 contribution to the inelastic scattering cross-section should be almost vanishing[4] and the L=2 component would be expected to dominate the cross-section. Since the L=2 contribution fits the angular distribution poorly,[1] the $^{14}N(p,p')^{14}N^*$ (Ex=2.31), $1^+(T=0)$ to $0^+(T=1)$ reaction is a good case for which to consider the effects of a possible tensor component of the effective interaction.

To explore tensor effects in the effective two-body interaction and possible energy dependences 29.8, 36.6, and 40.0 MeV protons from the MSU Sector-Focussed Cyclotron were scattered from ^{14}N targets and cross-sections for the excitation of the 2.31 and 3.95 states in ^{14}N and elastic scattering were obtained. Most of the 28.9 MeV data and the foreward angle points of the 36.6 and 40.0 MeV elastic angular distributions were obtained using gas targets and silicon solid state detectors. The 36.6 and 40.0 MeV data and check points for the 2.31, 29.8 MeV angular distribution were obtained using targets of melamine evaporated on carbon foil backings in conjunction with the MSU Enge split-pole spectrograph and a 300μ thick, 3.0 cm long position sensitive solid state detector. The gas cell data was taken with a $\Delta E,E$ detector telescope consisting of a 500μ thick surface barrier silicon detector and a 5000μ Si(Li) back detector. The $\Delta E,E$ signal pairs from particles of different masses are separated into different mass bands and energy spectra by the code TOOTSIE[5] running in the Sigma-7 computer. The position sensitive detector data was acquired through the XE/E option of TOOTSIE. Here two signals are obtained from the detector. One is proportional to the product of the position of the incident particle along the face of the detector and the energy lost by the particle and the other proportional only to the energy lost. The code does the numerial division necessary to define the particles' incident position. Point to point normalization of the spectrograph data was done by means of a 5000 mm Si(Li) detector used as a monitor, while overall normalization was obtained from the gas cell data.

The angular distributions for the elastically scattered protons and the reactions to the 2.31 and 3.95 states in ^{14}N for 29.8, 36.6 and 40.0 MeV incident protons are given in Figs. 1, 2, and 3. The errors shown on the data points are preliminary estimates of the total errors. The elastic cross-sections should be good to within 5%. A problem particular to the 2.31 angular distribution for 29.8 MeV incident protons taken with the E, E silicon detector telescope is the excitation of the 1.78 MeV state of ^{28}Si by inelastic proton scattering in the solid state detectors. Figure 4 is one of the spectra taken in the spectrograph.

A good bit of effort has gone into finding optical model parameters for the elastic scattering angular distributions. Using GIBELUMP, an optical model search code,[6] and starting with parameters similar to those used by van Oers and Cameron[7] to fit $p-^{16}O$ elastic scattering from 23-53 MeV, the optical model parameters in Table 1 were obtained. The explicit optical potential used was:

$$U(r)=U_c-V_R f_R(x)+\left(\frac{\hbar}{2m_p c}\right)^2(V_s+iW_s)\vec{L}\cdot\vec{\sigma}\frac{1}{r}\frac{d}{dr}f_s(x)$$

$$-i[W_s-4W_D\frac{d}{dx_I}]f_I(x).$$ Where U_c is the potential of a uniformally charged sphere of radius $r_c A^{1/3}$.

$$f(x)=(1-e^x)^{-1} \qquad x=\frac{r-R}{a} \qquad R=r_o A^{1/3}$$

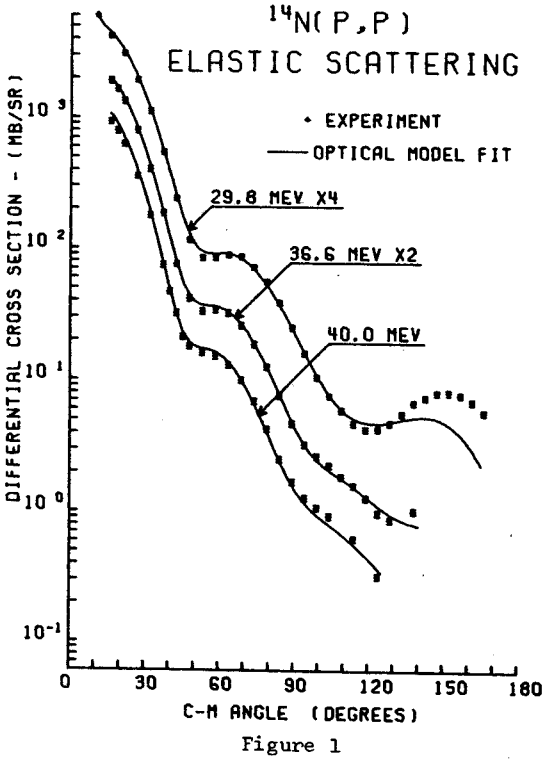

Figure 1

The hope was to fit 24.9, 29.8, 36.6 and 40.0 MeV $p-^{14}N$ elastic scattering data with average real and imaginary well geometries while the spin-orbit well geometry was set equal to the real

geometry. The geometry used was $R_R=R_S=1.133$fm, $A_R=A_S=0.6515$fm, $R_I=1.345$fm, and $A_I=0.5090$fm. The fits in Fig. 1 were obtained with slightly different parameters than those in Table 1. The final fits whose parameters are in Table 1 were actually better than shown in Fig. 1 especially at forward angles for 40.0 MeV.

Table 1

E_{LAB} (MeV)	V_R (MeV)	W_S (MeV)	W_O (MeV)	V_S (MeV)	X^2/N
24.9	51.36	1.56	4.75	766.0	4.2
29.8	48.50	2.65	3.52	959.1	4.7
36.6	46.45	6.26	1.63	1012.6	1.2
40.0	43.84	5.74	2.07	1555.2	0.56

The transition to the 2.31 state well be analyzed using a microscopic DWBA code (DWBA 70 by Raynal and Schaeffer) in which exchange effects as well as the tensor and L·S interactions may be included.

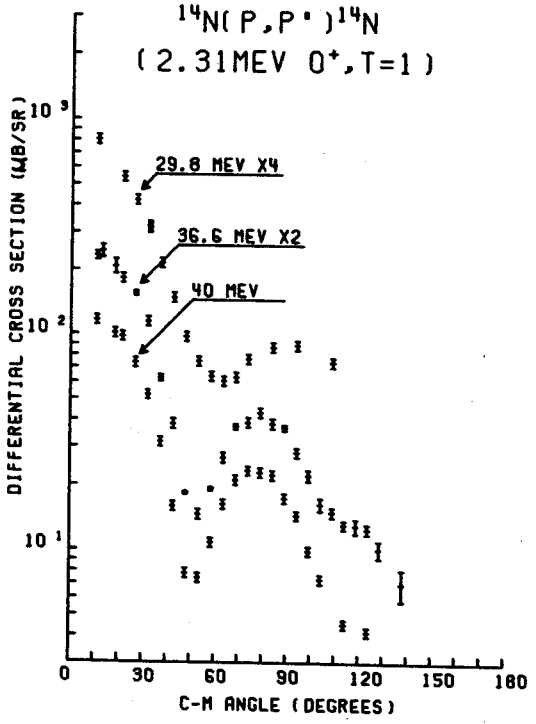

Figure 2

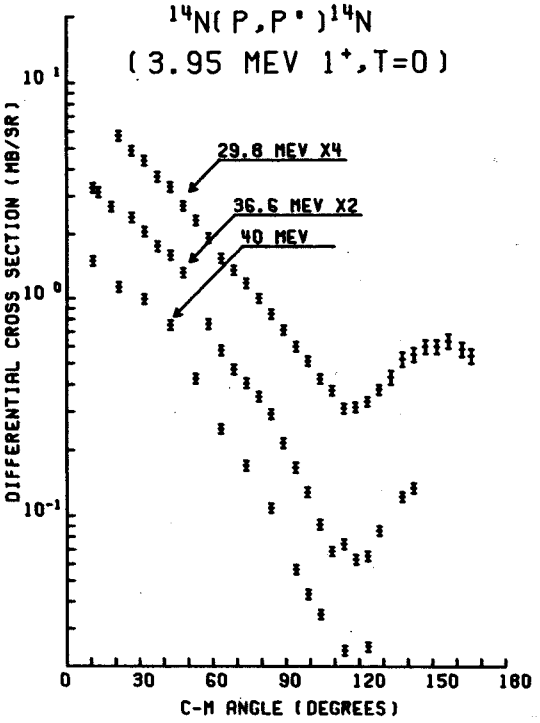

Figure 3

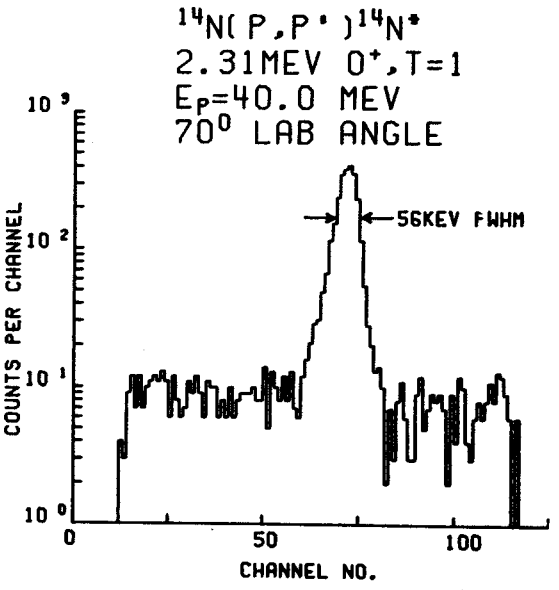

Figure 4

References

1. G.M. Crawley, S.M. Austin, and W. Benenson, and V.A. Madsen, F.A. Schmittroth and M.J. Stomp, Phys. Letters 32B, 92(1970).
2. J.L. Esceidie, A. Tarrats, and J. Raynal Proceedings of the Third International Symposium on Polarization Phenomena in Nuclear Reactions edited by H.H. Barschall and W. Haeberti (The University of Wisconsin Press) p. 705-707.
3. C. Wong, J.D. Anderson, V.A. Madsen, F.A. Schmittroth and H.J. Stomp, Phys. Rev. C3, 1904(1971).
4. C. Wong, J.D. Anderson, J. McClure, B. Pohl, V.A. Madsen, F.A. Schmittroth, Phys. Rev. 160, 769(1967).
5. D.L. Bayer, MSUCL-31 (MSU, East Lansing, Michigan (1971).
6. Written by F.G. Perey and modified by R.M. Haybron.
7. W.T.H. van Oers and J.M. Cameron, Phys. Rev. 184, 1061(1969).

Inelastic Proton Scattering on Zr at 40 MeV and Monopole Transitions

R.A. Hinrichs, B.M. Preedom,* and D. Larson

We have initiated a study of inelastic proton scattering on the Zr isotopes at 40 MeV with a special interest in the excitation of the well known excited 0^+ states in these nuclei. Such 0^+ to 0^+ transitions in the Zr isotopes have only been observed at much lower energies[1] (12.7 MeV); a study of these monopole transitions is particularly interesting in that their angular distributions are quite sensitive to the radial shape of the interaction form factor. Core polarization effects should also not cloud a microscopic description of the interaction as first order monopole collective oscillations of the core should be zero.

Data has been taken so far on $^{90,92}Zr$ at angles from 10° to 120° using plates in our Enge split-pole spectrograph. Long and short exposures were taken at each angle to study the 0^+ as well as other more strongly excited states. Figure 1 shows a partial angular distribution for excitation of the first excited 0^+ state in ^{90}Zr at 1.75 MeV. Pronounced structure is seen, as well as the smallness of the cross-section.

Data for the sequence of levels 2^+, 4^+, 6^+, 8^+ (due to re-coupling of two $g_{9/2}$ protons) has also been obtained. This sequence is interesting as it can provide information on the importance of exchange and spin-orbit effects as a function of angular momentum transfer. Analysis along these lines is being carried out with the use of the recently acquired computer code DWBA-70, written by R. Schaeffer and J. Raynal.

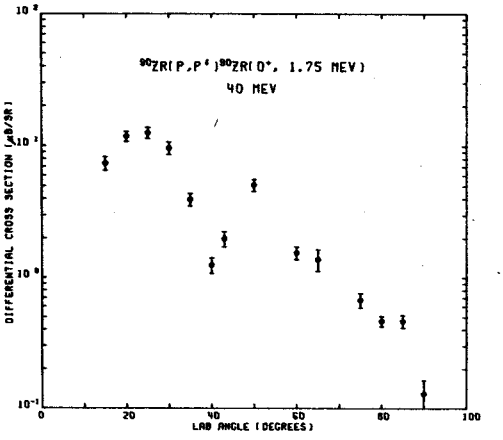

Fig. 1 Angular distribution for the reaction $^{90}Zr(p,p')$ at a bombarding energy of 40 MeV for excitation of the 0^+ state at 1.75 MeV.

Reference

1. J.K. Dickens, E. Eichler, and G.R. Satchler, Phys. Rev. 168, 1355(1968).

*Univ. of South Carolina, Columbia, S.C.

Inelastic Proton Scattering from N=82 Nuclei

Duane C. Larson Sam M. Austin B.H. Wildenthal S.H. Fox

We are using 30 MeV protons to study inelastic scattering from nuclei with 82 neutrons. There are seven such stable nuclei, with four to twelve valence protons outside the Z=50 shell. Since the density of states is quite high, we are using the speculator system developed by Blosser et al.[1] which allows us to routinely obtain resolutions of 10 keV or less at 30 MeV. The speculator system is basically a feedback system which operates on the elastic peak. It regulates the magnetic field of the spectograph in a compensating manner to keep the elastic peak at a constant point on the focal plane. During setup it is used to minimize the line widths of the peaks of the scattered particles. Dispersion matching is used to compensate for the beam energy spread, thus eliminating the need for slits to minimize the beam energy resolution. Beam currents on target were 100 na for Ba^{138} and 900 na for Pr^{141} and Sm^{144}.

Targets were made by vacuum evaporation of isotopically enriched Ba^{138}, Sm^{144} and natural Pr^{141} onto 20 $\mu g/cm^2$ carbon foils. The targets were stored and transferred under vacuum to prevent oxidation. Typical target thicknesses ranged from 50-300 $\mu g/cm^2$.

Data on Ba^{138}, Pr^{141} and Sm^{144} is now being analyzed. Typical spectra are shown in Fig. 1-2. Figure 1 shows a spectrum from Ba^{138} taken at a lab angle of 35°. The resolution here is 11 keV fwhm. The elastic peak is not shown. The first excited 2^+ state at 1.436, and the 3^- at 2.880 MeV were uncountable on this plate. The 4^+ state at 1.899 is followed by a state at 2.09 MeV which has not been seen in gamma ray work on this nucleus, but has been seen in La^{139} (d,He^3).[2] A 6^+ assignment for this state is consistent with the shell-model calculations of Wildenthal,[3] both with respect to the energy position and the spectroscopic factors for proton pickup.

Figure 2 shows a spectrum from Sm^{144} taken at a lab angle of 40°. The resolution is 7 keV fwhm. The elastic peak is not shown. The first excited 2^+ state at 1.67 and the 3^- at 1.82 MeV were uncountable on this plate. The strong state in the region of 2.43 MeV is probably the 2^+ seen by Barker and Hiebert[4] and is not the 0^+ level which is known at 2.48 MeV.[5]

Figure 3 shows that the cross-sections for the first 2^+ excited states in Ba^{138} and Sm^{144} are nearly identical in shape and differ in magnitude by less than 10%. In Fig. 4 we see that for the first 3^- states in these nuclei the shapes are again the same, but the Sm^{144} cross-section is 25% larger than the Ba^{138} cross-section.

Future work includes extending the experiments to the remaining N=82 nuclei, and doing microscopic DWBA calculations using the wave functions of Wildenthal with realistic forces.

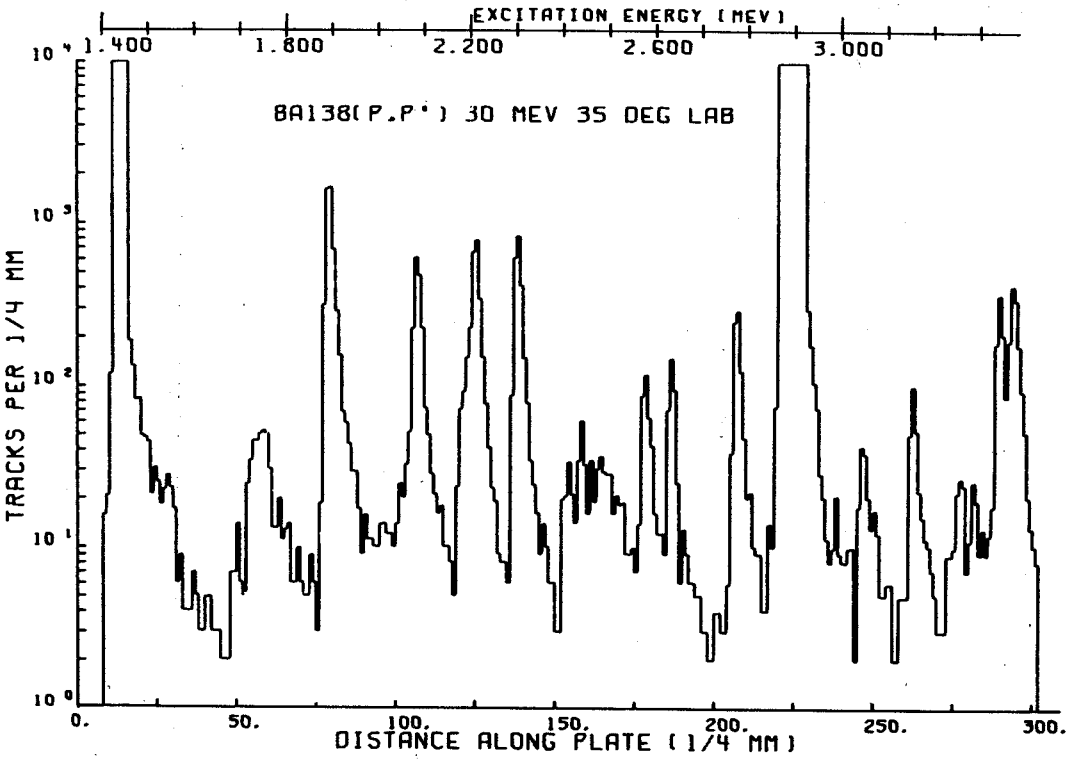

Figure 1

REFERENCES

1. H.G. Blosser et al., Nucl. Instr. and Meth. 91(1971)61.
2. W.P. Jones, L.W. Borgman, K.T. Hecht, John Bardwick, and W.C. Parkinson, Phys. Rev. 4, (1971)580.
3. B.H. Wildenthal, to be published.
4. J.H. Barker, J.C. Hiebert, to be published.
5. J.S. Geiger, R.L. Graham, Ark. Fys. 36(1967)191.

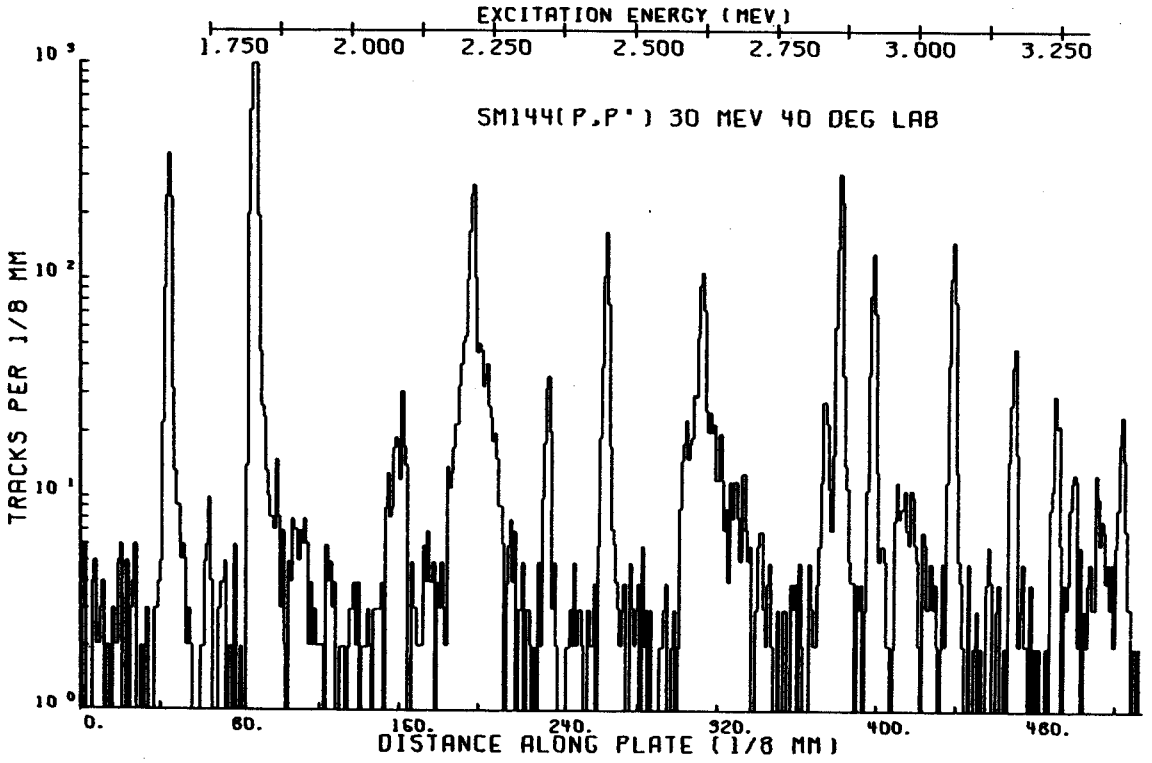

Figure 2

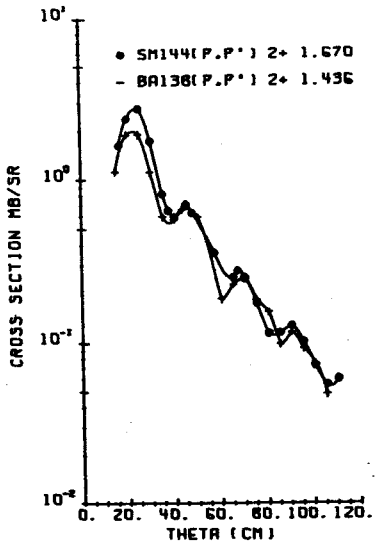

Figure 3

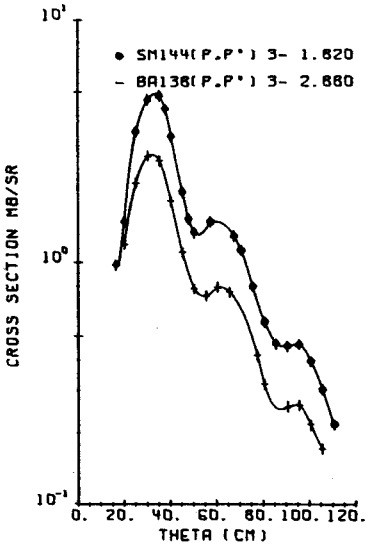

Figure 4

Inelastic Scattering from Pb and Bi Isotopes

W.T. Wagner, G.M. Crawley and P.S. Miller

Information on both nuclear structure and nuclear reaction mechanisms can be obtained from inelastic scattering experiments. However, experimental difficulties have limited the range over which various models and theories can be tested effectively. The shell-model structure of many Pb and Bi isotopes has been well established and good predictions of scattering and related phenomena have been given via a microscopic description of these nuclei. Also, the weak coupling model has seen success when applied to low-lying multiplets in this region and it would be of interest to extend this treatment to higher energies. Inelastic scattering also gives information on the collective properties of the predominantly single particle states in the odd A isotopes. With facilities for ultra-high resolution nuclear experiments, the Michigan State University Cyclotron Laboratory allows previous experimental difficulties to be overcome.

Therefore, much new information can now be obtained by a study of proton inelastic scattering from ^{206}Pb, ^{207}Pb, ^{208}Pb, and ^{209}Bi. While an inelastic study of the three lead isotopes has been done,[1] resolution and choice of bombarding energy were not optimum. Because of the MSU accelerator stability and predicted sensitivity of the data at this energy, the experiment will be performed at 40 MeV incident energy. With the use of the ultra-high resolution spectrometer system[2] recently developed at MSU, resolution of about 5 keV has been obtained.

Preliminary data have been taken at a few angles on ^{207}Pb and ^{208}Pb in the Enge spectrograph using photographic plates. Such data provides necessary information regarding exposure length versus total charge collected and their relation to plate fogging. The targets used in this preliminary run were made by vacuum evaporation of isotopically enriched lead on a thin carbon-formvar backing. It was found necessary to subject the backing to a glow discharge (exposure to low pressure, low energy ionized gas bombardment) to insure adhesion of the Pb. The targets were stored in reasonable vacuum to prevent unnecessary oxygen contamination. Another study is being made to determine the optimum relationship between target thickness, counting rate, and energy resolution.

Most of the reaction theories to be compared with the final inelastic scattering data require optical model parameters which are, of course, obtained from elastic scattering angular distributions. Also for a normalization aid in the inelastic experiments and to give data on the more strongly excited states, we are currently using the 40" scattering chamber and a ΔE-E detector telescope arrangement using two 5 mm Si(Li) detectors to study proton scattering at 40 MeV. The angular distributions for scattering from the ground state and first excited 3^- state of ^{208}Pb are shown respectively. In Figs. 1 and 2, similar studies on ^{206}Pb, ^{207}Pb, and ^{209}Bi are planned.

References

1. G. Vallois, Thesis, CEN-Saclay, Report CEA-R-3500 (unpublished).
2. H.G. Blosser, G.M. Crawley, R. deForest, E. Kashy, and B.H. Wildenthal, Nucl. Instr. and Methods 91, 61(1971).

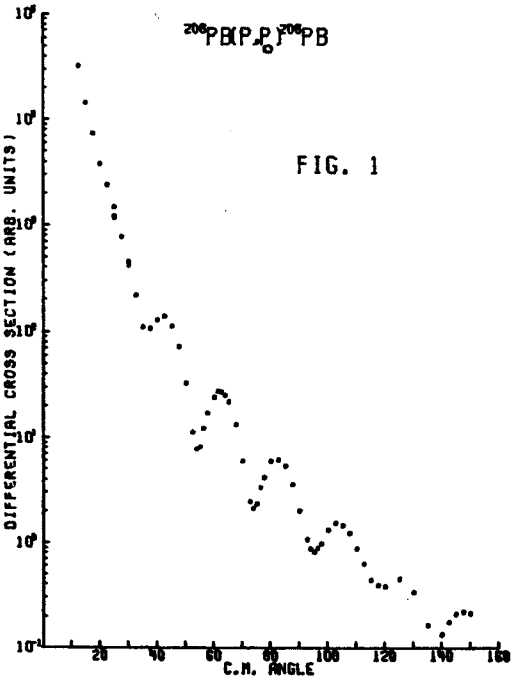

FIG. 1

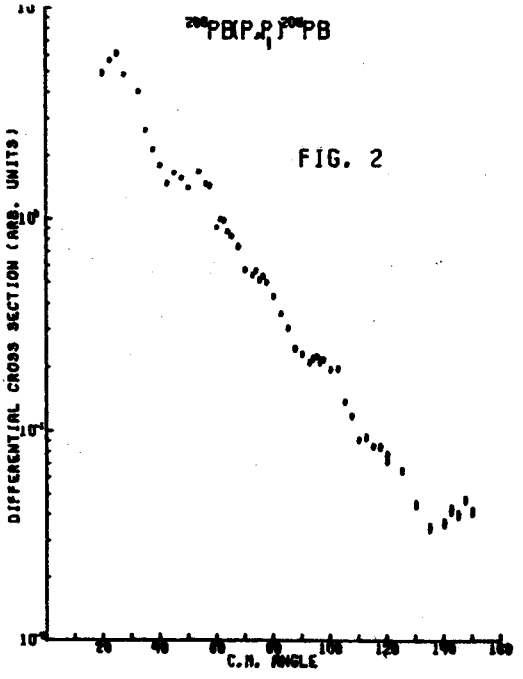

FIG. 2

The (p,n$\bar{p}$) Reaction Near A=208

G.M. Crawley and P.S. Miller

Studies of the (p,n$\bar{p}$) reaction allow the determiniation of the position and in some cases the width of the isobaric analogue state populated in the (p,n) reaction without the difficulty of neutron detection. In principle proton decay widths can also be measured but this is usually difficult because of uncertainties in the (p,n) cross section. This situation is improved in the lead region where decay to more than one final state is observed and therefore relative proton decay widths can be obtained. Another advantage of the (p,n$\bar{p}$) reaction is that can be used to study nuclei not readily reached by resonant elastic and inelatic scattering.

Earlier measurements of the partial widths for decay of the IAS in ^{208}Bi had shown agreement between the resonance measurements[1] and the (p,n$\bar{p}$) experiment.[2] However measurements of the ^{209}Bi(p,n$\bar{p}$) reaction[3] gave relative proton widths for the IAS in ^{209}Po which were significantly different from the measurements in ^{208}Bi. This discrepancy encouraged us to repeat the ^{208}Pb(p,n$\bar{p}$) experiment as a check on the earlier measurement. In addition, the (p,n$\bar{p}$) reaction on ^{206}Pb, ^{207}Pb was also studied.

The experiment used protons of various energies from 21.3 to 35 MeV from the Michigan State Isochronous Cyclotron. A standard counter telescope of cooled silicon detectors was used to detect the protons. Deuteron spectra were taken simultaneously since these reach the same final nuclei and help provide an energy calibration. The deuteron resolution also gives an accurate check of the target thickness measurements. Spectra were taken at many angles to avoid contaminant peaks and to check kinematic effects.[3]

The results of the Coulomb energy measurements are shown in Fig. 1 together with the results of other Coulomb energy measurements in the Pb isotopes. These data are plotted relative to the predictions of Fox and Long[4], which appear to be a reasonable approximation although the experimental values are consistently lower than the predictions. It should be noted that the measurements for ^{206}Pb and ^{209}Bi cannot be obtained from resonance measurements since no suitable target is available.

A spectrum of protons from ^{208}Pb at a laboratory angle of 158° is shown in Fig. 2. The low lying excited states of ^{208}Pb including the ground state have been excluded from the figure. The peaks observed correspond to decays to the first three single particle states in ^{207}Pb with J^π of $1/2^-$, $5/2^-$, and $3/2^-$ respectively. It is clear that although the peaks are broad, presumably due to the intrinsic width of the IAS, the $f_{5/2}$ state can be distinguished.

Similarly a proton spectrum from ^{207}Pb showing the large $\bar{p}$ feature at backward angles is shown in Fig. 3. The situation is more complex here since decays take place to a number of excited states of varying J^π too close in energy to be distinguished. A feature of this spectrum is the large width of the $\bar{p}$ peaks which are significantly broader than the ^{208}Pb case.

In contrast, the $\bar{p}$ peaks from the ^{206}Pb(p,n$\bar{p}$) reaction shown in Fig. 4 are narrower than even the ^{208}Pb case, the decays here going again to the hole states in ^{205}Pb with spins $5/2^-$ (plus possibly $1/2^-$) and the $3/2^-$ state at 262 keV. The ^{206}Pb target has more impurities and care must be taken to position the $\bar{p}$ peak in a reasonably clear region of the spectrum by suitable choice of bombarding energy and observation angle.

The yield for proton decay to a particular final state (or multiplet in the case of ^{209}Bi) of the residual nucleus is given by

$$\frac{d\sigma}{dr}(\bar{p}) \alpha \sum_i \frac{\Gamma_{pi}}{(E-E_i)^2+1/4\Gamma^2}$$

where in general the sum is over all members of a multiplet. Penetrability corrections are made to the partial decay widths (Γ_i) appearing in the equation. Corrections for target thickness and kinematics are also folded into the fitting equation. A smooth background was substrated from the original experimental spectrum as were contributions from impurity peaks. The remaining spectrum was fitted using a least squares method searching on the relative partial widths and gridding on the total width.

An example of such a fit is shown in Fig. 5. Although the total width is not well determined by the fitting procedure, a smaller χ^2 is ob-

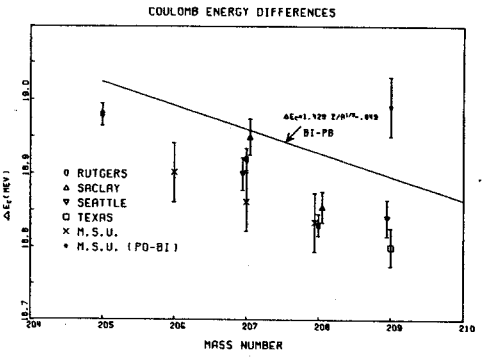

Figure 1

tained for total widths near 380 keV rather than the value of 22 keV obtained from resonance measurements.[1] However the partial widths extracted are relatively stable for a range of total widths. These calculations are still proceeding and the indications are that the earlier measurements did indeed give too low a value for the $f_{5/2}$ decay width although reasonable agreement is obtained with more recent measurements.

References

1. G.H. Leng and G.M. Temmer, Phys. Letters 24B, 370(1967) and B.L. Anderson, J.P. Bondorf, and B.S. Madsen, Phys. Letters 22, 651(1966).
2. G.J. Igo, C.A. Whitten, Jr., Lean-Luc Perreuoud, J.W. Verba, T.J. Woods, J.C. Young, and L. Welch, Phys. Rev. Letters 22, 724(1969).
3. G.M. Crawley, W. Benenson, P.S. Miller, D.L. Bayer, R. St.Onge, and A. Kromminga, Phys. Rev. 2, 1071(1970).
4. J.D. Fox, and D.D. Long, FSU preprint 1969 and D.D. Long, P. Richard, C.F. Moore and J.D. Fox, Phys. Rev. 149, 906(1966).
5. P.S. Miller, Ph.D. Thesis, Princeton University 1968 (unpublished), P.S. Miller and G.T. Garvey, Nucl. Phys. A163, 65(1971).

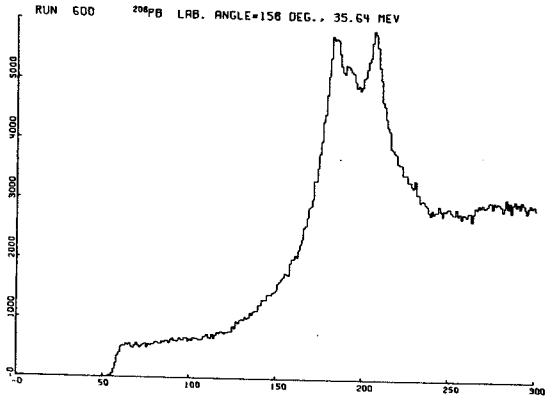

Figure 2

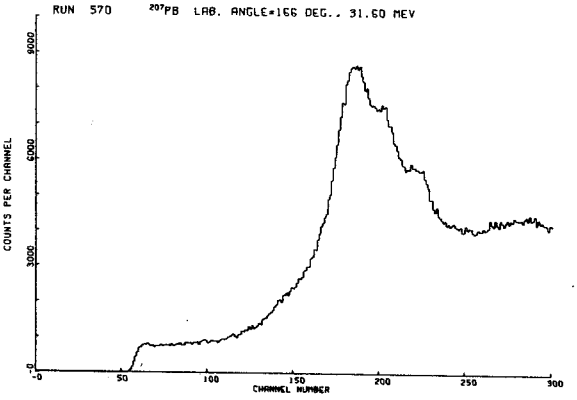

Figure 3

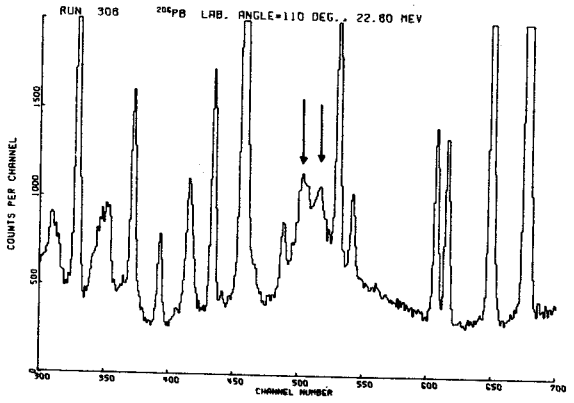

Figure 4

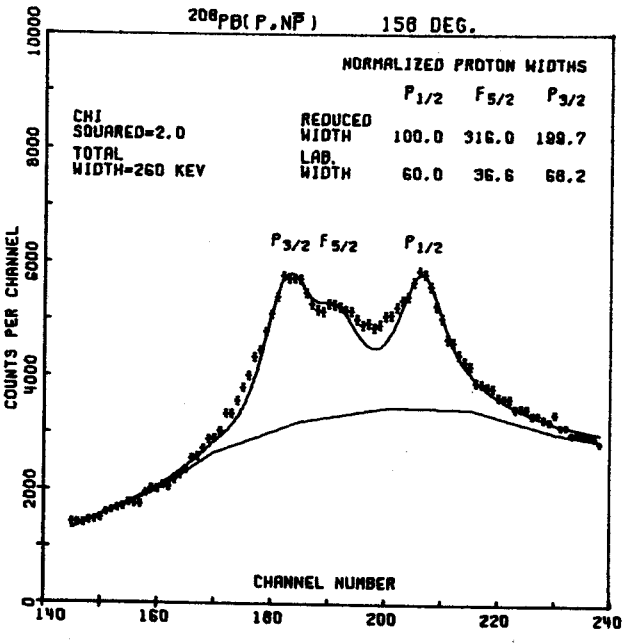

Figure 5

PROTON SPIN-FLIP

R.H. Howell and A.I. Galonsky

Experiments are being conducted to measure the proton spin-flip in inelastic scattering using the (p,p'γ) coincidence technique. Measurements have recently been completed for the following reactions.

	Ep	Ex	J^π
$^{120}Sn(p,p'\gamma)^{120}Sn^*$	30 MeV	1.17 MeV	2^+
$^{124}Sn(p,p'\gamma)^{124}Sn^*$	30 MeV	1.13 MeV	2^+

The scattering chamber has been described.[1] A new lead shield with motor drive has been added to the gamma-ray detector assembly.

Targets were isotopically enriched foils of 5 mg/cm^2 for ^{124}Sn and 10 mg/cm^2 for ^{120}Sn. Detectors were a 2 inch diameter by 3 inch long NaI(Tl) gamma-ray detector and a cooled 500mm^{2}x5mm Si(Li) particle detector.

An electronics system was developed to collect coincidence events as a 2-dimensional function of proton energy and gamma-ray pulse height.

The data are seen in Figs. 1 and 2 . Finite solid angle corrections were calculated as a function of proton scattering angle and relative substate populations with a published formula.[2]

Optical Model parameters for all DWA calculations were taken from Becchetti and Greenlees.[3]

Collective-model DWA calculations were performed here with the code written by H. Sherif at the University of Washington. This code included the deformed spin-orbit part of the optical potential in the full Thomas form.[4] Varying the strength of the spin-orbit deformation effected the spin-flip fits slightly and produced much better fits to published asymmetry data.[5] (See Fig. 3.)

Microscopic DWA calculations were preformed with the real, central Kallio-Kolltveit interaction and the quasi-particle wave function of Clement and Baranger.[6] Fits to the spin-flip were acceptable but fits to the asymmetry were not as good as in the collective case (see Fig. 4). Addition of the imaginary part of the collective model improves the asymmetry fit while having little effect on the spin-flip fits. Addition of the imgainary term also showed improvement to the fits to the cross section (see Fig. 5).

REFERENCES

1. J.J. Kolata and A. Galonsky, Phys. Rev. 182, 1073(1969).
2. H.H. Hippelein, R. Jahr, J.A.H. Pfleger, F. Rott, and H.M. Vieth, Nucl. Phys. A142, 369(1970).
3. E.D. Becchetti and G.W. Greenlees, Phys. Rev. 182, 1190(1969).
4. H. Sherif and J.S. Blair, Phys. Letters 26B, 489(1968); H. Sherif, Thesis, Univ. of Washington, 1968 (unpublished).
5. O. Karban, P.D. Greaves, V. Hnizdo, J. Lowe, and G.W. Greenlees, Nucl. Phys. A147, 461 (1970).
6. D.M. Clement and E.U. Baranger, Nucl. Phys. A120, (1968) and private communication.

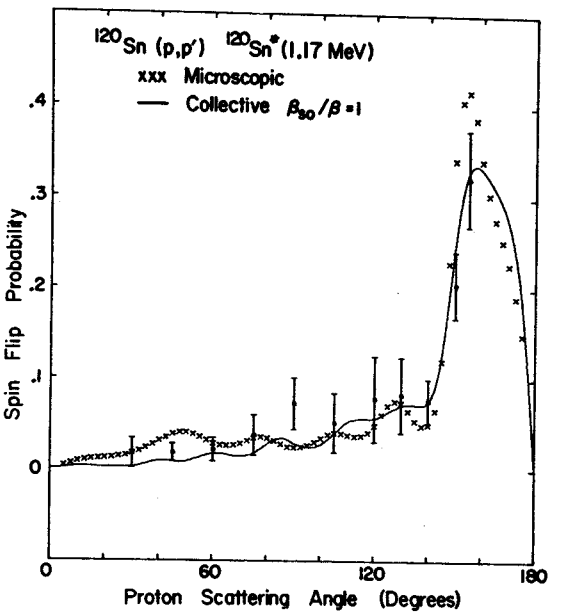

Fig. 1 Spin-flip probability for ^{124}Sn. The data have been corrected for the use of finite detector apertures. The curves are the collective model with a full Thomas term (solid line) and the microscopic model with the KK force (x's).

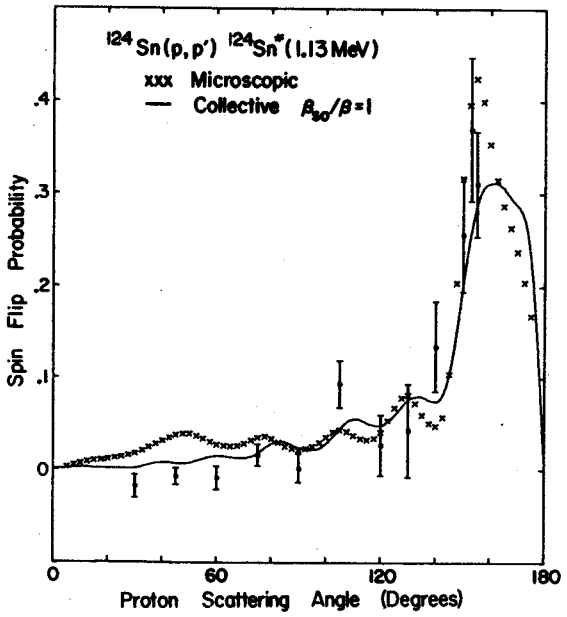

Fig. 2 Spin-flip probability for Sn. The correction for finite detector apertures reduces the values of the data at forward angles. The curves are the collective model with a full Thomas term (solid line) and the microscopic model with the KK force (x's).

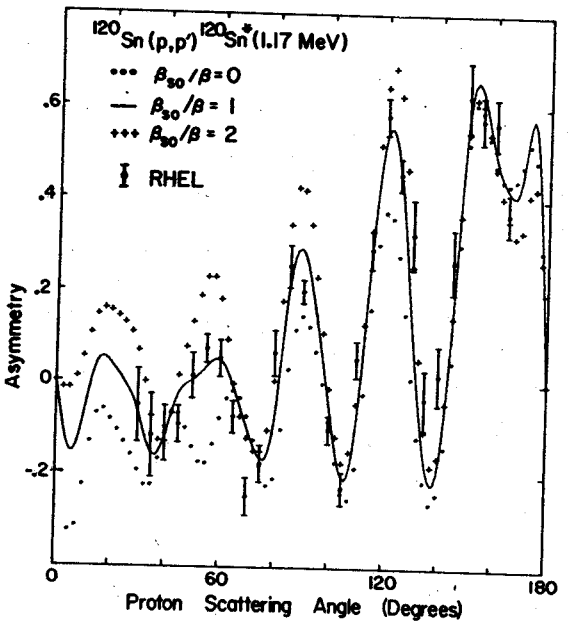

Fig. 3 Collective model calculations of the asymmetry with the full Thomas term. Increasing the strength of the spin orbit deformation from 0 to 2 has the greatest effect at forward angles where the central collective model is in least agreement with the data.

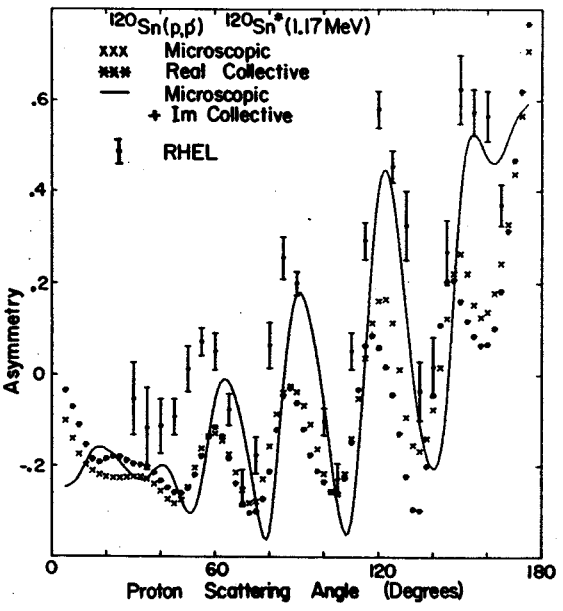

Fig. 4 The fits to the asymmetry with the real microscopic force (x's) and real part of the collective model (star's) are degraded at all angles. Adding an imaginary part to the microscopic form factor (solid line) improves the fit over most of the angular range.

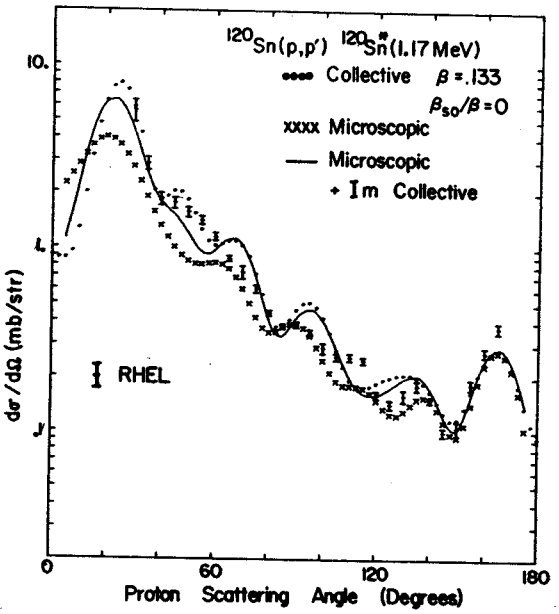

Fig. 5 Adding an imaginary part to the real microscopic form factor (solid line) improves the fit to the cross-section over that of the real microscopic form factor alone (x's). The complex collective model (dots) without spin orbit deformation also fits the data well.

Study of the Asymmetry Potential by (p,n) Quasi-Elastic Scattering

R.K. Jolly, T. Amos, A. Galonsky, and R. St. Onge

The proton-nucleus potential is more strongly attractive than the neutron-nucleus potential. This "asymmetry effect" can be described by a term in the scattering potential proportional to $\frac{N-Z}{A}$ or, alternatively, by one proportional to $\frac{\vec{t}\cdot\vec{T}}{A}$, where $\vec{t}$ and $\vec{T}$ are the nucleon and nucleus isospin vectors, respectively. Attempts to determine both the shape and strength of the asymmetry potential by systematic analysis of nucleon scattering data have not producted entirely conclusive results, the basic reason being that the asymmetry potential is a small part of the total potential responsible for scattering.

In (p,n) reactions between analogue states, however, the asymmetry potential is the entire potential responsible for the transition. To begin our study we have measured (p,n) angular distributions on aluminum with protons of 22, 30 and 40 MeV. In this case the analogue transition leads to the ground state of the residual nucleus, ^{27}Si. The data are shown in the figure along with DWBA fits computed with the code JULIE using a derivative surface form factor and optical model parameters of Perey[1] (22 and 30 MeV) and of Fricke and Satchler[2] (40 MeV). A pure volume interaction does not give a good fit at any of the three energies.

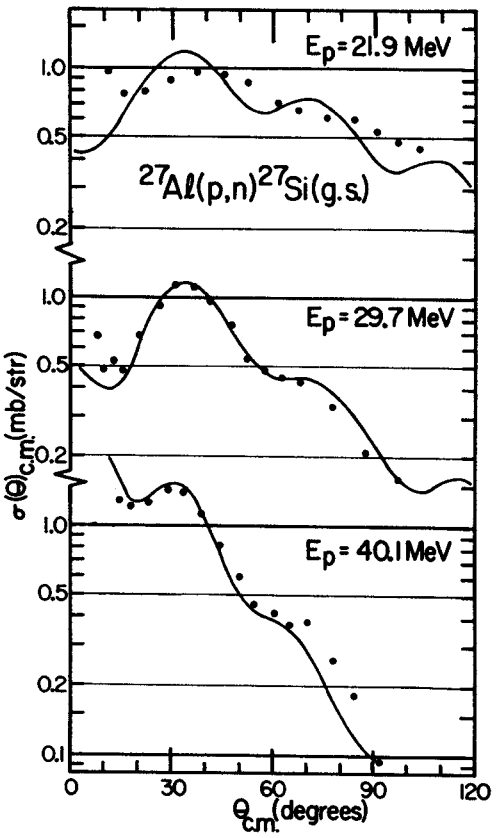

The eyeball normalizations in the figure of theory to experiment are for strengths of the surface interaction V_1' given in the table below. The asymmetry potential most commonly used in elastic scattering analyses has a volume shape with a depth $V_1 \simeq 27$ MeV. From the VR^n ambiguity in elastic scattering, we can relate an effective volume strength, V_1(eff), to our surface strengths through the relation $V_1(\text{eff}) = \frac{na}{R} V_1'$. The values of V_1(eff) in the table are for n=2.

Ep	V_1'	V_1(eff)
22	80	28
30	67	23
40	71	28

All values in MeV.

References

1. F.G. Perey, Phys. Rev. 131, 745(1963).
2. M.P. Fricke and G.R. Satchler, Phys. Rev. 139, B567(1965).

The Ghost Anomaly in the $^{9}Be(p,d)^{8}Be$ Reaction

P.S. Miller, G.M. Crawley, W.F. Steele, and F.C. Barker*

A ghost anomaly is a distortion of the line profile of a nuclear level caused by the occurrence of a breakup threshold near the energy of the level. The ground state of ^{8}Be, which has a measured decay width in the range 6 to 8 eV, possesses an interesting ghost because the state lies just 92 keV above the α-α breakup threshold. The spectrum of deuterons from the $^{9}Be(p,d)^{8}Be$ reaction in Fig. 1 shows this ghost which is the broad group extending from near the ground state to beyond 2 MeV excitation energy. This anomaly is a feature of the ground state line shape, so it cannot vary with respect to the main peak except in so far as the line shape may be further distorted by interference from other 0^{+} states. The ghost can be calculated by a reaction theory, such as R-matrix theory, which includes the effects of the barrier and the interference of several levels on the line shape of the ground state.[1] The ghost line shape can help to constain the R-matrix parameters for the 0^{+} states used to fit α-α scattering phase shifts. The ghost is especially sensitive to the channel radius a_{o}, whose value is ambiguous in the fits to scattering data ($5.5\ fm \leq a_{o} \leq 7.0\ fm$).[2] An earlier measurement of the ghost by the Be(p,d) reaction[3] was done at 5.2 MeV bombarding energy where the compound nucleus contribution to the cross section may not be negligible. This weakened the conclusion that could be drawn because of practical difficulties in the analysis. The ^{8}Be ghost has been investigated recently by several different reactions[4] at low energies, but only a preliminary theoretical analysis has been performed on the data. We are measuring the ghost line shape near 40 MeV bombarding energy where the direct (p,d) amplitude is expected to predominate over compound nucleus.

The deuterons from the natural Be target (thickness 1.8 mg/cm^{2}) enter the Enge split-pole magnetic spectrograph and are detected in the focal plane. Preliminary measurements of the line shape were made with 3cm- and 5cm-long position sensitive solid state detectors, but they required large corrections for efficiency variation and non-linearity of the detector response. In addition the short lengths made splicing together several runs a necessity and introduced normalization difficulties.

Nuclear emulsions were used to obtain the spectrum shown in Fig. 1. Due to the large dynamic range required to see both the ghost and the main peak, three exposures (for approximately 1, 10 and 100 microcoulombs of integrated beam current) were taken and the countable parts of each were scanned. Similar data were recorded at a laboratory angle of 15°.

Recently an experimental position sensitive gas proportional counter has been used successfully at 30 MeV bombarding energy (see Fig. 2). A practical model of this detector is under construction, and we intend to use it shortly to measure angular distributions of the ghost at several energies to try to verify the hypothesis that compound nuclear effects are negligible.

Analysis of the spectra using a 3 level approximation for the 0^{+} and the 2^{+} states will be performed as described elsewhere.[5]

References

1. F.C. Barker and P.B. Treacy, Nucl. Phys. 38, 33(1962).
2. F.C. Barker, H.J. Hay, and P.B. Treacy, Aust. J. Phys. 21, 239(1968).
3. H.J. Hay, E.F. Scarr, D.J. Sullivan, and P.B. Treacy, Aust. J. Phys. 20, 59(1967).
4. E.H. Berkowitz, S.L. Marolt, A.A. Rollefson, C.P. Browne, B.A.P.S. 15, 520(1970), and to be published.
5. P.S. Miller, G.M. Crawley, W.F. Steele, and F.C. Barker, B.A.P.S. 16, 35(1971).

*Australian National University, Canberra, Australia.

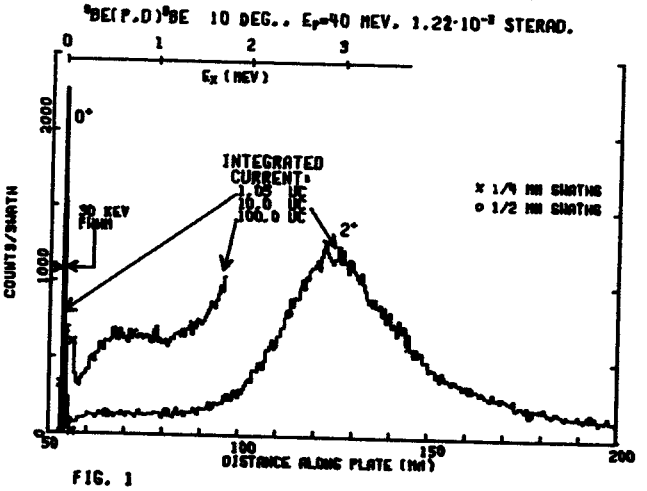

FIG. 1

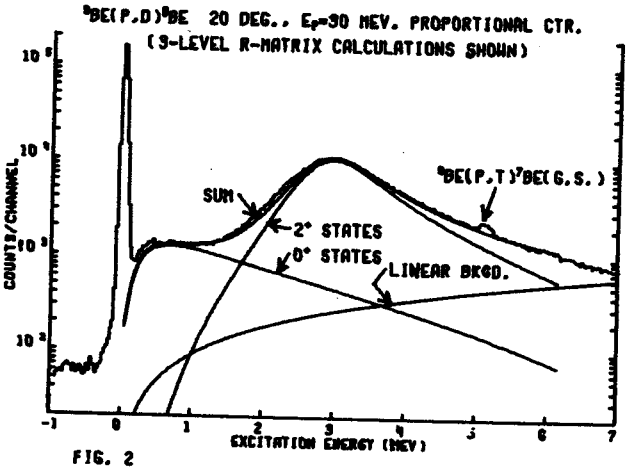

FIG. 2

Studies of Odd-Odd Nuclei in the sd-Shell

J.A. Rice, B.H. Wildenthal, and B.M. Preedom

Examination of the results of recent detailed shell-model theories[1,2] for the nuclei of the sd-shell (A=17-39) shows that nuclei with odd numbers of both neutrons and protons occupy pivotal positions in so far as evaluation of these theories is concerned. We are studying several such nuclei with the (p,d) reaction. Our experimental goals are to resolve and identify as many levels in the residual nuclei as possible and assign accurate excitation energies to them, and to measure the (p,d) angular distributions to very small angles so as to allow an unambiguous extraction of both ℓ=0 and ℓ=2 spectroscopic factors. The experiments are carried out with photographic plates and the split-pole spectrograph. Bombarding proton energies are 35 MeV. Targets of $Na^{35}Cl$, $Li^{35}Cl$, ^{23}Na, $Na^{37}Cl$, and ^{34}S have been studied to date. Plate scanning and analysis of the energy level spectra have been completed for the Na and ^{35}Cl target data and DWBA analysis of these angular distributions is in progress. Representative spectra are shown in Fig. 1. The FWHM energy resolution for these data is approximately 14 keV. The energy levels we identify in ^{34}Cl and ^{22}Na are listed in Tables I and II, along with the results of gamma-ray and other charged particle studies. Our excitation energy assignments are obtained by making a small correction to our absolute momentum vs. focal plane position calibration in order to produce an rms best fit to the set of ±1 keV energy assignments available from Ge(Li) gamma-ray detector studies. We find that in order to simultaneously fit both the ^{22}Na and ^{34}Cl energies we must use a value $Q[^{23}Na(p,d)^{22}Na]-Q[^{35}Cl(p,d)^{34}Cl] = +229$ keV rather than the value +218±9 keV in the literature.[3,4]

Table I

Energy Levels in ^{34}Cl

E_x^a(MeV)	E_x^b(MeV)	E_x^c(MeV)
0.000	0.000	0.000
0.147	0.146	0.147
0.462	0.461	0.461
0.667	0.666	0.666
1.232	1.230	1.229
1.886	1.888	1.886
		1.924
2.156	2.158	2.157
2.178	2.181	
2.374	2.377	
2.578		2.579
2.609	2.611	2.608
2.720	2.722	2.720
3.127		3.126
3.333		3.332
3.382		3.381
3.543	3.545	3.544
	3.601	
3.632	3.632	3.630
	3.771	3.771
3.860		
3.942		
3.965		
3.983	3.982	3.982
4.079	4.075	4.075
	4.137	4.143
4.149		
4.219		
4.331		
	4.353	4.352
	4.416	4.416
4.447		
4.467		
	4.514	4.514
4.612		4.605
4.641	4.639	4.636
4.719		

References

1. E.C. Halbert, J.B. McGrory, B.H. Wildenthal, and S.P. Pandya, Advances in Nuclear Physics, Vol. 4.
2. B.H. Wildenthal, E.C. Halbert, J.B. McGrory, and T.T.S. Kuo, to be published in Physical Review.
3. C. Maples, G.W. Goth, and J. Cerny, Nuclear Reaction Q-Values, Lawrence Radiation Laboratory, Berkeley, California, 1966.
4. J.H.E. Mattauch, W. Thiele, and A.H. Wapstra, Nuclear Physics 67, 32(1965).

Table II

Energy Levels in ^{22}Na

E_x^a(MeV)	E_x^d(MeV)	E_x^e(MeV)
0.000	0.000	
0.583	0.583	
0.657	0.657	
0.891	0.891	
1.529	1.528	
	1.937	
1.950	1.952	
1.983	1.984	
2.210	2.211	
2.569	2.572	
2.968	2.969	
3.057	3.059	
3.518	3.521	
3.708	3.708	
3.943	3.944	
4.071	4.069	
4.295	4.294	
4.321	4.319	
4.361	4.360	
	4.466	
	4.522	
4.585	4.583	
4.625	4.622	
4.707	4.708	
4.773	4.770	
5.062	5.061	
5.100	5.099	
	5.117	
5.129		
5.173	5.165	
5.321	5.317	
5.441	5.446	5.440
5.606	5.605	5.605
5.726	5.734	
5.754	5.745	
	5.837	5.803
5.868	5.871	5.858
	5.938	
5.925	5.953	
5.964		
5.998	5.988	5.995
6.089	6.089	6.088
6.183	6.190	6.185
6.245	6.241	6.247
6.329	6.329	6.326
6.436	6.435	

Table I Con't.

E_x^a(MeV)	E_x^b(MeV)	E_x^c(MeV)
4.860		
4.943		
4.963		
4.975		
5.005		
5.118		
5.186		
5.339		
5.368		
5.452		
5.560		
5.583		
5.614		
5.643		
5.760		
5.873		
5.948		
5.984		
6.057		
	6.167	
6.187		
	6.206	
6.228	6.226	
6.279		
6.372		

[a] Present work (±1 keV/MeV)

[b] A.K. Hyder, Jr. and Gale I. Harris, to be published. (±1 keV)

[c] J.R. Erskine, D.J. Crozier, J.P. Schiffer, and W.P. Alford, Phys. Rev. 3C, 1976(1971).

Table II cont.

E_x^a(MeV)	E_x^d(MeV)	E_x^e(MeV)
	6.450	
6.534	6.528	6.521
6.569	6.556	6.557
	6.591	6.582
	6.640	
6.670	6.671	6.664
6.722	6.713	6.715

[a] Present work (±1 keV/MeV)

[d] Olness, Harris, Paul, Warburton, Phys. 1c, 958(1970). for levels below 5.2 MeV (±0.5 keV/MeV) and Hinds, Marchant and Middleton, Nucl. Phys. 51, 427(1964) for levels above 5.2 MeV (±10-15 keV).

[e] J.D. Garrett, Ph.D. Dissertation, University of Pennsylvania, (1970) (±4 keV).

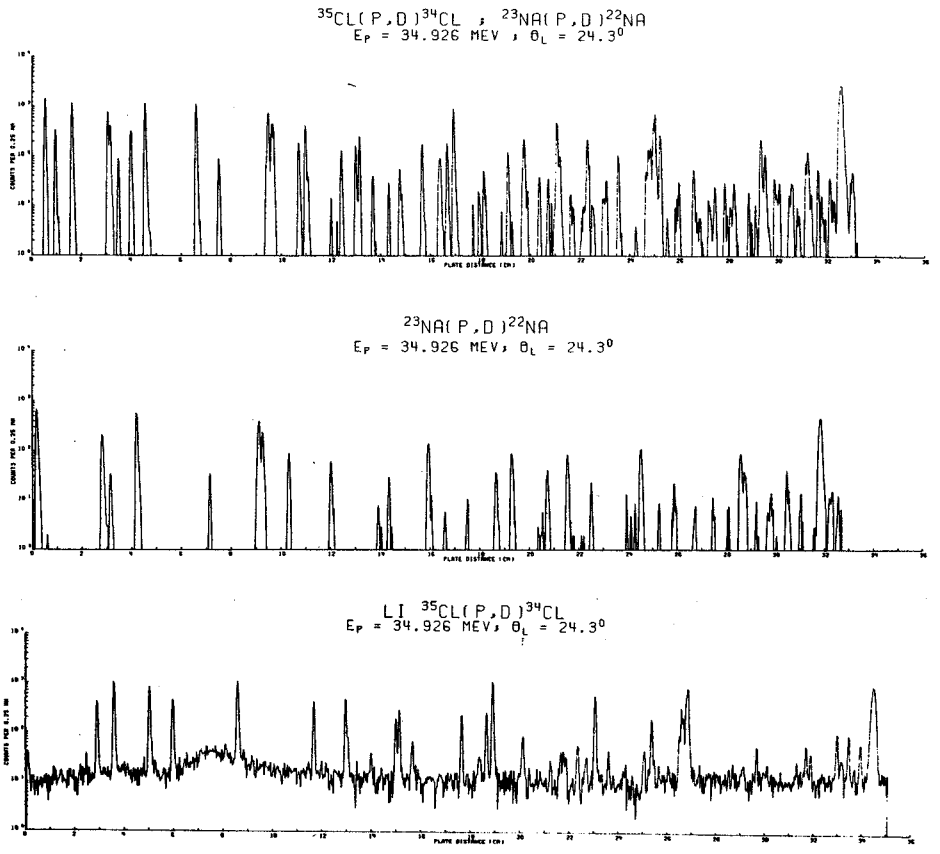

The $^{48}Ca(p,t)^{46}Ca$ Reaction at 39 MeV

G.M. Crawley, P.S. Miller and G. Igo*

This reaction has been investigated by a number of authors[1-3] but the previous work has suffered from either a lack of good energy resolution or too low a bombarding energy. Both of these difficulties can be overcome using the Enge spectrometer with the MSU Cyclotron. One of the major aims in such an experiment is to obtain accurate cross sections for various 0^+ states excited in this reaction since this serves as a good test of shell-model configurations in the Ca isotopes. Since there have also been some careful (t,p) studies[4,5] populating the same states from ^{44}Ca, a complete comparison of all the 0^+ states populated by these two reactions serves as an even more stringent constraint on both the reaction theory are the nuclear wave functions used. Unfortunately the previous (p,t) studies have only been able to observe the first excited 0^+ state at 2.43 MeV and have not been able to make comparisons with the remaining four 0^+ states observed in the (t,p) reaction.

Preliminary data have been obtained at three laboratory angles 20°, 24°, 28° for this experiment using a beam of 39 MeV protons from the MSU Cyclotron. The proton energy has chosen so that the maximum energy tritons were obtained which could be bent by the Enge spectrometer. A thin ^{48}Ca isotopically enriched target (60 μgm/cm² 96% enriched), evaporated onto a carbon backing and transferred under a vacuum, was used in the preliminary run. The 28° triton plate is the only one scanned yet, and this spectrum is shown below. The energy resolution is approximately 11 keV FWHM and the initial indication is that at least some single states are resolvable up to 7.5 MeV. Since the speculator system[6] was used with the ground state peak, this peak does not appear in the spectrum on the plates.

All of the states seen in the previous (t,p) and (p,t) experiments are also observed here although states at 4.29, 4.99, 5.64, and 5.85 MeV are very weakly excited. One state which was seen in a (p,p') experiment[7] at 3.780 MeV is completely missing in our data and in fact has not been observed in any other experiment. However we do observe about 10 or 12 new states up to 6 MeV excitation including what appear to close doublets at 4.43, 4.47, 4.78, 4.80, and 5.93, 5.94 MeV where for the 1st two cases the higher energy number is weakly excited. In addition new states are observed at 4.01, 4.52, 5.03, 5.09, 5.26, 5.47, 5.49, 5.79 MeV although it should be remembered that some of these may be impurity peaks which will become distinguishable when spectra at other angles are compared.

It is also interesting to note that the strong excitation of the first 4^+ and 6^+ states at 2.58 and 2.98 MeV which one might class mainly as members of the $(\nu_{f7/2}^{-1})^2$ configuration. At 20 MeV these are much weaker than the first 2^+ state but at 39 MeV all three states are of comparable strength at this angle (which should probably enhance the lower J states). Similarly the 3^- and 5^- states at 3.61 and 4.75 MeV are in the ratio 1:3 at 39 MeV whereas at 20 MeV the ratio was closer to 3:1.

The six 0^+ states observed in $(t,p)^4$ are all observed at approximately the same energy in this experiment the main difficulty being with the state observed in (t,p) at 5.628 MeV, where only a weak peak is seen in the (p,t) reaction at about 5.64 MeV. The intensities of these 0^+ states, relative to the 1st excited 0^+ at 2.43 MeV are shown in Table 1, although these numbers should be treated with great caution since they are only derived from one spectrum.

Further experiments and analysis on this reaction are being carried out.

Table 1

Relative Strengths of 0^+ States in ^{46}Ca, Normalized to 0^+ State at 2.43 MeV

(Energy (MeV))	Relative Strength at 28° Lab
2.43	10.0
5.29	2.5
5.59	5.0
5.64	0.3
6.05	4.5

References

1. R. J. Peterson, Phys. Rev. 170, 1003(1968).
2. Y. Dupont, P. Martin and M. Chambre, Phys. Letters 31B, 68(1970).
3. H. Hefele, U. Lynen and R. Santo, Nucl. Phys. A157, 93(1970).
4. D.C. Williams, J.D. Knight and W.T. Leland, Phys. Rev. 164, 1419(1969).
5. J.H. Bjerregaard, O. Hansen, O. Nathan, R. Chapman, S. Hinds and R. Middleton, Nucl. Phys. A103, 33(1967).
6. H.G. Blosser, G.M. Crawley, R. deForest, E. Kashy, and B.H. Wildenthal, Nucl. Instr. and Methods 91, 61(1971).
7. T.A. Belote, J.H. Bjerregaard, O. Hansen and G.R. Satchler, Phys. Rev. 138, B1067(1965).

*Univ. of California, Los Angeles, California.

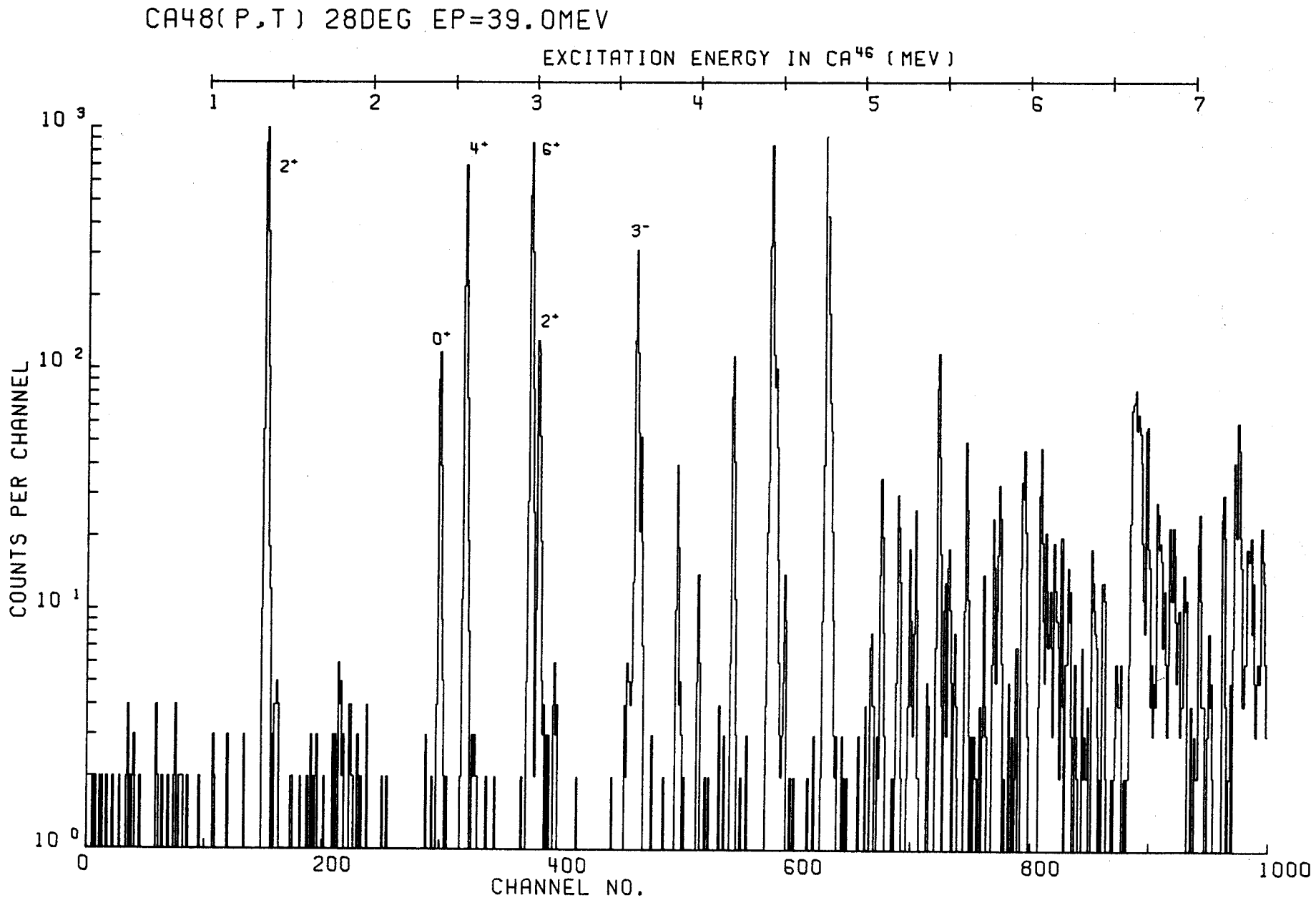
CA48(P,T) 28DEG EP=39.0MEV
EXCITATION ENERGY IN CA46 (MEV)
1
2
3
4
5
6
7
10 3
10 2
10 1
10 0
COUNTS PER CHANNEL
2+
0+
4+
6+
2+
3-
0
200
400
600
800
1000
CHANNEL NO.

Direct (p,α) Reactions

Jerry Nolen and Paul Zemany

We have recently begun to use the direct (p,α) reaction to obtain nuclear structure information about several nuclei. Very few angular distributions have yet been measured, but preliminary data indicate this promises to be a very useful nuclear probe.

The data are being recorded on nuclear emulsions with the dispersion-matching technique in the Enge-split-pole magnetic spectrograph. The resolution is partially limited by target thickness due to the relatively low cross-sections for many of the energy levels of interest. However, typical data recorded at a proton energy of 30 to 35 MeV has about 15 keV (1/2 mm) FWHM resolution.

The reactions currently being studied are ^{46}Ti(p,α)^{43}Sc and ^{44}Ca(p,α)^{41}K. In both of these cases one primary interest is in determing to what extent the high spin states are populated. A $15/2^+$ state from the configuration $(\pi d_{3/2}^{-1})(\nu f_{7/2}^{2})$ is expected around 4 MeV excitation in ^{41}K, this would be populated via L=8 angular momentum transfer in this reaction. Similarly, the $19/2^-$ state from the $(f_{7/2}^{3})$ configuration in ^{43}Sc has recently been located by the Stockholm group as a short-lived isomer at 3.123 MeV excitation energy. Shell-model selection rules generally inhibit the population of these seniority three high spin states in one and two nucleon direct transfer reactions, but allow them to be populated in three nucleon transfer. Preliminary DWBA calculations also indicate that the (p,α) reaction is not restricted kinematically from a wide range of angular momentum transfer, i.e. it does not enhance particular L-values to a large extent. Thus it is hoped these "extended" shell-model configurations can be located and identified with the (p,α) reaction. If so, the resulting information on these states will provide valuable new tests of shell-model calculations.

A sample spectrum of the ^{46}Ti(p,α)^{43}Sc reaction is given in the figure. It is clear that many states of the $f_{7/2}^{3}$ as well as states involving s-d proton holes are strongly populated. Since this scattering angle was small the lower spin states are emphasized in this spectrum. It had been previously inferrred from their low yields in proton stripping reactions as well as life-time work that the low-lying $3/2^+$ and $1/2^+$ states in ^{43}Sc were dominately proton hole states. Their strong yields in the (p,α) pickup reaction confirm this interpretation. The energy levels indicated on the figure are largely from particle-gamma and gamma-gamma correlation work. The (p,α) data will help to clear up many of the existing ambiguiities in spin and configuration assignments.

The preliminary angular distributions for the ^{44}Ca(p,α) reaction to the low-lying levels of ^{41}K indicate some probable new spin assignments. For example, the doublet at 1.560-1.582 MeV was well resolved with the lower member having an L=2 shape and the upper an L=0 shape. Thus the probable spin assignments are 1.560 MeV $(3/2,5/2^+)$ and 1.582 MeV $(1/2^+)$.

An example of the difference between (p,α) and (d,^{3}He) reaction is indicated by the different relative yields to states of the same spin. The (d,^{3}He) reaction essentially measures the relative amounts of $2s_{1/2}$ proton hole configuration in these two $1/2^+$ states of ^{41}K. However, in the (p,α) reaction coherence between the simple proton hole components and seniority three components can greatly change the relative yields. Thus the two reactions yield complementary information about the wave functions.

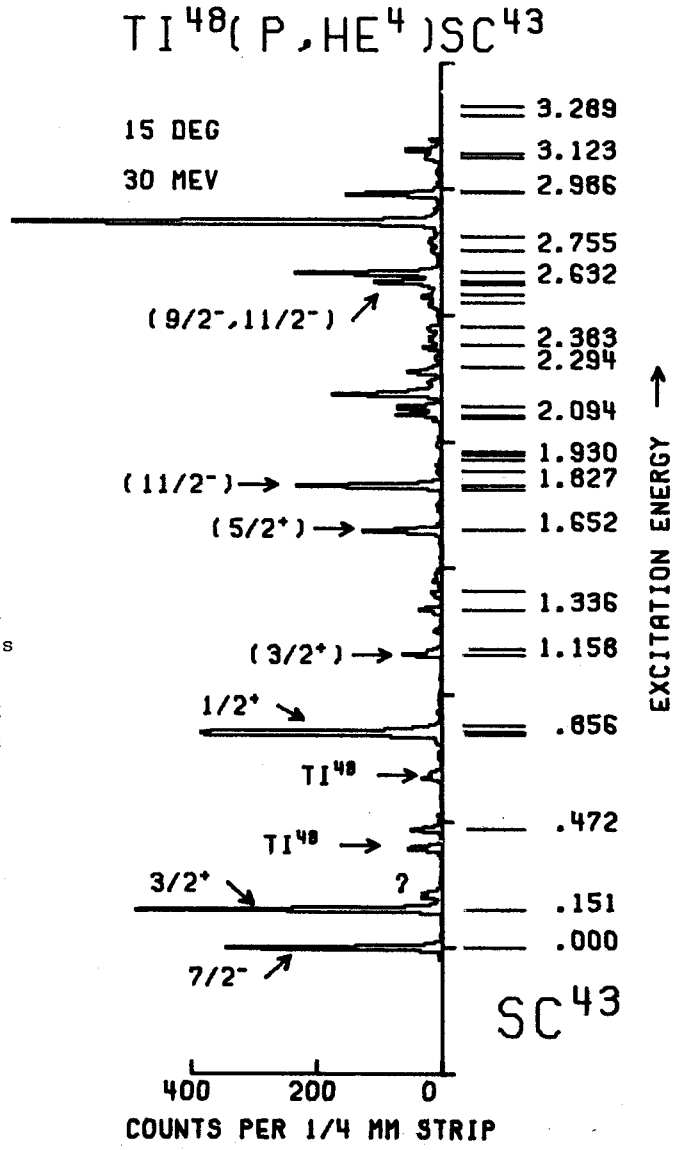

70 MeV ^{3}He Elastic Scattering

R.R. Doering, R.A. Hinrichs, and A. Galonsky

We have begun an investigation of ^{3}He elastic scattering from $f_{7/2}$-shell nuclei at 70 MeV. Thus far we have bombarded ^{51}V, ^{50}Ti, and ^{46}Ti targets. The positive Q-values (~10 MeV) of the (^{3}He,^{4}He) reactions on these nuclei necessitate the use of particle identification. Thus, with E-ΔE detector telescopes we have also collected data on the associated neutron pickup and inelastic scattering reactions. Preliminary elastic angular distributions for ^{51}V and ^{50}Ti are presented in Fig. 1. We are currently in the process of extracting final angular distributions for as many of the aforementioned reactions as our resolution will allow.

The dominant feature of the ^{50}Ti and ^{51}V elastic scattering cross-sections is a dramatic drop-off with increasing angle. From 5° to 140° they span about ten orders of magnitude, which is a source of major experimental difficulties. To measure the small cross-sections, we used "thick" (>1 mg/cm^2) targets, large solid angles, and minimal beam energy selection. These factors coupled to give $\gtrsim$150 keV FWHM resolution. Thus we do not expect to analyze more than a few of the low-lying excited states.

The principal objective of this study is to extend the optical model to 70 MeV for ^{3}He scattering. A secondary interest has been to obtain further information relevant to the question of the necessity for target-spin dependent terms in the optical model potential, such as: $\vec{\ell}\cdot\vec{I}\ U_1(r)$ and/or $\vec{\sigma}\cdot\vec{I}\ U_2(r)$. We have employed the optical model code GIBELUMP to search for parameters yielding reasonable fits to our preliminary ^{51}V and ^{50}Ti angular distributions. The parameters obtained differ little from the starting sets, which were found at 30-37 MeV by Gibson[1] and by Luetzelschwab and Hafele[2] for various $f_{7/2}$-shell nuclei. In particular, the discrete ambiguity in the strength of the real potential is still present. Of the various parameter families giving reasonable fits, the one with $V \gtrsim 110$ has the least χ^2, especially if large angle data are included (Fig. 2a). In general, the back angle cross-sections were difficult to fit. However, significant improvements resulted from including a spin-orbit potential of about 2-3 MeV (Fig. 2b) and using a surface rather than volume form of the imaginary potential. Some of the best fits were obtained with the parameter sets listed in the table.

At Oak Ridge Hafele and Fulmer have done similar studies with 50 MeV helions scattering from ^{59}Co and ^{60}Ni.[3] They interpret an observed damping of the ^{59}Co elastic angular distribution oscillations with respect to those of ^{60}Ni beyond 70° as evidence for including a target-spin dependent term in the optical model potential. We chose ^{51}V and ^{50}Ti as our initial targets because they are another pair of neighboring nuclei with the same spins as ^{59}Co and ^{60}Ni ($7/2^-$ and 0^+, respectively). However, we have not observed a similar damping of back angle cross-section oscillations for ^{51}V with respect to ^{50}Ti. In fact the data for both nuclei are strikingly similar (Fig. 1). Two possible explanations of this result have been suggested. Hafele and Fulmer also have a ^{60}Ni angular distribution at 71 MeV which is much smoother beyond 70° than the one at 50 MeV.[4] Thus, it may be that the target-spin effect is more pronounced at 50 MeV. The other obvious difference between our experiments is the choice of targets. Perhaps ^{60}Ni is "anomalously spherical" for its neighborhood of the nuclide spectrum and yields larger elastic scattering oscillations than ^{59}Co due to a smaller diffuseness rather than greater target-spin forces. To explore these possibilities, we have decided to include ^{58}Ni, ^{59}Co, and ^{60}Ni in our next series of targets.

References

1. E.F. Gibson, et al., Phys. Rev. 155, 1194(1967).
2. J.W. Luetzelschwab and J.C. Hafele, Phys. Rev. 180, 1023(1969).
3. J.C. Hafele, C.B. Fulmer, and F.G. Kingston, Phys. Letters 31B, 17(1970).
4. C.B. Fulmer and J.C. Hafele, ORNL-4649, 48(1970).

OPTICAL MODEL PARAMETERS - 70 MEV

	V	R_0	A	W_D	R_I	A_I	V_{SO}	CHISQ
^{51}V	155.0	1.24	.621	26.1	1.16	.805	2.9	130
	102.1	1.24	.715	18.9	1.24	.830	1.6	55
^{50}TI	158.3	1.24	.641	25.1	1.13	.860	1.3	33
	157.1	1.24	.628	28.1S	1.43	.891	0.7	70
^{50}TI	106.7	1.24	.739	20.0	1.29	.765	2.4	27
	107.0	1.24	.742	20.2	1.31	.744	0.0	31
	30 MEV ^{51}V (LUETZELSCHWAB, HAFELE)							
	156.5	1.24	.639	23.7	1.04	.934	3.2	29

Note: All parameter sets shown are with a surface form of the imaginary potential except the one labelled S, which is spherical. The set at 30 MeV was obtained from our fit to the data of Luetzelschwab (Ref. 2).

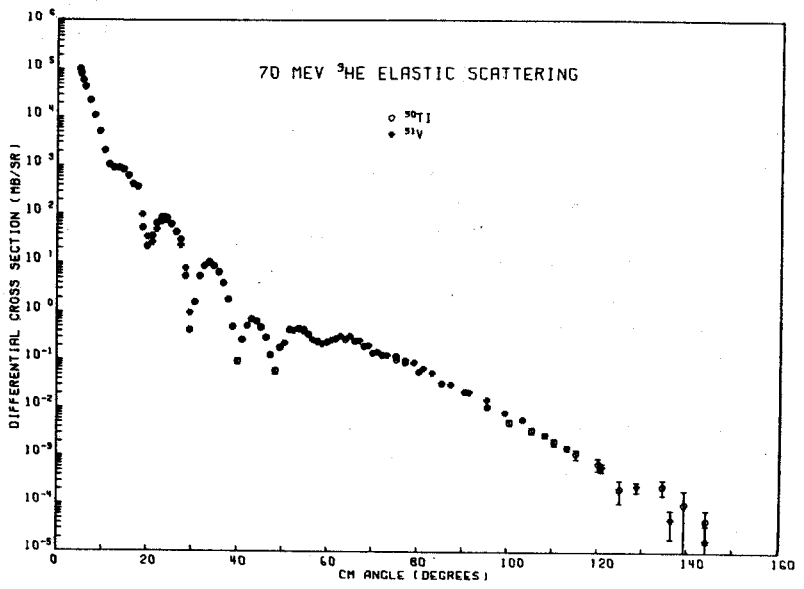

Fig. 1 Comparison of ^{3}He elastic scattering from ^{50}Ti and ^{51}V at 70 MeV.

Fig. 2 Optical Model Calculations

(a) Fits to ^{51}V elastic scattering from different real well depths. Only the real well radius was held fixed in the search. Final parameters for the fits shown are given in the table.

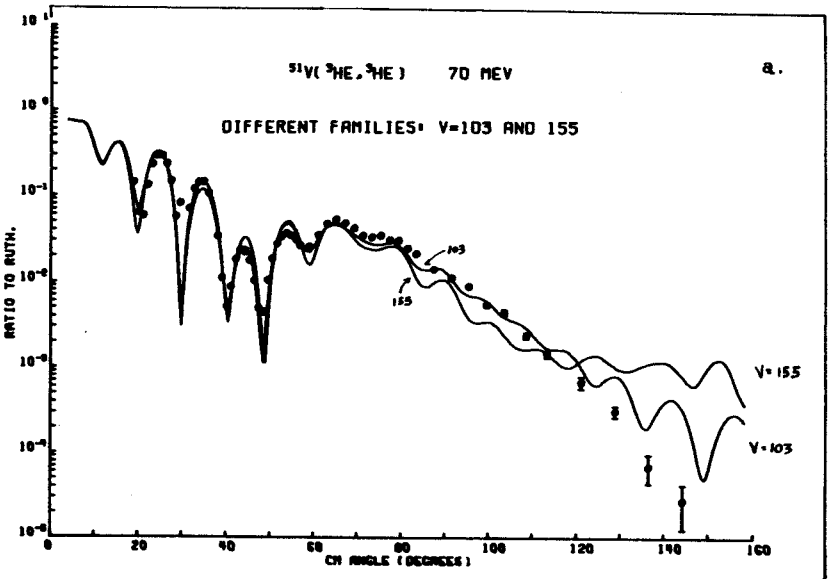

(b) Fits to ^{50}Ti elastic scattering with and without a spin-orbit potential. Starting parameter sets were otherwise the same. Only the real well radius was held fixed. Final parameters for the fits shown are given in the table.

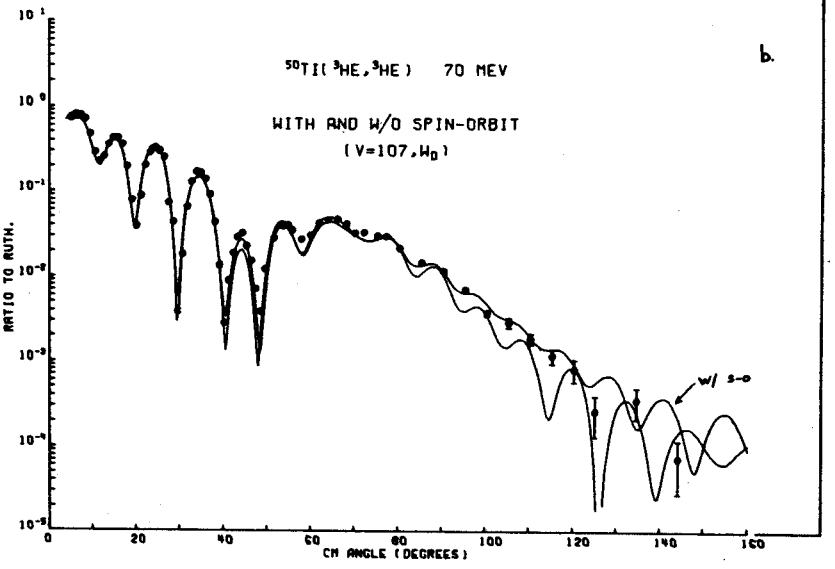

Reaction Mechanism and Spectroscopic Studies with the (^{3}He,t) Reaction

The (^{3}He,t) charge exchange reaction has served in recent years as a valuable spectroscopic tool in determining spins and parities of states in many odd-odd nuclei. The density of levels in such nuclei and the low cross-sections encountered have not deterred experimentalists from making many measurements. As in other types of reactions the hope is that the level spins (or at least the angular momentum transfer) can be determined by the shapes of the angular distributions. In most instances for (^{3}He,t) this has been the case,[1] although, as brought out by work here in the past year, there are some notable exceptions to this surmise, that is, cases have been observed in which standard DWBA descriptions fall short of providing reasonable fits to the data and thus reliable spectroscopic information.

1. Transitions to 0^+ Antianalog States in ^{64,66}Ga and ^{40}K.

R.A. Hinrichs, R. Sherr,* G.M. Crawley, and I. Proctor

The (^{3}He,t) reaction can populate both $T_>$ (analog) and orthogonal $T_<$ states (states of isospin one less than the target) that have the same spin and configuration as the analog state (antianalog states). If spin 0 states are selected for both the initial and final nuclei, then the interaction responsible for the transition, in usual microscopic terminology, is only the pure charge-exchange operator $V_\tau(\vec{t}\cdot\vec{\tau})g(r)$, with the transition proceeding via an L=0 angular momentum transfer. We have studied such 0^+ to 0^+ transitions to analog and antianalog states in ^{40}K and ^{64,66}Ga.[2] The 0^+ $T_<$ states in these nuclei are at 1.64, 0.0, and 0.0 MeV, respectively, and are well determined. Figure 1 shows angular distributions to these states, as well as the 0^+ isobaric analog state. Also shown are macroscopic DWBA calculations. The analog state is fit very well in all cases by an allowed L=0 transfer but the antianalog state is shifted relative to the predicted angular distribution and is fit much better by the L=1 curve. Macroscopic calculations with several sets of optical model parameters, as well as microscopic calculations with different values of the range of the Yukawa interaction, failed to change the general shape of the L=0 curve. The spatial dependence of each excess neutron orbital contributing to the microscopic wave functions was also varied by changing the geometrical well parameters r and a, but the maxima and minima of the angular distributions remained at the same positions. Such observations have led to the conclusion that modifications need to be made in the conventional treatment of (^{3}He,t) reactions. Recent calculations by R. Schaeffer and G. Bertsch seem to show that two-step processes, for example those of the form (^{3}He,α)-(α,t), are responsible for the observed anomalies.

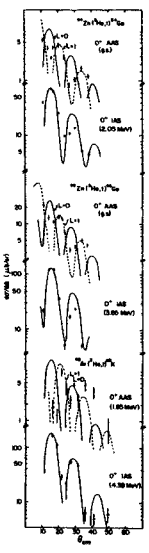

Fig. 1 Angular distributions for (^{3}He,t) transitions to the 0^+ analog (IAS) and anti-analog (AAS) states in ^{64,66}Ga and ^{40}K. The curves are macroscopic DWBA calculations (with the indicated L transfers) and normalized to the data.

2. The Reaction ^{89}Y(^{3}He,t) to $T_<$ States

R.A. Hinrichs and G.F. Trentelman

In continuing the study of (^{3}He,t) reactions to antianalog and other $T_<$ states, the target ^{89}Y was selected.[3] The $1/2^-$(.59 MeV) and $9/2^+$(1.51 MeV) states in ^{89}Zr are antianalog states. Other well-known $T_<$ states nearby can also be observed. The transitions to these antianalog states can be expected to be complicated as more than one L value can contribute and the tensor term in the effective interaction is important. Figure 2 shows angular distributions to the isobaric analog (8.0 MeV) and antianalog (.59 MeV) $1/2^-$ states in ^{89}Zr. The microscopic DWBA calculations shown included a tensor term in the interaction; for the antianalog state they are out of phase with the data (as in the 0^+ to 0^+ transitions), which is fit better by a (macroscopic) L=1 transfer calculation.

Figure 3 shows angular distributions to the $9/2^+$ excited antianalog state at 1.51 MeV and to the $9/2^+$ ground state of ^{89}Zr. The data in both cases is quite similar and shows more forward angle strength than the calculations would allow. The microscopic calculations, which emphasize the higher L transfer (L=5) with the inclusion of the tensor term, peak at a much larger angle than the data, which is fit better by an L=2 (macroscopic) calculation. Because of the similarity of the two $9/2^+$ angular distributions, it appears that the anomaly noted in the last section is not dependent solely upon the uniqueness of the antianalog state. Shifts in the angular distributions for

(^{3}He,t) reactions to $T_<$ states has been noted for other nuclei, especially for transitions involving high L transfers.[4] Our data for other $T_<$ states in ^{89}Zr show some shifts in angle from the calculated shapes, even for lower L transfers, but no trend seems to be apparent for such reactions. It should be noted that there are quite a few cases in which good fits to the data for $T_<$ states do exist. The anomalous effects may thus be configuration dependent and so a determination of final state spins from the (^{3}He,t) reaction, by either a comparison of the experimental shapes with transitions to known states or calculations with the present microscopic interaction, may be misleading. Two-step processes, as mentioned in the last section, may provide a firmer foundation for spectroscopy; however, additional modifications probably have to be added to explain the enhanced forward angle data seen in some of this work.

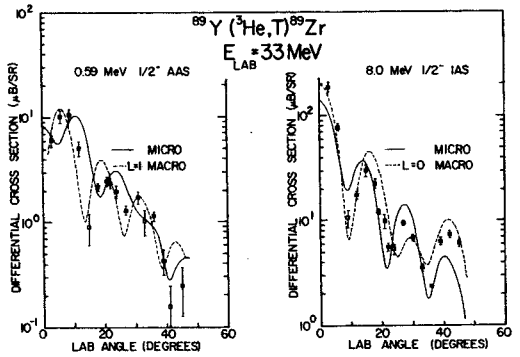

Fig. 2 ^{89}Y(^{3}He,t) angular distributions for transitions to the 1/2⁻ analog (IAS) and anti-analog (AAS) states in ^{89}Zr. The curves are DWBA calculations normalized to the data. The L transfers used in the macroscopic form factor are indicated.

Further studies (on the Sn isotopes) have begun to explore other examples of (^{3}He,t) transitions with large L transfers.

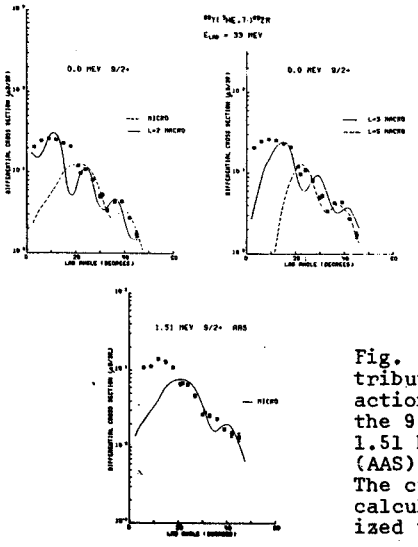

Fig. 3 Angular distributions for the reaction ^{89}Y(^{3}He,t) to the 9/2⁺ ground and 1.51 MeV anti-analog (AAS) states in ^{89}Zr. The curves are DWBA calculations normalized to the data.

3. Spectroscopy of ^{34}Cl via the ^{34}S(^{3}He,t) Reaction

R.A. Hinrichs, B.H. Wildenthal, D. Show, and J.A. Rice.

The level structure of ^{34}Cl has been investigated in a variety of different ways, including the reaction ^{35}Cl(p,d) as found in this report. We have studied the levels of ^{34}Cl below 5 MeV via the (^{3}He,t) reaction on ^{34}S at 35 MeV; this reaction selects proton-particle, neutron-hole excitations of the target ground state. Plates were exposed in the spectrograph and a resolution of 20-30 keV was obtained, with angular distributions taken between lab angles of 3° and 45°. Figure 4 shows the energy levels determined in this experiment for ^{34}Cl. The energies agree quite well with those found in (p,γ)[5] and (^{3}He,d)[6] studies. Previously unindentified states are observed at 4.21 and 5.00 MeV. The determination of the energies of the states above 4.3 MeV has not been completed. The spin assignments listed are those determined by other reactions and confirmed in this (^{3}He,t) study—by comparison with angular distribution shapes for transitions to known levels or by DWBA calculations. If a discrepancy exists in the assignments, the present determinations are underlined.

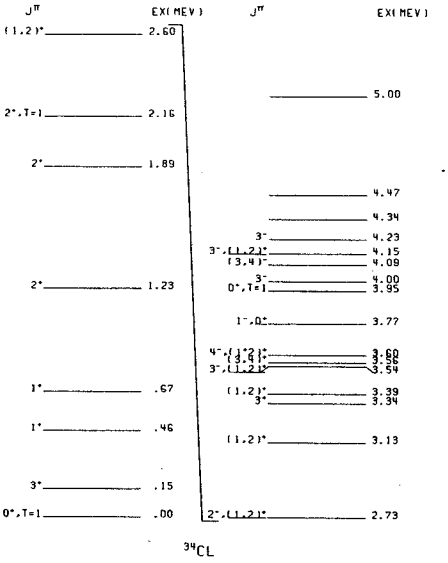

Figure 4

Three obvious discrepancies are noted in these assignments; the states at 2.72 and 3.60 MeV have been found in (^{3}He,d) and (p,γ) studies to be 2^- and 4^- respectively, but our assignments indicate either 1^+ or 2^+, based upon macroscopic DWBA calculations and comparisons with the shapes of other known 1^+ or 2^+ states. Some of these angular distributions with macroscopic DWBA calculations are shown in Fig. 5. The state at 3.77 MeV is very similar to the known 0^+, T=1 state at 3.94 MeV, but its 0^+ assignment is doubtful as (p,γ) measurements indicate a 1^- spin-parity and a strong transition to the 0^+ ground state for this level. One wonders whether these discrepancies could be

due to the shifts in angular distributions observed in the previous two subsections. In general though there is good agreement between expected spin-parity assignments and the theory.

References

1. See, e.g., J.J. Schwartz and B.A. Watson, Phys. Rev. Letters 24, 322(1970) and H.H. Duhm, K. Pterseim, R. Seehars, R. Finlay and C. Detraz, and references cited therein.
2. R.A. Hinrichs, R. Sherr, G.M. Crawley, and I. Proctor, Phys. Rev. Letters 25, 829(1970).
3. R.A. Hinrichs and G.F. Trentelman, to be published.
4. J.R. Comfort, J.P. Schiffer, A. Richter, and M.M. Stantberg, Phys. Rev. Letters 26, 1338(1971).
5. A.K. Hyder and G.I. Harris, to be published.
6. J.R. Erskine, D.J. Crozier, J.P. Schiffer, and W.P. Alford, Phys. Rev. C3, 1976(1971).

---

*On leave from Princeton University, Princeton, New Jersey.

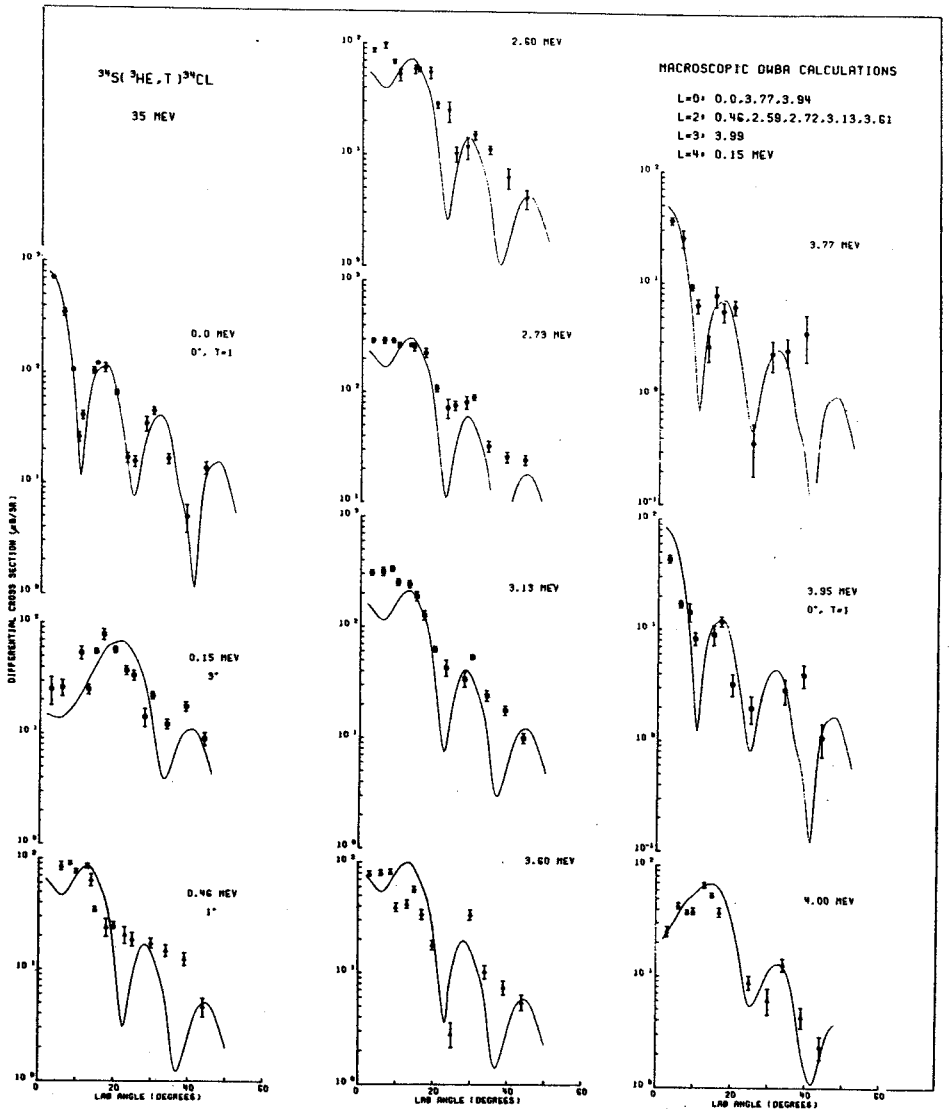

Fig. 5 Angular distributions for transitions to a multitude of representative states in ^{34}Cl populated by the reaction ^{34}S(^{3}He,t). The curves are macroscopic DWBA calculations (normalized to the data) with the L transfers as given in the right-hand corner.

Study of Proton Rich Nuclei Using the (^{3}He,^{6}He) Reaction at 70 MeV

W. Benenson, J. Dreisbach, E. Kashy, B.M. Preedom#, I. Proctor, and F. Trentelman

The (^{3}He,^{6}He) reaction at 70 MeV is being used to measure ground state masses and to study proton-rich nuclei the level structure of which was previously completely unknown. The experimental method consists of using low-sensitivity photographic plates in the Enge split-pole spectrograph. Previous (^{3}He,^{6}He) measurements in this laboratory[1,2,3] have been of ground state masses of some of these nuclei and have made use of position sensitive solid state detectors on the focal plane of the spectrograph. Some of the advantages of plates over the counters are 1) larger energy bite, 2) better resolution, 3) better particle discrimination of weak ^{3}He groups from background α's, and 4) insensitivity to neutrons and gammas.

Ilford Kminus 1 plates are used with absorbers stepped in thickness to give ^{6}He energies between 20 and 25 MeV everywhere along the plate. This amount of absorber leaves the α's at the same focal plate position with typical energies of 50-60 MeV. The tracks left by the much more ionizing He's are readily distinguishable from the α's except at the peak of very intense α-groups.

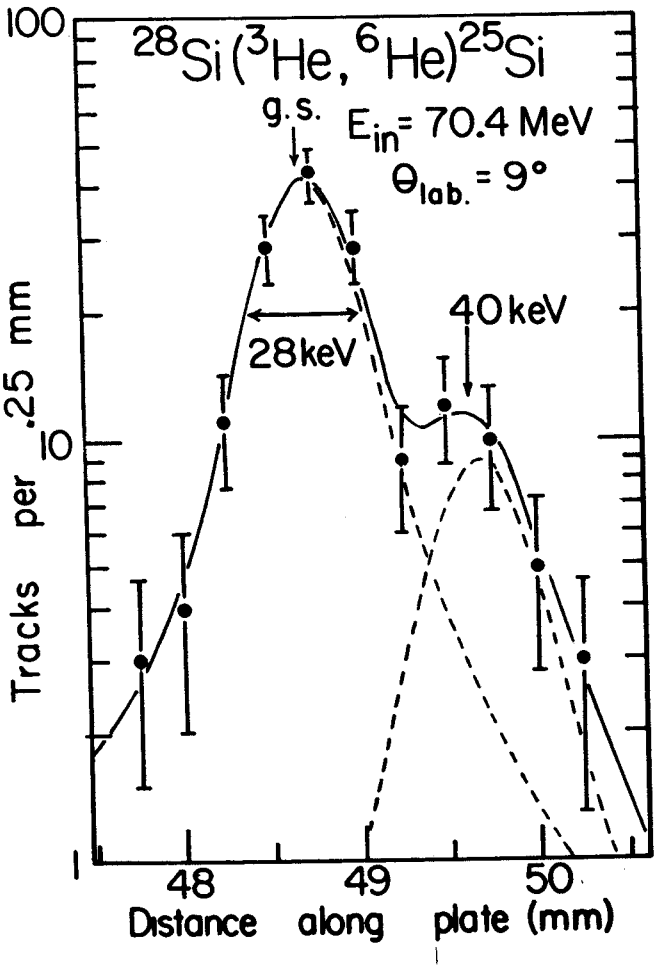

Figure 1

The kinematic compensation, dispersion matching and large solid angle of the spectrograph permit collection of ^{6}He spectra in 4 to 12 hours. The energy resolution is limited by target thickness effects. The best resolution obtained was 25 keV for the ^{28}Si(^{3}He,^{6}He)^{25}Si reaction at 9° and permitted resolving the ground-first excited state doublet. The presence of an excited state in ^{25}Si at about 40 keV (shown in Fig. 1) means a readjustment of the ^{25}Si mass downward by about 8 keV but does not effect the conclusions concerning the isobaric multiplet mass equation in Ref. 3. In addition to the 40 keV state, seven other states in ^{25}Si where found as is shown by the spectrum

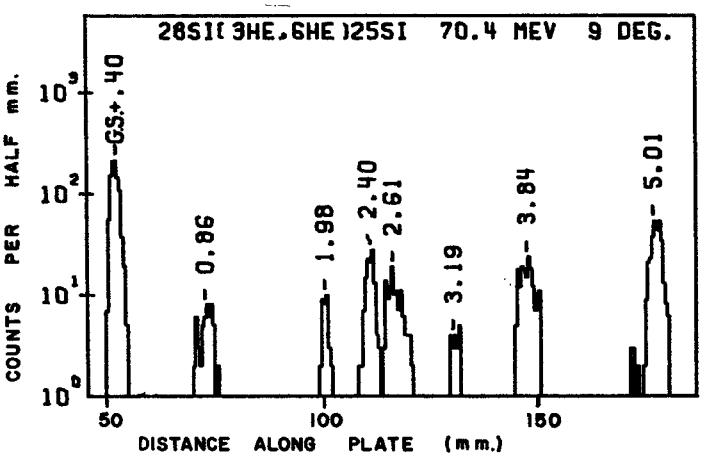

Figure 2

These levels line up well with the T=3/2 levels in ^{25}Mg, ^{25}Al, and ^{25}Si as can be seen from the table.

Table 1

^{25}Na T_z=3/2	^{25}Mg T_z=1/2	^{25}Al T_z=-1/2	^{25}Si T=-3/2
0.0	0.0(E_x=7.782)	0.0(E_x=7.915)	0.0
0.090	0.081[x]	0.072[x]	0.040
1.068	1.009		0.86
2.201			1.98
2.417			2.40
2.788			2.61
2.914	2.836		
3.353			3.19
3.455			
3.685			
3.928	3.943		3.84
3.950	3.965		
3.995	3.993		
5.190	5.116		5.01

Except for the first excited state, at least one member of each quartet is still missing. Using the multiplet mass equation the missing energy level can be predicted accurately. The energies cited are preliminary. In addition to ^{25}Si, the energy levels of ^{9}C, ^{10}C, and ^{21}Mg are being studied. In ^{9}C only the ground state was observed

and in ^{10}C no states that were not previously observed[5] in $^{12}C(p,t)$ were seen. Figure 3 shows a

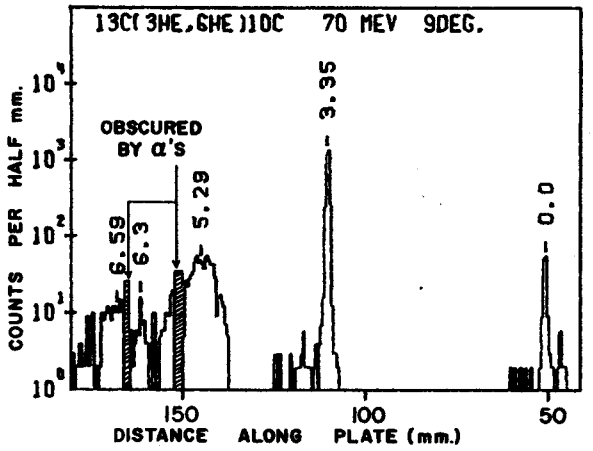

Figure 3

spectrum of $^{13}C(^{3}He,^{6}He)$ at 9°. The location of very strong peaks from the $^{13}C(^{3}He,^{4}He)^{12}C$ reaction is shown on the figure. In spite of the low sensitivity to α's it was not possible to scan right at the top of these peaks. Of interest in the spectrum is the very strong yield to the 2^{+} first excited state. In addition ^{9}C, ^{10}C, ^{21}Mg, and ^{25}Si work has begun on the masses and energy levels of ^{37}Ca, ^{47}Cr, ^{51}Fe, and ^{55}Ni. Other nuclei to be studied in the near future are ^{13}O, ^{16}F, ^{24}Al, ^{29}S, and ^{33}Ar.

References

1. G.F. Trentelman, B.M. Preedom, and E. Kashy, Phys. Rev. Letters 35, 530(1970).
2. G.F. Trentelman, B.M. Preedom, and E. Kashy, Phys. Rev. 3C, 2205(1971).
3. G.F. Trentelman and I.D. Proctor, Phys. Letters 35B, 570(1971).
4. C. Detraz and R. Richter, Nucl. Phys. A158, 343(1970).
5. W. Benenson, G.M. Crawley, J.D. Dreisbach, and W.P. Johnson, Nucl. Phys. A97, 510(1967).

*Visiting from the University of South Carolina.

A Survey of the (^{3}He,^{7}Be) Reaction

G.M. Crawley, P.S. Miller, and W.F. Steele

In recent years interest has grown in the field of multinucleon transfer reactions. Due to the extreme complexity of such reactions, no satisfactory theory has yet been developed for them. The reaction mechanism appears to be simplest in the case of α-transfer reactions. Because of the tight binding of the alpha particle, the four nucleons may, to some degree of approximation, be treated as an alpha cluster rather than four separate uncorrelated nucleons. Consequently, interest has been greatest in α-transfer reactions. To date most work has been done with α-stripping via the (^{6}Li,d)[1] (^{7}Li,t),[2] and (^{16}O,^{12}C)[3,4] reactions. Very little study has been given to α-pickup.

The present work is a study of the (^{3}He,^{7}Be) α-pickup reaction at 70 MeV incident beam energy. Earlier work on this reaction has been done at 30 MeV.[5] Preliminary data has been taken from ^{12}C, ^{16}O, ^{24}Mg, ^{28}Si, and ^{58}Ni targets. Figures 1 and 2 show spectra taken from the ^{12}C and ^{24}Mg target respectively. These data were taken in a 30-inch scattering chamber using silicon surface barrier detectors in an E-ΔE telescope arrangement. As can be noted from the spectra, each peak is a doublet since the ^{7}Be nucleus may be ejected from the reaction in its particle-stable first excited state (432 keV) as well as the ground state.

Cross sections have been found to be small and they decrease systematically with increasing atomic number. For example, ^{12}C(^{3}He,^{7}Be)^{8}Be (g.s.) has a maximum cross section of 80 μbarn/str. whereas ^{58}Ni(^{3}He,^{7}Be)^{54}Fe (g.s.) has a cross-section of 2 μbarn/str. More detailed angular distributions for states in ^{8}Be have been measured. The results for the 0^+ ground state and the 2^+, 2.9 MeV first excited state are shown in Figs. 3 and 4. The doublet structure of each level was not resolved so the indicated cross sections are roughly twice the value for a single peak.

Because of the small cross sections and the need to resolve the doublet structure, the consequent counting rates make impractical a detailed study of a variety of targets using the detector telescope system. Therefore an effort has been made to develop a practical position sensitive detector system for use in the focal plane of the laboratory's split-pole broad range magnetic spectrograph. A larger solid angle becomes feasible because of the spectrograph's kinematic focusing property. Nuclear emulsions cannot be used to detect the ^{7}Be particles since a variety of other ions would also strike the plate in the region of interest. Solid state position sensitive detectors are typically about 5 cm long, allowing one to collect data in only a small region of a spectrum at one time.

For the present work, position sensitive gas proportional counters are well suited. They can be made sufficiently long, can identify particles, and are capable of adequate resolution. Test counters have been built and used to detect ^{7}Be ions in the spectrograph. The tests show that indeed the gas counters are very suitable for detecting ^{7}Be ions. Although the resolution of the initial counter was not optimum, it nevertheless produced better energy resolution (sufficient to resolve the ^{8}Be g.s. doublet) than was obtained with the detector telescope arrangement.

Presently, improved position sensitive gas proportional counters are being designed. When available, they will be used for a detailed and comprehensive study of the (^{3}He,^{7}Be) reaction.

References

1. K. Meier-Ewert, K. Bethge and K.O. Pfeiffer, Nucl. Phys. A110, 142(1968).
2. R. Middleton, L.M. Polsky, C.H. Holbrow, and K. Bethge, Phys. Letters 21, 1398(1968).
3. A.M. Friedman, H.T. Fortune, G.C. Morrison, R.H. Siemssen, Proc. Int. Conf. Nuclear Reactions Induced by Heavy Ions, R. Bock, W. Hering eds. (North-Holland, Amsterdam), p. 171.
4. H. Faraggi, A. Jaffrin, M-C. Lemaire, M.C. Mermaz, J-C. Faivre, J. Gastebois, B.G. Harvey, J.M. Loiseaux, A Papineau, de-Shalit Memorial Volume (Annals of Physics 1971).
5. C. Détraz, H.H. Duhm, H. Hafner, Nucl. Phys. A147, 488(1970).

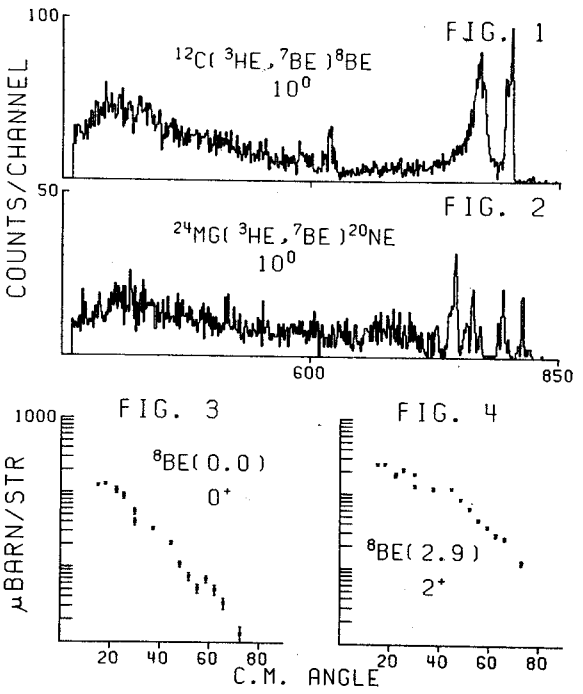

Search for ^{64}Ge

R.G.H. Robertson, S.M. Austin, and Wm.C. McHarris

The nuclide ^{64}Ge has N=Z and is predicted[1] to be stable against α- and proton emission. It is thus of considerable astrophysical interest as it would be the heaviest N=Z member of the α-capture chain believed to be established in explosive nucleosynthesis. An accurate knowledge of its mass is needed in order to make predictions about the abundances of heavier nuclei.[2]

We are attempting to produce ^{64}Ge by the ^{64}Zn(^{3}He,3n)^{64}Ge reaction at $E_{^3He} \simeq 45$ MeV. A 70 MeV He beam is degraded by an absorber and allowed to pass through a 10 mg/cm^2 target enriched to 99.66% in ^{64}Zn. Recoil nuclei from the target are stopped (thermalized) in helium gas at 2 atm. and pumped at sonic speeds through a capillary to a low-background counting area, using the technique first described by Macfarlane et al.[3] and implemented here by Kosanke and Giesler.[4] The decays of reaction products are then observed with a Ge(Li) detector.

It is probable that the ground state of ^{64}Ga is 0^+, and therefore the isospin selection rule will require much of the beta-decay of ^{64}Ge to lead to excited states in ^{64}Ga. Since little is known about states in ^{64}Ga a preliminary study of the ^{64}Zn(p,nγ)^{64}Ga reaction has been undertaken. The (p,nγ) reaction should reveal many of the γ-rays likely to follow the decay of ^{64}Ge, since both will favor low-spin states.

A large number of low-energy γ-rays appear when the beam energy is raised well above 7.98 MeV, the threshold for ^{64}Zn(p,n)^{64}Ga. These are tabulated below, where an x signifies that a γ-ray has been observed clearly.

E_γ (keV)	Ep (MeV)					
	8.193	8.225	8.251	8.305	8.418	8.577	9.530
42.8	x	x	x	x	x	x
85.7	x	x	x	x	x	x
128.5	x	x	x	x	x	x
152.4					x	x
280.4					x	x
291.2						x
323.1					x	x
363.8					x	x
367.5						x
384.6						x
420.4						x
427.2					x	x
434.8						x
491.8						x
495.3						x
550.2						x
583.9						x
592.8						x
666.9						x
885.9						x

Based on energy sums a possible level scheme for ^{64}Ga has been drawn up as shown. Some support for this scheme comes from earlier studies in this laboratory of the ^{64}Zn(^{3}He,t)^{64}Ga reaction by Hinrichs.[5] However, the cross-sections in that reaction are so low that the number of counts obtained was small, and the levels shown must be considered open to question.

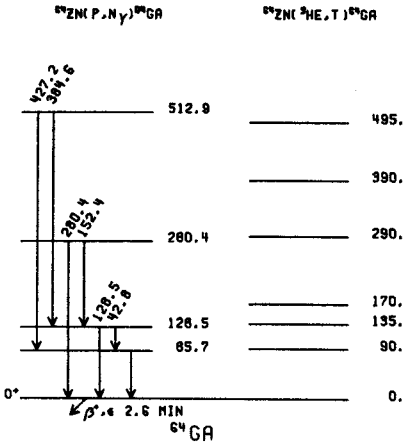

Thus far, none of the above γ-rays has been observed in the thermalizer experiments, although ^{61}Cu, ^{61,62,63}Zn, ^{63,64,65}Ga and possibly ^{65}Ge activities have all been recognized. Present efforts are being directed towards reducing the background caused by long-lived activities, as it seems probable that the half-life of ^{64}Ge will be quite short.

References

1. G.T. Garvey, W.J. Gerace, R.L. Jaffe, I. Talmi and I. Kelson, Rev. Mod. Phys. 41, S1(1969).
2. W.D. Arnett, private communication (1971).
3. R.D. Macfarlane, R.A. Gough, N.S. Oakey, and D.F. Torgerson, Nucl. Instr. and Methods 73, 285(1969).
4. K. Kosanke and G. Giesler, MSU report COO-1779-49(1970) p. 247.
5. R.A. Hinrichs, private communication (1971).

The Decay of ^{40}Sc to ^{40}Ca

J. Black

The bulk of the available information on the levels in ^{40}Ca has been obtained through scattering experiments.[1-5] Although some earlier work on the ^{40}Sc decay has been performed,[6-8] the rather short half-life of this isotope has hindered detailed γ-ray investigation of the levels in ^{40}Ca populated by this decay. However, with the advent of slow-pulsing for the MSU Cyclotron, together with good on-line detection systems, it has now been possible to study the γ decay of ^{40}Sc to obtain the levels in ^{40}Ca with a relatively high degree of accuracy.

For these experiments, the beam pulsing and routing of the data was accomplished with a special timing module designed by Dr. P. Miller of this laboratory.[9] The beam was pulsed by modulation of the cyclotron RF. The timing module also provided adjustable routing outputs and an adjustable inhibition period after the beam burst. A typical period of modulation started with a 0.4-sec beam burst, during which data was stored in one 4096-channel spectrum, followed by a total beam-off period of 0.6 sec, divided into four additional 0.15-sec counting intervals. No inhibition period was used in these experiments.

Several kinds of targets were tried in attempts to reduce the background of unwanted γ rays. Slurries of $CaCO_3$ (natural and isotopically enriched) were prepared in polystyrene or Duco-Cement binders on thin mylar. Good results, however, were not obtained until a 2-mg/cm^2, 99.973% isotopically-enriched ^{40}Ca foil, prepared at Oak Ridge National Laboratory, became available for this experiment. This foil was bombarded in a small chamber equipped with a vacuum-transfer port. A well-shielded Faraday cup was located about 2 m beyond the target. Background activity, induced by ions which suffered multiple scattering in the target, was minimized by removing all constrictions of less than 4-in. diameter between the target and Faraday cup. The target plane was inclined at 45° to the beam. At 90° to the beam, a 2.5%-efficent Ge(Li) detector was used to observe the γ rays following the β^+ decay of ^{40}Sc. This detector had a resolution of 2.1 keV and a peak-to-Compton ratio of 16.5:1. The ^{40}Sc was produced by the ^{40}Ca(p,n)^{40}Sc reaction, using a 24-MeV proton beam from the cyclotron.

The resulting γ-ray spectra were accumulated in the laboratory's Sigma-7 Computer.

Four beam-off routed spectra from this study are shown in Fig. 1. These resulted from a 32-hour accumulation of data in the slow-pulsing mode. From the half-lives, and comparison with scattering data, seven γ rays were found to belong in the ^{40}Ca level scheme. The energies and intensities of these γ rays are given in Table I. Although the intensities are in good agreement with most of the values reported by earlier workers,[6-8] the energies are not. The proposed decay scheme for ^{40}Sc is shown in Fig. 2.

Table I

γ-ray Energies and Intensities from the Decay of ^{40}Sc to ^{40}Ca

Energy (keV)	Intensity
754.5±0.2	48±3
1121.4±0.6	13±2
1875.5±0.5	25±2
2043.6±0.3	27±3
3166.4±0.6	14±2
3736.9±0.7	100
3919.5±1.0	10±2

References

1. C.M. Braams, Phys. Rev. 101, 1764(1956).
2. P.M. Endt and C. Van Der Leun, Nucl. Phys. A105, 1(1967).
3. J.R. Erskine, Phys. Rev. 149, 854(1966).
4. W.S. Gray, R.A. Kenefick, and J.J. Kraushaar, Nucl. Phys. 67, 542(1965).
5. A. Springer and B.G. Harvey, Phys. Letters 14, 116(1965).
6. A.J. Armin, J.W. Sunier, and J.R. Richardson, Phys. Rev. 165, 1194(1968).
7. W.C. Anderson, L.T. Dillman, and J.J. Kraushaar, Nucl. Phys. 77, 401(1966).
8. E. Kashy and J.L. Snelgrove, Phys. Rev. 172, 1124(1968).
9. Nuclear Chemistry Annual Report, Michigan State University, 1970, p. 257.

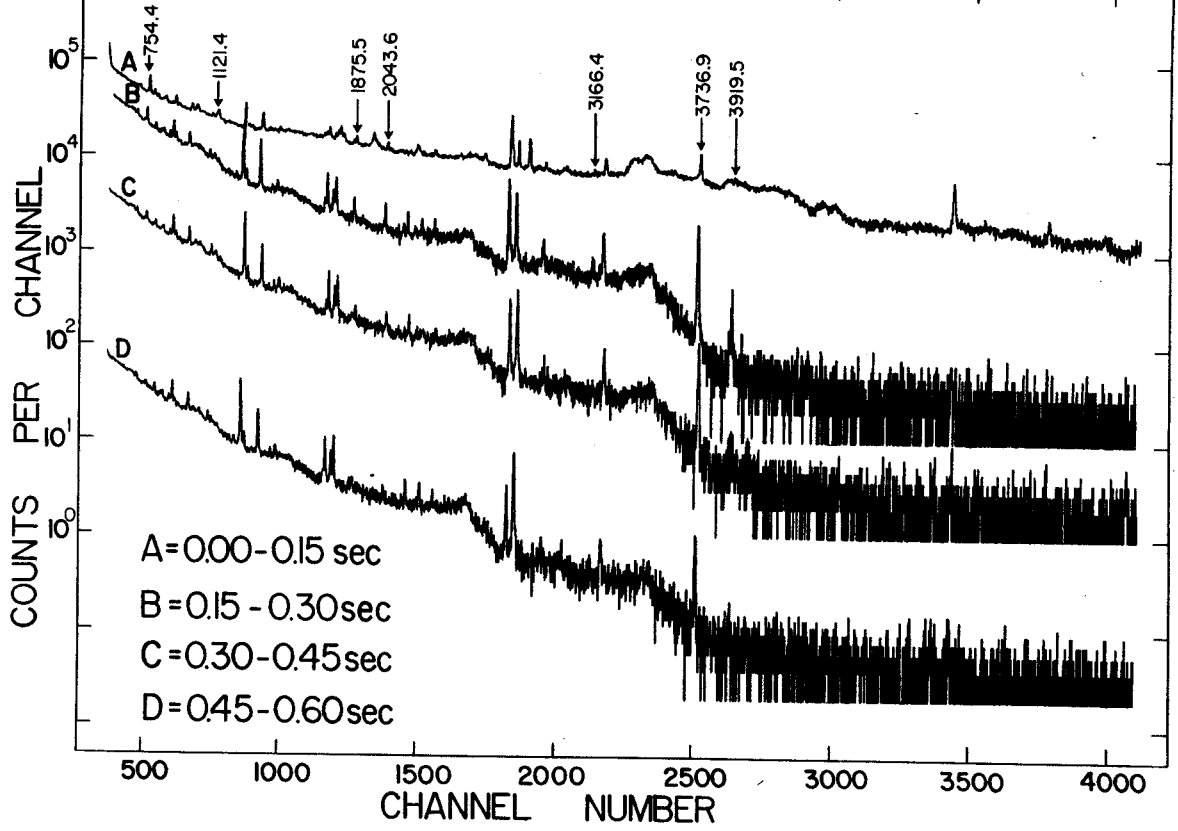

Fig. 1 Routed γ-ray spectra from the pulsed-beam study of ^{40}Sc.

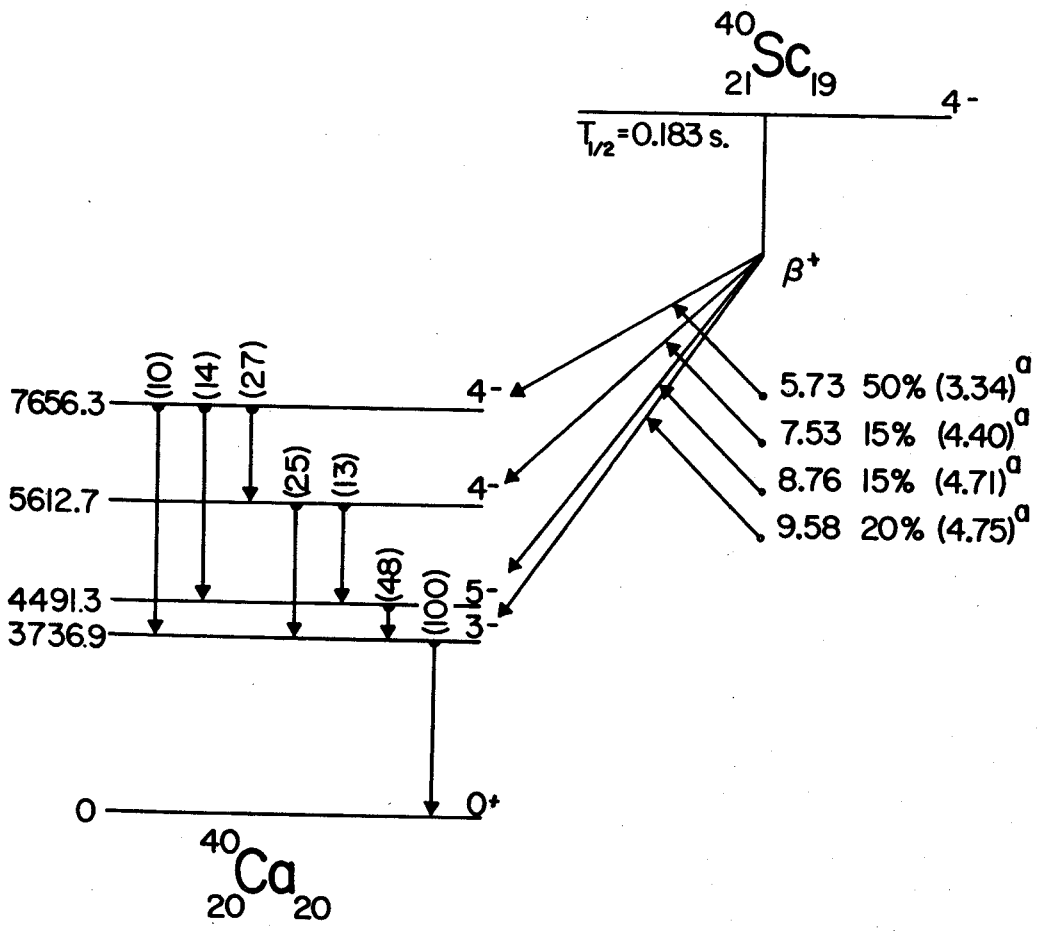

Fig. 2 The proposed γ-decay scheme for ^{40}Sc.

[a]Values taken from Ref. 6.

Use of the He Thermalizer-Jet Transport

K.L. Kosanke, G.C. Giesler, Wm.C. McHarris

Our initial motivation for construction of the He thermalizer-jet transport was its proposed use in an on-line mass filter (see Section 21 of this report). While this remains the case, the thermalizer-jet transport has become a popular research tool in itself. It is being used with increasing frequency for the rapid transport cyclotron produced activities to low background counting areas for conventional γ and α counting experiments. To facilitate this use we have just completed a tape transport system to move the activity to successive detector locations after it is collected from the He-jet. We anticipate that the He thermalizer-jet transport will remain an important research tool in and of itself even after we have developed our on-line mass separation capability.

The thermalizer we constructed was patterned after that developed by R.D. Macfarlane[1] and we are grateful to him for his continued help in developing our system. We are continuing to use polyethylene capillary (0.034" ID) which was extended to about 60 feet in length. However, we will soon start using a larger diameter capillary in an attempt to reduce the recoil collection time by pumping a larger quantity of gas. The set up of the thermalizer shown in Fig. 1 is one in which three targets were used and the recoils collected at 90° to the cyclotron beam. Here the targets are staggered in the holder so that the He flow entering the teflon blocks from the right sweeps infront of each target successively We have found the use of multiple targets to be a useful method of increasing the recoil yield in cases where the added time necessary to sweep the recoils from the larger volume into the capillary could be afforded. Further we have found collecting at 90° to the beam to be a more reliable technique than 0° (described in Ref. 1 and 2) for collecting and transporting the recoils. We do expect to use the 0° technique when working with extremely short lived activities.

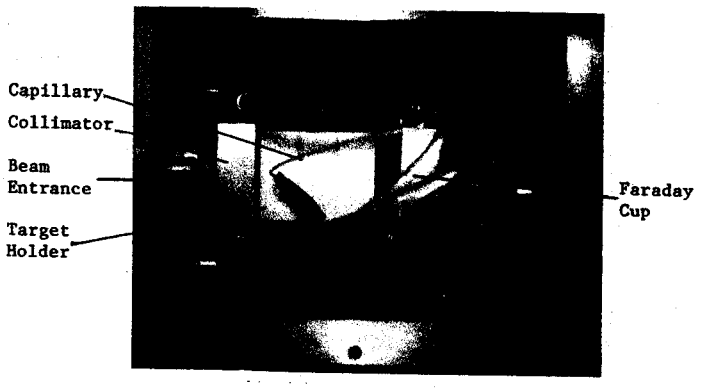

Fig. 1a Recoil thermalizer showing target holder-collector and Faraday Cup.

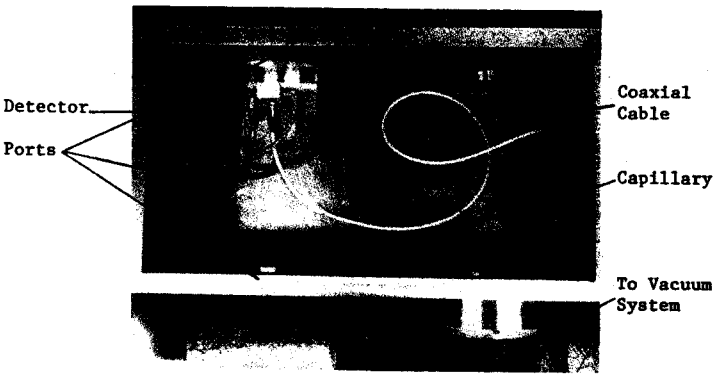

Fig. 1b Recoil counting chamber showing capillary and detector in cooled mount.

References

1. R.D. Macfarlane, R.A. Gouch, N.S. Oakey, and D.F. Torgeson, ORO-3820-2 (1969); Nucl. Instr. and Methods 73, 285(1969).
2. K.L. Kosanke and G.C. Giesler. Michigan State University. Nuclear Chemistry Annual Report for 1970 (COO-1779-49) 247-50.

Progress with the On-Line Isotope Separator

K.L. Kosanke, Wm.C. McHarris, and H.P. Hilbert

To date our work toward an on-line isotope separation has been directed at two areas of the overall system. First has been the development of our He thermalizer-jet transport (See next section of this report) with a tape transport that will later be used in our complete system. Second has been with our electric quadrupole mass filter. We have directed the initial work on our overall system to these areas because we felt they would each prove to be useful research tools in themselves and could be used before the complete system was constructed. The remaining work on the system will be the linking of these two pieces of hardware together.

The on-line mass separation system under construction and its operation are shown schematically in Fig. 1. A collimated cyclotron beam enter the apparatus, striking a thin target (or a series of thin targets if half-lives are sufficiently long) in an atmosphere of helium (1 to 3 atm. of pressure). Those nuclei near the back of the targets interacting with the beam will be recoiled out of the target into the helium. The recoils are then slowed to thermal energies through collisions in the helium. Recent work by R.D. Macfarlane[1] suggests that the next step is the attachement of the recoils to large molecule collectors (with masses up to 10^8 amu) formed from impurities in the helium in the plasma generated by the cyclotron beam as it leaves the target passing through the helium atmosphere. The recoils then leave the thermalizer attached to these large moleculor clusters through a polyethylene or teflon capillary[2] (0.02 to 0.06 in ID) accelerator ing to near the sonic velocity of He (~3ft/msec). The capillary is run through concrete shielding to a low background area about 60 feet away. At the end of the capillary the helium will be skimmed off using a one or two stage skimmer. Quite efficient skimming of the helium should be possible[1] just by directing the flow from the capillary at a conical orifice. The molecular clusters with their horendus masses are extremely well collimated and should be passed quite efficiently through the orifice whereas the helium will diverge and be largely pumped off. If our pumping capacity is not sufficent to reduce

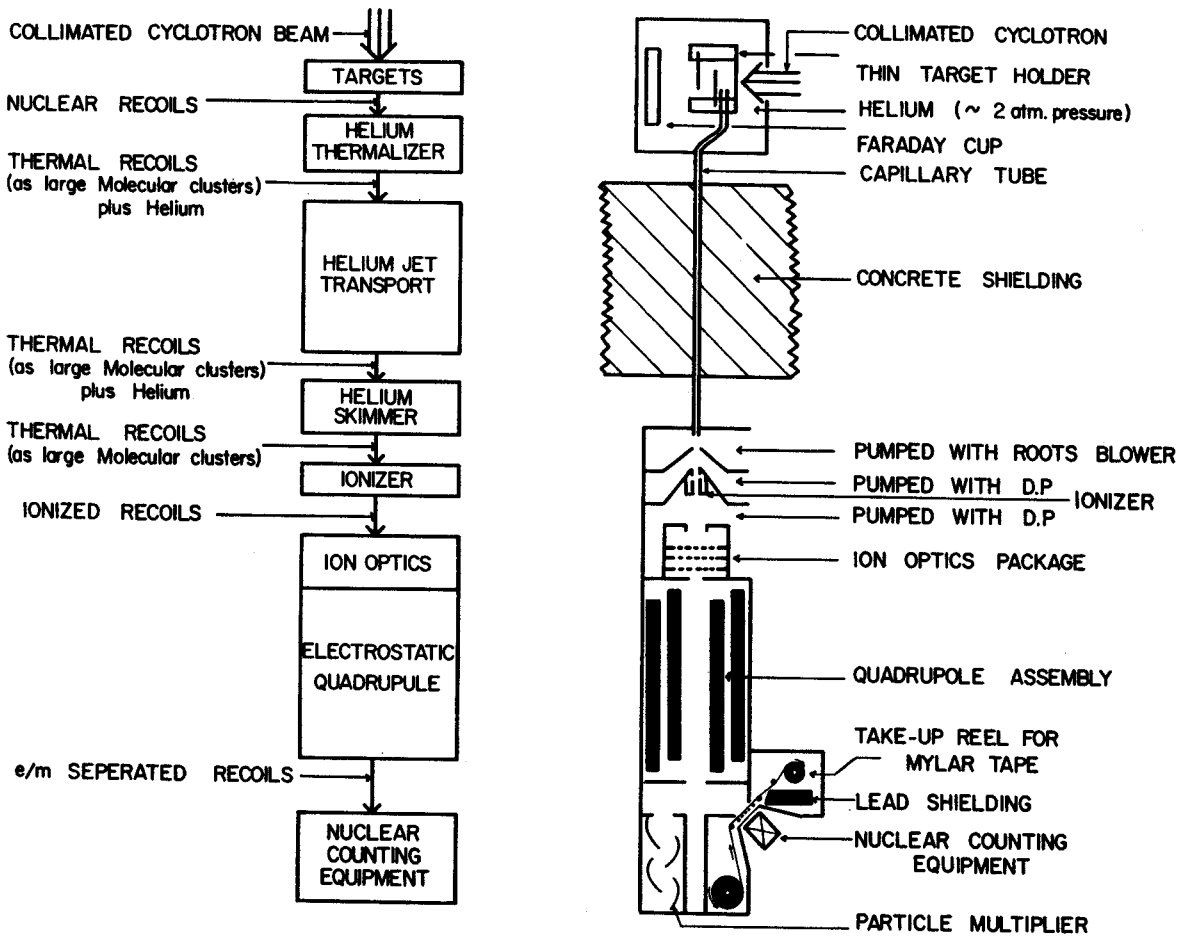

Fig. 1 Block and schematic diagrams of the on-line isotope separator.

the pressure to $\sim 10^{-5}$ ton after the first skimming stage, a second stage will be added. The molecular clusters will be broken up and the recoils ionized in an RF or DC induced discharge setup in one of the skimming stages with the recoils directed into the ion optics associated with the electrostatic quadrupole.[3] With the quadrupole setup properly only selected masses are transmitted through it.[4] At the exit of the quadrupole the recoils will either be directed into an electron multipler such that it is possible to obtain a mass scan or onto paper or aluminized mylar tape for conventional nuclear counting. A typical mass scan from the quadrupole is shown in Fig. 2.

References

1. H. Jungclas, R.D. MacFarlane, and Y. Fares, to be published.
2. K. Kosanke, G. Giesler, MSU Nuclear Chemistry Annual Report for 1970 (COO-1779-49) p. 247-50.
3. Electric quadrupole supplied by Extranuclear Labs. P.O. Box 11512, Pittsburgh, Penn.
4. For a theoretical description of the Electric Quadrupole sec: W. Paul, H.P. Reinhard, and U. von Zahn, Z. Phys. 152, 143(1958).

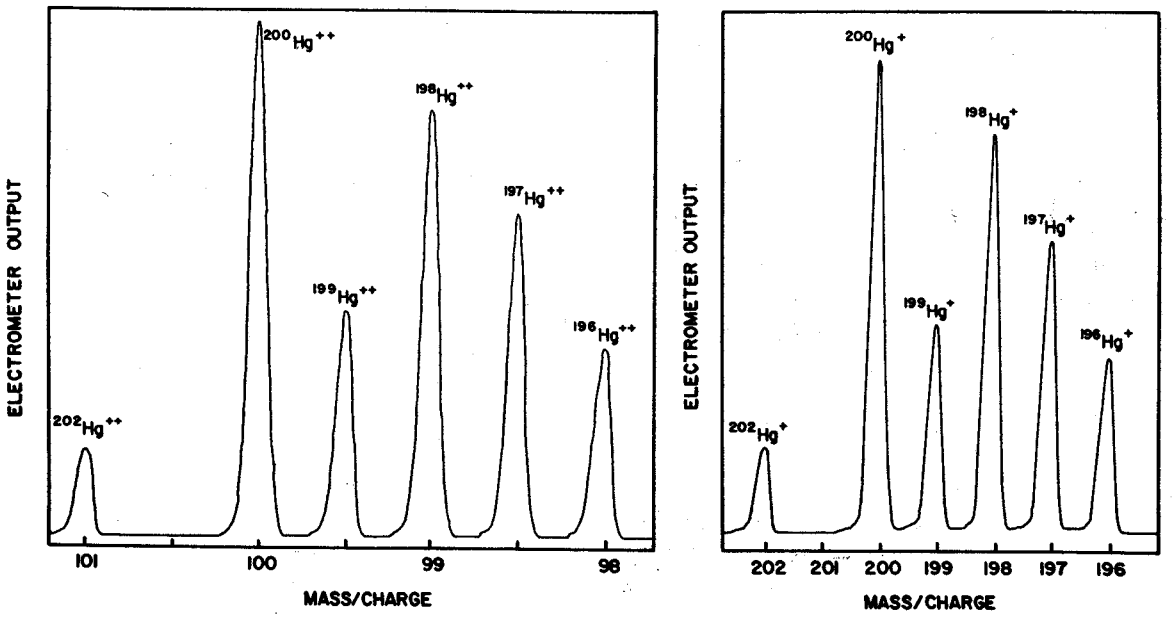

Fig. 2 Tyipcal Hg mass spectra taken with the extranuclear electric quadrupole mass filter.

Rabbit-Pneumatic Target System

K.L. Kosanke, H.P. Hilbert and C.B. Morgan

A pneumatic target system (rabbit) has been developed to aid in the study of moderately short-lived nuclides ($t_{1/2} \gtrsim 3$ seconds) and to make more efficient use of the cyclotron time in general. The functioning of the rabbit system is diagramed in Fig. 1. The rabbit has proven so successful that for the past two years all sources prepared for off-line study by the Nuclear Chemistry and Physics groups here in the lab were made using the rabbit system.

Target holders (rabbits) and the terminals of the system (rabbit hutches) are shown in Fig. 2. Rabbits used for irradiation are 2 inches in diameter and 3 inches long, with target material and associated absorbers carried in the central region. The targets are air cooled directly and water cooled by conduction through the target holder. The rabbit can be reproducibly oriented (±5°) with respect to the cyclotron beam. The mechanism used to orient the rabbit is to rotate it by directing a jet of air onto a set of fins near its base. The rotation is stopped by the attraction between a small permanent magnet mounted in the top portion of the rabbit and an electromagnet in the rabbit hutch. The rabbit shown with an exploded view of its sample container in Fig. 2 has been quite useful in preparation of multiple separated isotope targets. The central bolt-like piece contains one sample, and a series of sample containers and/or absorbers are stacked before it. In this way, we have prepared as many as four sources at once. The rabbit is constructed such that only the fraction of cyclotron beam that passes through the 5/16-inch diameter target container reaches the Faraday cup, so only that portion of the beam passing through target material is monitored.

The rabbit is propelled through a cellulose acetate pipe (with bends made of poly-vinyl-chloride pipe) by setting up a pressure differential across the rabbit. We are now using 3psi pressure on one side of the rabbit and a partial vacuum, created by a commercial vacuum cleaner, on the other. At the end of its path the rabbit is stopped with an air cushion, initiated by a small unit attached to the rabbit pipe to sense the passage of the magnet mounted in the rabbit. Transit times for the rabbit are now usually ≳5 seconds. This is almost twice as long as previously reported. This is because we have lengthened rabbit line to about 250 ft. We felt the added transit time, allowing us to move to a more convenient location was acceptable in that our searches for shorter lined isotopes are now being conducted using our He thermalizer-ject transport (see another section of this report).

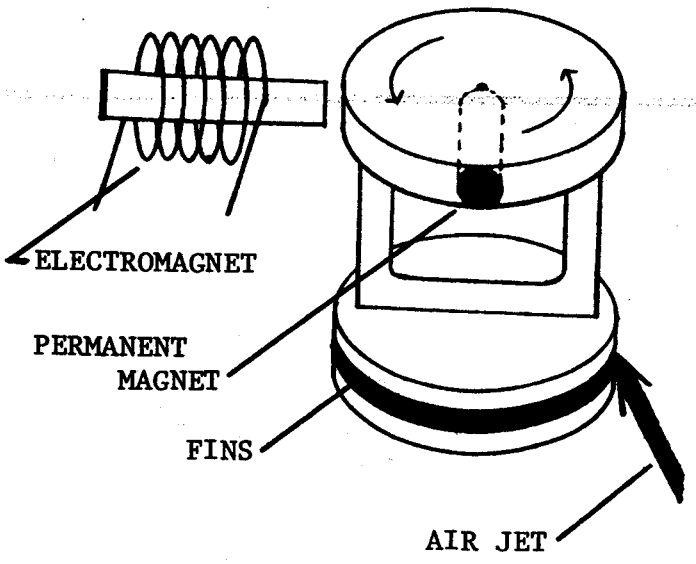

Figure 3

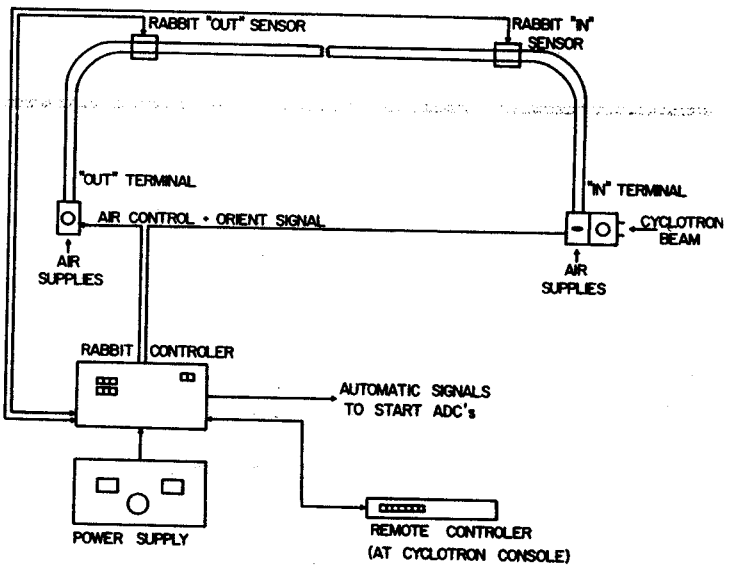

Fig. 1 Schematic lay-out of "Rabbit" system.

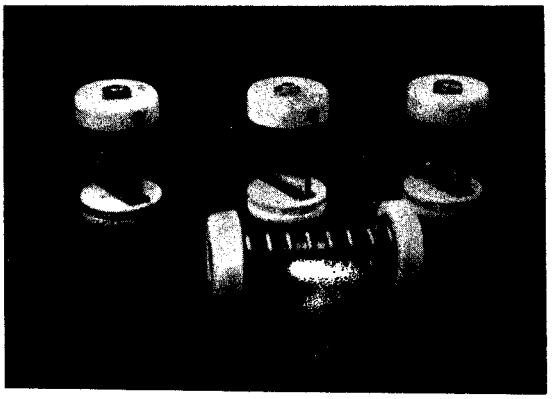

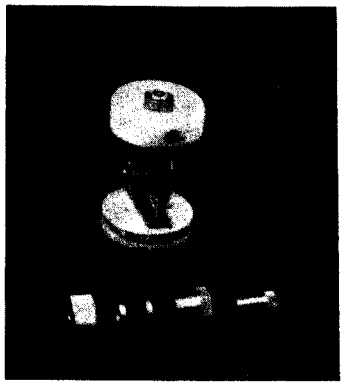

Fig. 2a "Rabbits" used in system.

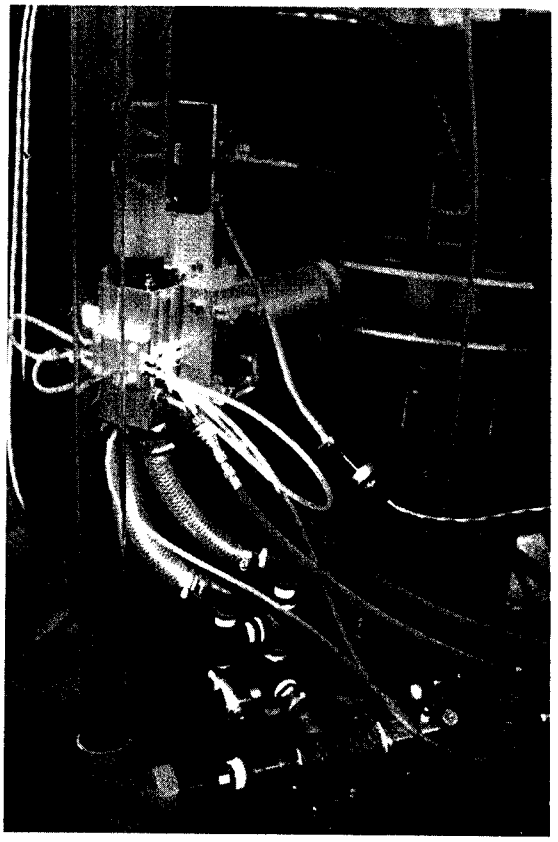

Fig. 2b "In-Terminal" of system.

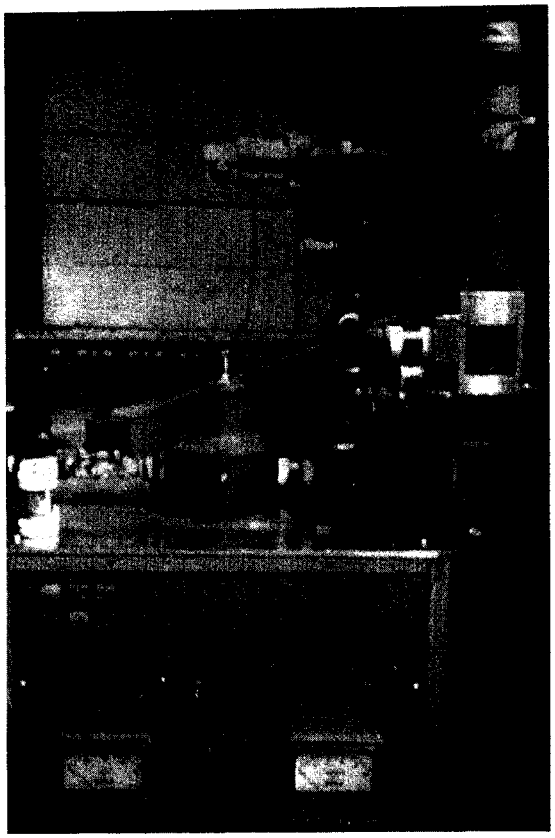

Fig. 2c "Out-Terminal" of system.

Electron Capture Decay of ^{205}Bi

K.L. Kosanke, Wm.C. McHarris and W.H. Kelly

Our initial γ sources were prepared by bombarding natural Pb foils with 36 MeV protons to induce the ^{208}Pb(p,4n)^{205}Bi reaction. The targets were aged from 6 to 10 weeks to optimize the 15·3d ^{205}Bi activity. Before counting, the ^{205}Bi activity was chemically separated from the targets.[1] Additional γ sources were prepared by bombarding mass separated ^{206}Pb with 19 MeV protons to induce the ^{206}Pb(p,2n)^{205}Bi reaction and also by bombarding natural Tl with 37 MeV alphas to induce the ^{205}Tl(^{4}He,4n)^{205}Bi reaction. The primary detector used was a Ge(Li) detector with 3.6% efficiency relative to a 3"x3" NaI(Tl) detector and had a photopeak resolution (FWHM) of 2.1 keV at 1.332 MeV. In our γ singles experiment we identified and determined intensities for 97 definite and 15 possible transitions as belonging to the decay of ^{205}Bi. Also we have placed upper intensity limits on 12 transitions reported by other investigators and not observed in this study.

The primary thrust of our study was the conduction of two megachannel Ge(Li) vs Ge(Li) coincidence experiments.[2] In the second run of the experiment >3.5 million coincidence events were recorded on magnetic tape. Detectors having 2.5% and 3.6% relative efficiencies and placed at ≃75° to each other with a graded level absorber between them were used to collect the coincidence events. Subsequent to collecting the coincidence events the tapes were played back having set various gates to be scanned on each pass. In addition to generating spectra by setting gates on peaks, backgrounds adjacent to peaks and normalized peak to background difference spectra could be generated. Accordingly using these 3 different types of coincidence spectra it was readily possibly to make coincidence assignments. More than 300 different gates were set on 95 areas of interest in the spectrum. In a few cases where the coincidence results were ambiguous, the event tapes were played back in a sum coincidence mode[3] allowing a few additional coincidence assignements. On the basis of this coincidence study, we have placed 80 transitions in our first confidence decay scheme (see Fig. 1). Also, less conclusive coincidence data helped place 14 of 27 additional transitions included in our second confidence decay scheme.

Another area of investigation of the ^{205}Bi decay was the β^+ feedings to states in ^{205}Pb. For this study we used a 2.5% Ge(Li) detector with a resolution (FWHM) of 2.3 keV at 1.33 MeV in conjunction with an 8"x8" NaI(Tl) split annulus having a resolution of ≃10% at 1.33 MeV. The Ge(Li) detector was located just outside the annulus with the source placed inside the annulus. The events analyzed required a triple coincidence between the Ge(Li) detector and the halves of the annulus each gated on the 511 keV region and had a resolving time of ≃150 nsec. After correcting for chance energy sums, compton events, and pair producing transitions a ratio of the triple coincidence to singles count rate was determined. Repeating the experiment using ^{22}Na with a known ε/β^+ ratio we were able to report the following percent β^+ feeding in ^{205}Bi: 703.4-keV level 0.095 0.02%, 987.5-keV level 0.006±0.002%, 1043.7-keV level <0.002%.

The final area of investigation was the search for the n and o conversion of the 2.3-keV first excited to ground state transition.[4] This was accomplished using the Michigan State University $\pi\sqrt{2}$ beta spectrometer with a post accelerator which extended its range to <1. keV. Needless to say the chemistry involved in the source preparation required exceptional care to maintain the necessary parity. We observed definite n_{II} and n_{III} lines with the ratios, n_{II}/n_{III}=0.70 0.25 and $n_{II}+n_{III}/L_I$ (26.22 keV) = $0.48^{+0.15}_{-0.05}$.

References

1. K.L. Kosanke, W.H. Kelly, Wm.C. McHarris, to be published in Phys. Rev.
2. Event Recorder/Recovery described in MSU Cyclotron Annual Report for 1969-70, pp. 107.
3. G.C. Giesler, K.L. Kosanke, R.A. Warner, Wm.C. McHarris, Nucl. Instr. and Methods, 93, 211(1971).
4. W.C. Johnston, W.H. Kelly, S.K. Haynes, K.L. Kosanke, Wm.C. McHarris, Phys. Rev. Letters 26, 1043(1971).

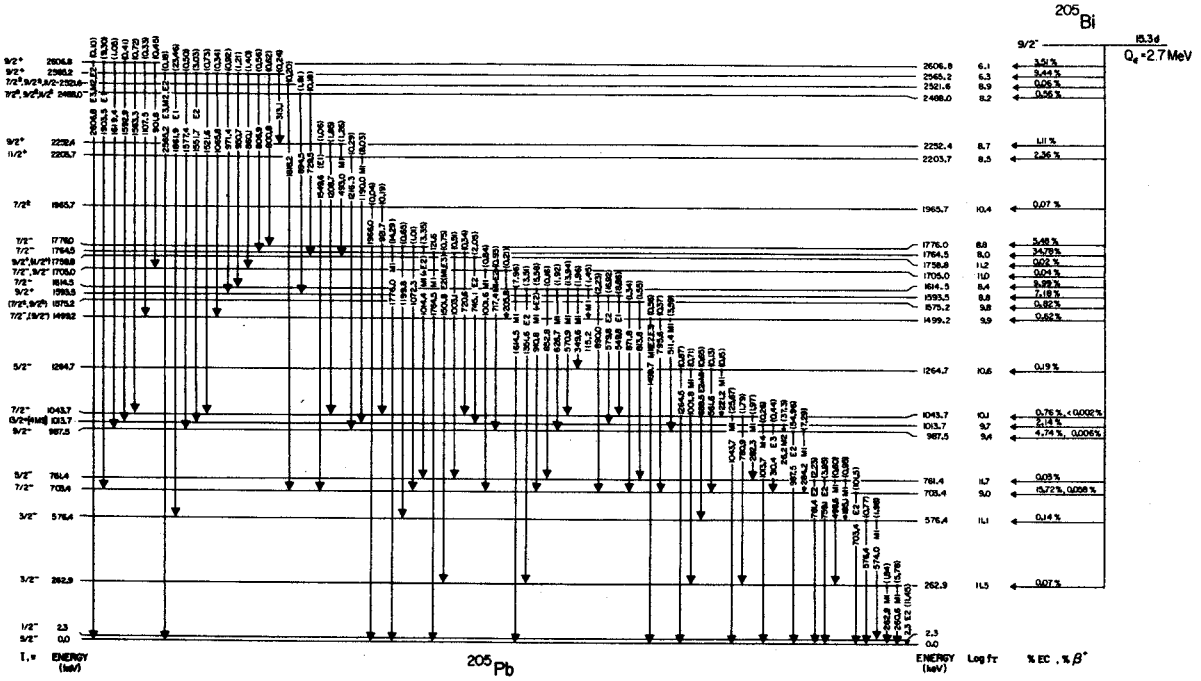

Fig. 1a ^{205}Bi first confidence decay scheme.

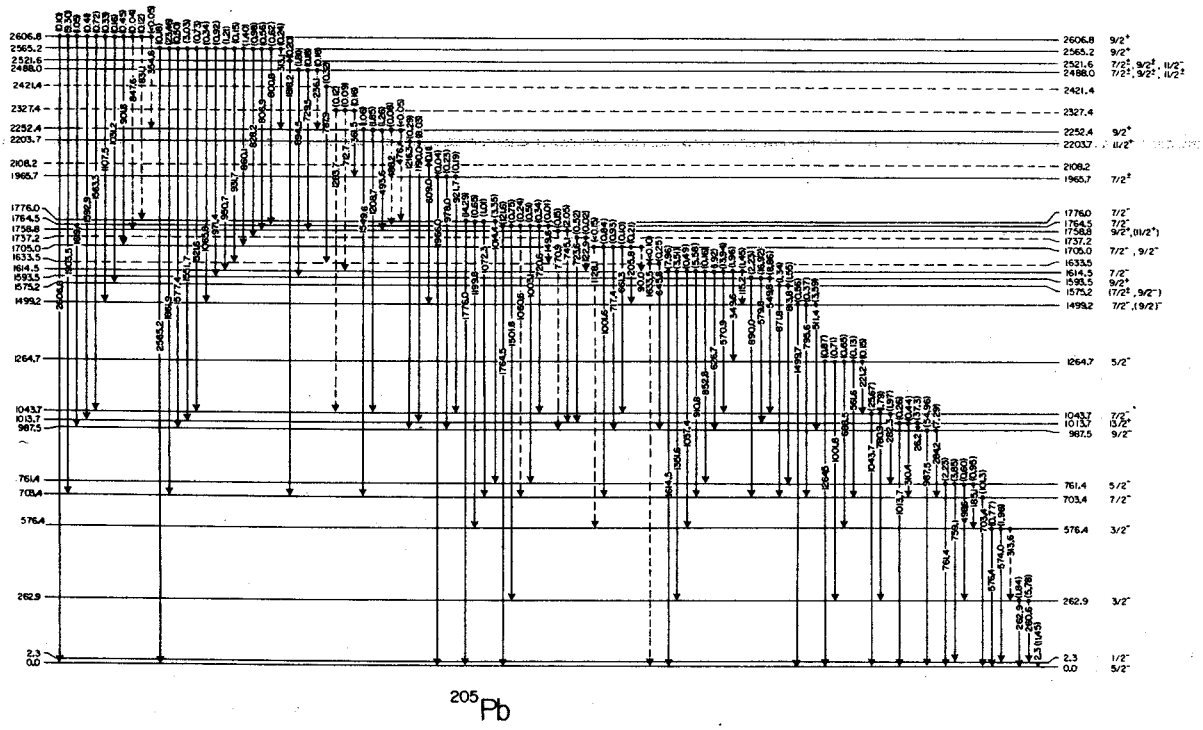

Fig. 1b ^{205}Bi second confidence decay scheme.

The Decay of ^{202m}Pb

J. Guile

Since the existence of an isomer associated with ^{202}Pb was first reported[1] in 1954, the decay of ^{202m}Pb has been the object of several further studies.[2-5] The most extensive of these was conducted by McDonell and co-workers.[4] Their investigation resulted in a decay scheme that has remained essentially unchanged until the present study.

Our renewed interest in this isomer was stimulated by work done in this laboratory on the decay of ^{201}Pb in which accurate γ-ray intensities of several of the ^{202m}Pb transitions were needed in order to correct for their contributions to the ^{201}Pb spectra. In our attempt to determine these intensities, several previously unreported γ-ray transitions with a 3- to 4-hour half-life were observed. It was, therefore, deemed worthwhile to conduct a more extensive investigation of ^{202m}Pb using the improved γ-ray spectroscopic techniques now available.

The ^{202m}Pb sources were prepared by bombarding natural thallium foils and enriched ^{203}Tl (70% ^{203}Tl, obtained from Oak Ridge National Laboratory) with a 16-MeV proton beam from the Michigan State University Cyclotron. The induced ^{203}Tl(p,2n)^{203m}Pb reaction produced the desired activity in good yield with a 7-10 min. bombardment at a beam current of 0.7 μA. No chemical separation was deemed necessary, but sources were allowed to age for a period of 2 to 3 hours before counting in order to minimize contamination from shorter-lived isotopes.

The energies and intensities of the γ-rays emitted in the decay of ^{202m}Pb were studied using a Ge(Li) detector with a photopeak efficiency of 10.4% at 1332 keV (compared with the efficiency of a 3x3 in. NaI(Tl) detector having the source at a distance of 25 cm) and an optimum resolution of 2.1 keV at that same energy. A typical ^{202m}Pb γ-ray singles spectrum is presented in Fig. 1. Seventeen

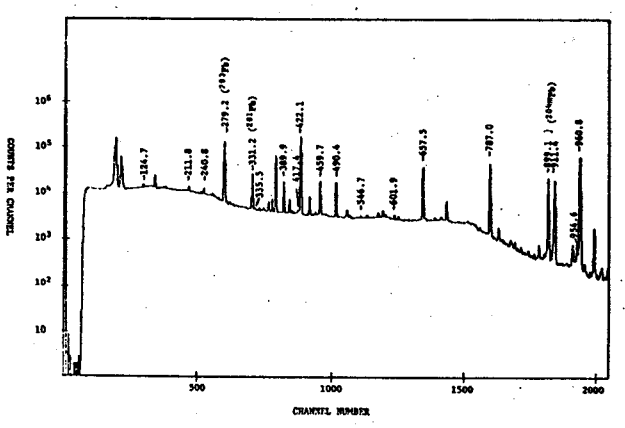

Fig. 1 A typical ^{202m}Pb γ-ray singles spectrum.

γ-rays with a half-life comparable to that of ^{202m}Pb were observed. Table I lists the energies and relative intensities of these γ-rays and compares our values with those obtained by McDonell et al.[4] Of the transitions in this table, those

Table I

Energies and Relative Intensities of γ-rays and Conversion Electrons from the Decay of ^{202m}Pb

Energy (keV)	Relative γ-ray Intensity	Relative Conversion Line Intensity[a]
124.75±0.09	1.3 ±0.4	---
211.88±0.07	1.12±0.5	---
240.83±0.08[b]	1.17±0.4	---
335.56±0.1	0.32±0.7	1.3±0.1
389.91±0.07	8.9 ±0.1	28. ±3.
417.44±0.1	0.68±0.08	---
422.13±0.06	128.1 ±0.3	66. ±5.
459.11±0.08	13.5 ±0.1	9. ±1. (ΣL)
490.44±0.07	14.9 ±0.2	1.7±0.2(ΣL)
546.7 ±0.5	0.25±0.1	1.1±0.1(ΣL)
601.95±0.09	1.05±0.08	---
657.48±0.06	60.6 ±0.3	4.4±0.4
787.00±0.06	100	100
954.62±0.09	1.9 ±0.2	---
960.77±0.3	194.8 ±0.4	13. ±1.
---	---	690. ±50.(ΣL)
---	---	17. ±3.
---	---	4.0±0.3
---	---	2.5±0.2

[a] From McDonell et al. (Ref. 7). Relative intensities are for the K-conversion lines unless otherwise specified.

[b] In our measurements we were unable to delineate between the 240.3- and 241.1-keV γ rays emitted in the decay of ^{202m}Pb. The energy and relative intensity given here, are therefore due to the total unresolved doublet peak.

with energies of 124.75-, 211.88-, 417.44-, 601.95-, and 954.6-keV have not been previously reported. Among these, the 417.44-keV transition was seen to fit into the existing decay scheme between the 2041- and 1624-keV levels in ^{202}Pb. The existence of a transition in this energy range was predicted by McDonell et al.,[4] but no experimental verification was available at that time. Energy sums and differences indicated that the remaining four transitions could be incorporated into the decay scheme by adding two new energy levels: one at 1916.6 keV in ^{202}Pb and one at 1552.1 keV in ^{202}Tl. These levels have been included in the decay scheme given in Fig. 2.

To determine the cascade relationships in the decay of ^{202m}Pb and help test the consistency of these new assignments, a γ-γ coincidence experiment was performed. For these measurements, the detector mentioned above was coupled with a 4.6% efficient Ge(Li) detector with an optimum resolution of 1.9 keV at the energy of 1332 keV. The addresses of coincidence events from both sides of the system were processed and listed on magnetic tapes, to be recoved later, off-line, as gated

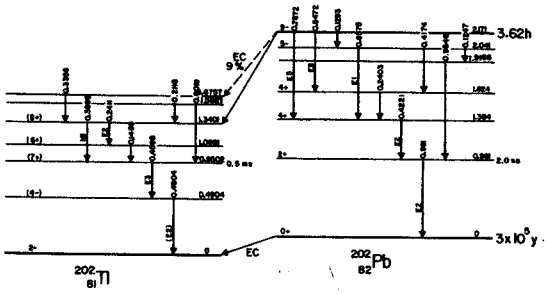

Fig. 2 Revised decay scheme of ^{202m}Pb.

slices. The integral coincidence spectra and five of the gated coincidence spectra of particular interest are presented in Fig. 3. Parts b) and c) of Fig. 3 show clearly the existence of a 124.7-945.6-keV cascade. Our assignment of this cascade to levels in ^{202}Pb, in preference to ^{202}Tl, was substantiated when spectra gated on the Pb K x-rays increased the relative intensities of these peaks with respect to those of transitions known to occur between levels in ^{202}Tl. By intensity considerations, it was also suggested that the 124.7-keV transition feeds the 954.6-keV transition and not vice versa. Parts e), f), and g), indicate that a 211.8-keV γ ray feeds the 1340.1-keV level in ^{202}Tl which de-excites by either a 3899- or 241.1-keV transition. No coincidence data were available for the 601.9-keV transition because of the 0.5-msec half-life of the 950.2 state in Tl. By gating on the Tl K x-rays, however, it was possible to place both the 211.8- and 601.9-keV transitions in the electron capture branch of ^{202m}Pb decay. The agreement between these 2-parameter coincidence results and our original placements leads us to place considerable confidence in our revised decay scheme.

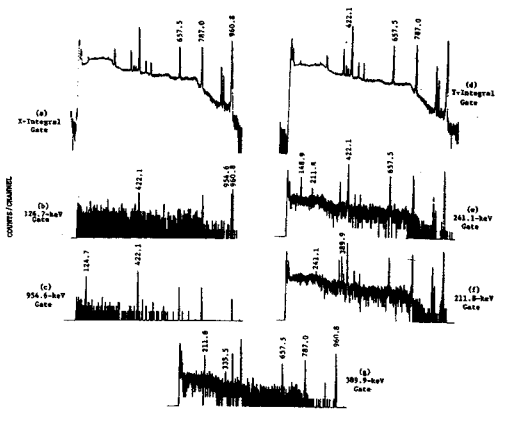

Fig. 3 Coincidence spectra.

REFERENCES

1. D. Maeder and A.H. Wapstra, Phys. Rev. 93, 1433(1954).
2. D. Maeder, A.H. Wapstra, G.J. Nijgh, and L.Th.M. Ornstein, Physica 20, 521(1954).
3. I. Bergström and A.H. Wapstra, Phil. Mag. 46, 61(1955).
4. J.A. McDonell, R. Stockendal, C.J. Herlander, and I. Bergström, Nucl. Phys. 3, 513(1957).
5. B. Johansson, T. Alväger, and W. Zuk, Arkiv Fysik 14, 439(1959).
6. R.E. Doebler, Ph.D. Thesis, Michigan State University, CO-1779-42(1971), R.E. Doebler, Wm.C. McHarris and W.H. Kelly, to be published.

The Decay of ^{170}Lu to Levels in ^{170}Yb*

D.C. Camp** and F.M. Bernthal

A detailed study of the complex decay of ^{170}Lu to levels in ^{170}Yb has recently been carried out at the Berkeley and Livermore Lawrence Radiation Laboratories and the MSU Cyclotron Laboratory.

The ^{170}Lu activity was produced by irradiating Tm_2O_3 with 40 MeV α-particles at the Berkeley 88-inch cyclotron. Ge(Li) and Si(Li) detectors were employed to obtain γ-ray singles, conversion electron, and γ-γ coincidence data. The γ-ray singles and pair-peak data were gathered with the Livermore anti-Compton spectrometer operated in the Compton-suppression and double-escape pair-peak modes simultaneously. Isotope-separated sources of ^{170}Lu were obtained for counting the low-energy portion of the spectrum and for the Ge(Li)-Ge(Li) γ-γ coincidence experiments. The conversion electron spectrum from 0-3 MeV was obtained with use of a 3-mm deep by 1cm² cooled Si(Li) detector.

A total of 550 γ-ray transitions has been observed in the ^{170}Lu decay spectrum, 217 of which are assigned to the ^{170}Yb level scheme on the basis of 112 γ-γ coincidence spectra. An additional 118 γ-ray transitions were placed in the level scheme on the basis of energy differences. The proposed ^{170}Yb level scheme is shown in Fig. 1. Spin and parity assignments are proposed for some 48 levels. Not included in Fig. 1 are those γ-rays that could be assigned from energy differences.

One of the most unusual features of the ^{170}Yb level scheme is the appearance of four low-lying 0^+ excitations, at 1069.4, 1228.9, 1479.9, and 1566.4 keV. The pairing energy gap 2Δ is thought to be about 1.7 MeV in this nucleus, so all four of the observed states lie within the gap and must be presumed to be influenced by collective interactions. Numerous explanations have been proposed to account for the presence of such multiple 0^+ excitations in doubly-even deformed nuclei.[1] None of these explanations has been very successful, however, and it appears that further progress in this area must await more detailed experimental data.

One useful property of the $K=0^+$ excitations that may be extracted from decay data is the ratio of monopole to quadrupole decay into other 0^+ bands. This ratio is usually expressed as the X-parameter, $\rho^2 e^2 R_o^4/B(E2)$.

Table 1 gives a summary of the X-parameters for the $I\pi K=0+0$ and $2+0$ excitations in ^{170}Yb. Also shown in Table 1 are derived values for the nuclear monopole transition moment, ρ(E0) for cases where B(E2) data from the Coulomb excitation work of Riedinger, et al.[2] are available. The most evident conclusion that may be drawn from these data is that the 1228.9-keV 0^+ state seems to carry the bulk of the quadrupole vibrational strength in ^{170}Yb. The exact character of the other 0^+ states is still in question.

Table 1. Values of the Parameters $X=\frac{\rho^2 e^2 R_o^2}{B(E2)}$ for ^{170}Yb

Level(keV)	$I\pi K$	X	ρ^+
1069.4	$0+0_1$	0.0049	≤0.009
1145.6	$2+0_1$	≤0.032	≤0.01
1228.9	$0+0_2$	0.080	0.13
1306.4	$2+0_2$	≤0.14	
1479.9	$0+0_3$	0.94	
1534.5	$2+0_3$	≤1.2	
1566.4	$0+0_4$	0.54	
1634.8	$2+0_4$	≤0.50	

+Values for ρ derived with use of preliminary data of Riedinger, et al.[2]

Also of interest in the ^{170}Yb level scheme is the 2+2 γ-vibrational state ostensibly at 1138.6 keV. The γ-ray branching data and Riedinger's B(E2) data indicate very strong mixing between this state and the $2+0_1$ state.

It is also noteworthy that we are able to observe the E0 transitions between several of the excited 0^+ states in ^{170}Yb. The E0 moment, ρ(E0), between these states seems to be comparable to the moment to the ground state.

Finally, we are unable to identify in ^{170}Yb a level at 2533.1 keV previously thought to be of the type $I\pi K=1+0$.[3] According to Gabrakov et al.[4] such a state would be predominantly $\{5/2[523\downarrow]_n - 5/2[512\uparrow]_n\}$, but would also exhibit a weak collectivity proposed to arise from oscillations of the spin part of the nuclear magnetic dipole moment.

Details of the ^{170}Yb level scheme will be discussed further in a forthcoming publication.[5]

References

1. N.I. Pyatov, JINR Report P4-5422(1970); F.M. Bernthal, J.O. Rasmussen, and J.M. Hollander, Bull. Am. Phys. Soc. 15, 523(1970).
2. L.L. Riedinger, private communication (1971).
3. N.A. Bonch-Osmolovskaya, H. Ballund, A. Plochocki, Z. Preibisz, and A. Zglinski, Nucl. Phys. A162, 305(1971).
4. S.I. Gabrakov, A.A. Kuliev, and N.I. Pyatov, Sov. Journ. Nucl. Phys. (trans.) 12, 44(1971).
5. To be submitted to Physical Review.

*This work was supported in part by the U.S. Atomic Energy Commission.

**Lawrence Radiation Laboratory, Livermore, California 94550

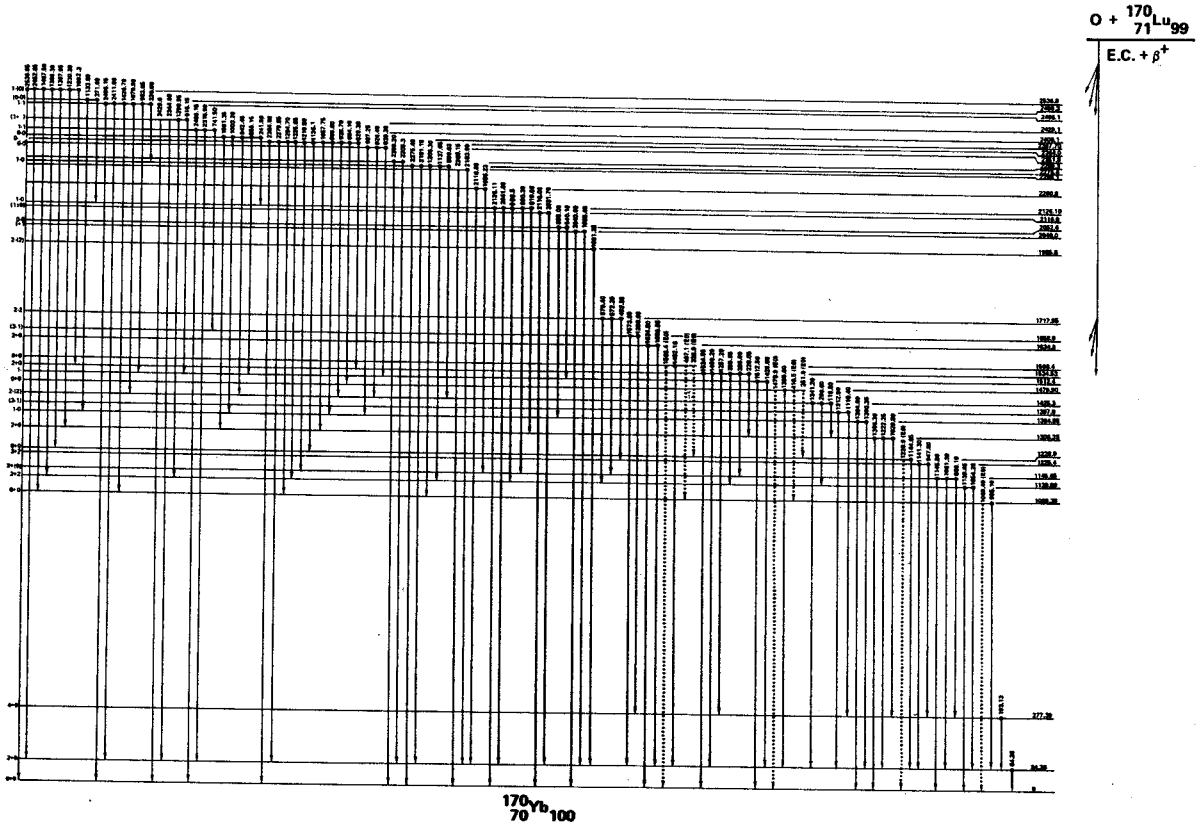

Fig. 1a Decay scheme for 0-2600 keV levels in ^{170}Yb populated by EC-β^+ decay of ^{170}Lu.

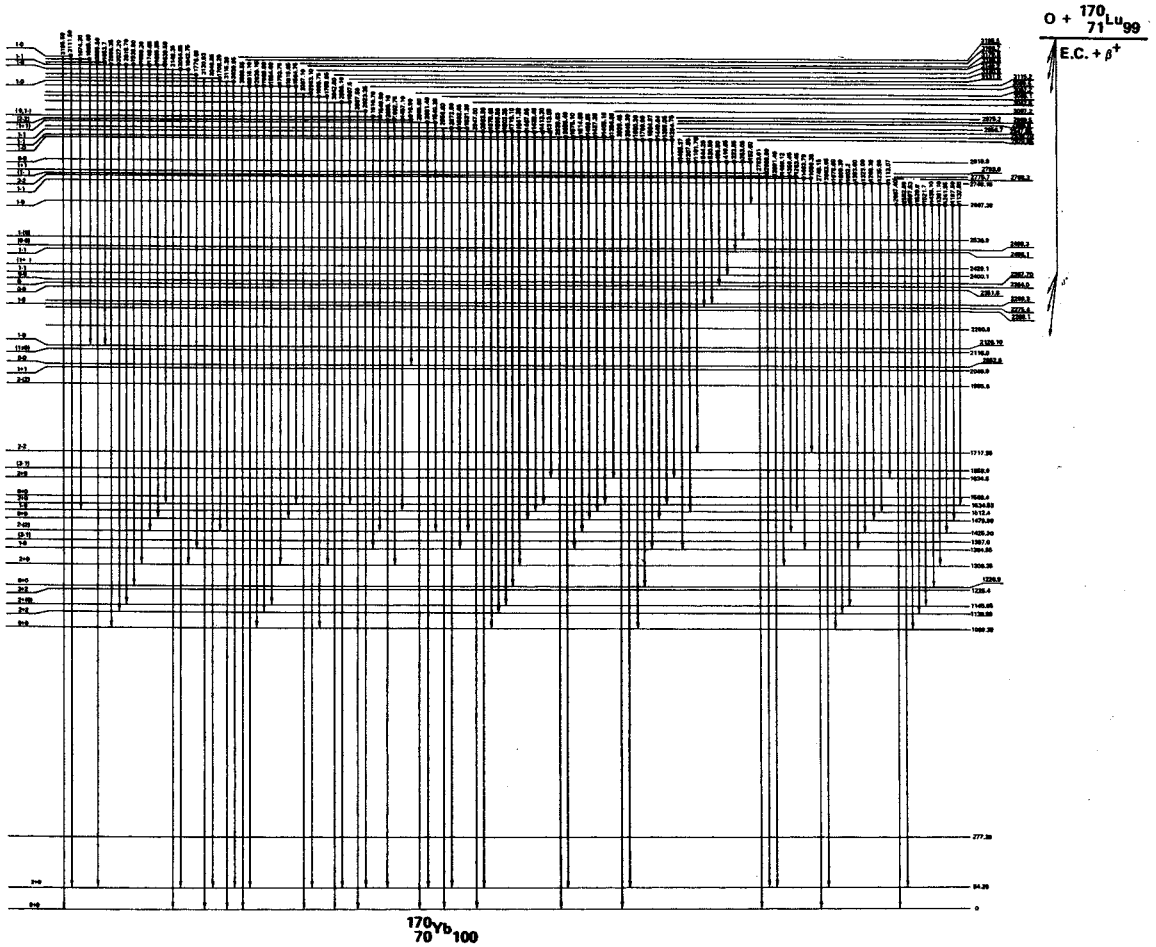

Fig. 1b Decay of 2600-3200 keV levels in ^{170}Yb populated by EC-β^+ decay of ^{170}Lu.

Study of Levels in Even-Even Deformed Nuclei by (^{3}He,d) and (^{4}He,t) Reaction Spectroscopy

F.M. Bernthal and R.A. Warner

One of the most puzzling phenomena discovered in recent years in the "well-understood" doubly-even deformed nuclei has been the systematic occurrence of multiple low-lying excited 0+ states. The energies of several of these states have commonly been found to lie within the pairing gap, 2Δ, a region once thought to be reserved for only 0+ states of the simplest quadrupole-type β-vibrations, and more recently, perhaps, for pairing vibrations. In ^{170}Yb for example,[1] no less than four 0+ states are observed below 1600 keV.

It has proved difficult to account for this phenomenon in ^{170}Yb as well as in other deformed nuclei. Though various explanations have been proposed,[2] none of them has been entirely satisfactory, and in the absence of detailed information on the structure of the multiple 0+ states, it has proved difficult to test the various collective interactions thought to influence these states.

Decay work has successfully identified the locations of many of the 0+ states, but details of their structure are perhaps best determined by other means. One such means is the use of single-particle and two-particle transfer reactions to deduce spectroscopic factors for populating the 0+ states. We have begun a program of study at the MSU Cyclotron Laboratory designed to extract the information on 0+ states that such transfer reactions can provide. Initial work has been carried out on levels in ^{170}Yb and ^{176}Hf by the ^{169}Tm(α,t), ^{169}Tm(^{3}He,d) and the ^{175}Lu(α,t) and ^{175}Lu(^{3}He,d) reactions. Multiple 0+ excitations in both residual nuclei are well characterized from earlier work. The experiments have been carried out with 33-MeV α-particles bombarding carbon-backed foils of the rare-earth metals. The outgoing particles were energy-analyzed in the MSU broad range Enge-type split-pole magnetic spectrograph and were collected on nuclear emulsion plates for counting.

To date, lower resolution studies ($\sim$25 keV FWHM for tritons) have revealed several qualitative features of the ^{170}Yb and ^{176}Hf nuclei in the region of interest, and it is already clear that there are wide variations in the proton-transfer cross-sections leading to the various 0+ levels in these nuclei. Further experiments are planned which will employ thinner targets in an effort to enhance the resolution. Also planned are (p,t) reaction studies of the same residual nuclei to measure the possible influence of neutron pairing vibrations on the observed 0+ states.

References

1. D.C. Camp and F.M. Bernthal, this report.
2. For an excellent review of current thinking on the subject, see N.I. Pyatov, JINR Report P4-5422(1970).

*This work supported in part by the U.S. Atomic Energy Commission.

In-Beam (α,xnγ) and (^{3}He,xnγ) Studies of Rotational Band Structure in Transitional Odd-Mass Deformed Nuclei*

F.M. Bernthal and R.A. Warner

Studies of the rotational band structure in deformed odd-A nuclei have yielded a substantial amount of information on the interaction between collective and single-particle motion in such nuclei. Most thoroughly studied has been the rotational band mixing that results from the Coriolis interaction. It has become common practice to solve for the perturbed quasi-particle wavefunctions at increasing rotational angular momentum by making use of the experimentally observed energies of rotational band members and then diagonalizing the complete Coriolis interaction matrix. The Nilsson wave-functions are most commonly used as a basis set in this type of calculation.

Such a procedure has apparently been quite successful in accounting for the highly perturbed band structure of the so-called "parity-unique" Nilsson states emanating from the $h_{11/2}$ and $i_{13/2}$ shell-model states. The behavior of odd-A nuclei near the edges of deformation is still poorly documented, however, and it appears that a substantially different treatment of the coupling between rotational and particle motion may be required in such nuclei.[1,2]

One method of tracing the transition from deformed to spherical equilibrium shape is to observe the breakdown of rotational band structure as one moves away from the regions of stable deformation. We have embarked on a program of study to elucidate the structure of such transitional nuclei. The techniques of (α,xn) and (^{3}He,xn) in-beam γ-ray spectroscopy are being employed. Because of the complex, poorly-ordered structure of these nuclei, γ-γ coincidence data are required to deduce band structure. Initial difficulties with electronic interference from the cyclotron RF oscillator seem now to have been overcome and excellent in-beam Ge(Li)-Ge(Li) coincidence data have been obtained. Full-width at half maximum time resolution for a detector system comprised of two large-volume coaxial detectors has been less than 15 nsec with a 20:1 dynamic range.

Initial studies are focusing on the N=105 and 107 isotones in an attempt to follow the behavior of the 9/2+[624] rotational band in the ^{179}W, ^{181}W, ^{181}Os, and ^{183}Os nuclei. This 9/2+ member of the $i_{13/2}$ family of Nilsson states has previously been shown to be highly perturbed.[3] Similar studies are planned for the transitional Sm and Gd nuclei. Preliminary data have now been obtained on ^{179}W, ^{183}Os, and ^{151}Gd.

References

1. P. Vogel, Phys. Letters 33B, 400(1970).
2. I. Rezanka, J.O. Rasmussen, and R. Needham, Preprint (1971).
3. F.M. Bernthal and J.O. Rasmussen, Nucl. Phys. A101, 513(1967); F.M. Bernthal, (Thesis) UCRL-18651(1969).

*This work supported in part by the U.S. Atomic Energy Commission.

The (p,t) Reaction on Rare Earth Nuclei

R. Goles

The (p,t) reaction on ^{141}Pr, ^{159}Tb, ^{165}Ho and ^{169}Tm has been carried out for the purpose of studying the general systematics of the (p,t) reaction on rare earth nuclei.

^{141}Pr(p,t) Experiment

In this study an ∿800 μg/cm metallic target of ^{141}Pr was bombarded with 40-MeV protons. An E-ΔE detector telescope consisting of two cooled Si surface barrier detectors was used to both identify and measure the energies of the outgoing scattered tritons. Triton spectra were collected between 15° and 65° at 5° intervals. Typical spectra taken at the lab angles of 25° and 35° are illustrated in Fig. 1. Overall experimental resolution for this study was 50 keV.

The experimental angular distributions obtained from this experiment together with distorted wave calculations[1] appear in Fig. 2. The $5/2^+ \rightarrow 5/2^+$ ground state transition clearly exhibits an angular distribution corresponding to a dominant $(d_{3/2})^2_{\ell=0}$ transfer.

The five distributions appearing below the $\ell=2$ designation in this figure all exhibit a characteristic $(d_{3/2})^2_{\ell=2}$ angular shape. Moreover this result is consistant with the vibrational character previously ascribed to these states.[2]

The remaining states in this figure all exhibit odd-ℓ angular shapes. This implies transitions corresponding to either an octupole core excitation or an $h_{11/2}$ neutron pickup. Both explanations eliminate the possibility of $\ell=1$ assignments for the 1.62-MeV and 2.05-MeV states.

The results of this experiment clearly illustrate the collective strength associated with the (p,t) reaction. Beside the ground state, only states having a collective and possibly $(\pi d_{5/2})^1 (\nu d_{3/2})^{-1} (\nu h_{11/2})^{-1}$ shell model origin were observed to be populated through this reaction.

^{159}Tb(p,t), ^{165}Ho(p,t), and ^{169}Tm(p,t) Experiments

In these studies a ∿300 μg/cm^2 target of the metallic rare earth was bombarded with 30-MeV protons. The scattered tritons were analyzed with an Enge-split-pole magnetic spectrometer and were collected on photographic plates. A typical spectrum obtained from these studies appears in Fig. 3. Overall experimental resolution obtained in these studies was in the range of 10-12 keV. Resolution obtained in the angular distribution study of the ^{159}Tb(p,t) reaction was in the 15-20 keV range.

In each of the deformed nuclei studied, a strong population of the ground state rotational band was observed with at least six band members being excited in each case. Moreover, a β vibrational band in ^{157}Tb and γ vibrational bands in ^{157}Tb and ^{163}Ho were also found to be strongly excited through this reaction. In addition, the ^{169}Tm(p,t) spectral results suggest the possible presence of a K=5/2 γ vibrational band at 1380 keV of excitation and the possibility of a K=1/2 β vibrational band at ∿1200 keV of excitation in ^{167}Tm. All bands were identified on the basis of systematics, previous results, consistant band member energy spacings and the proven directness of the (p,t) reaction at the bombarding energies used in these studies. The results of these studies which are summarized in Tables 1-3 clearly illustrate the power of using this reaction as a tool of probing the collective properties of deformed nuclei.

Angular distributions of low energy states populated through the ^{159}Tb(p,t) reaction were taken between 10° and 75° at 5° intervals and appear in Fig. 4 along with distorted wave predictions.[1] Of the members of the ground state rotational band populated through this reaction, only the ground state appears to be populated through a single dominant angular momentum transfer. The 5/2 and 7/2 members of this band appear to exhibit some $\ell=2$ strength, although the poor agreement between experiment and theoretical $\ell=2$ predictions make even this statement extremely uncertain.

The angular shapes exhibited by the first three members of the γ vibrational band are within statistical uncertainty identical, indicating a complete absence of $\ell=0$ strength in the transition to the 3/2 member of this band. Moreover, the angular shapes exhibited by these three states as well as the remaining two members of this band indicate that these states are populated by a complex mixture of several allowed ℓ values.

Unlike the γ vibrational band, the members of the β band appear to be populated through a single dominant angular momentum transfer. The overall shape and underlying strength of the $3/2^+$ experimental curve undoubtedly express its dominant $\ell=0$ character. The angular distributions of the remaining two members of this band both exhibit a characteristic $\ell=2$ angular shape.

Angular distributions of two additional states of unknown origin were determined in the study and appear under the heading "Other States".

References

1. R.W. Goles, Ph.D. Thesis, Michigan State University (1971).
2. D.B. Beery, W.H. Kelly, and Wm.C. McHarris, Phys. Rev. 188, 1851(1969).
3. G. Winter, L. Funke, K. Hohmuth, K.H. Kaun, P. Kemnitz, and H. Sodan, Nucl. Phys. A151, 337(1969).

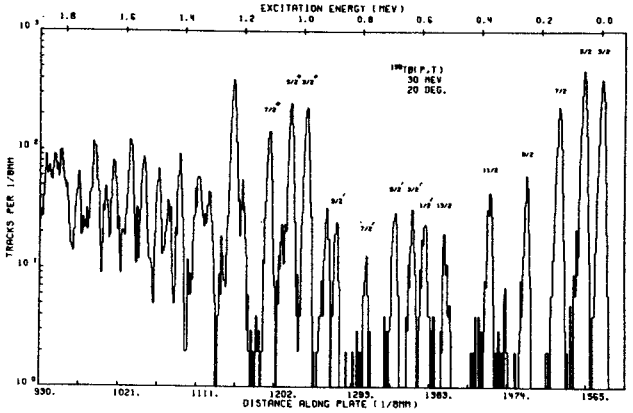

Fig. 3. $^{159}Tb(p,t)$ spectrum obtained at the laboratory scattering angle of 20°.

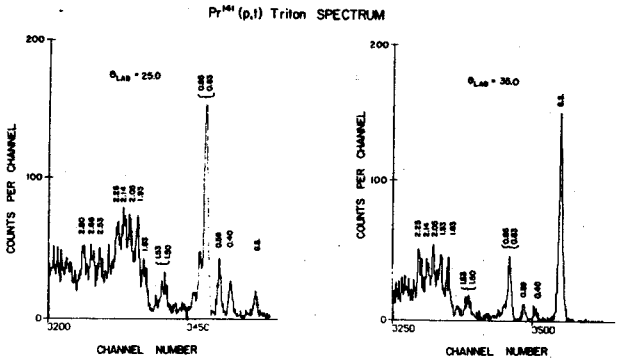

Fig 1. $^{141}Pr(p,t)$ triton spectra taken with an E-ΔE detector telescope.

Table 1. States Populated Through the $^{159}Tb(p,t)$ Reaction.

Energy (keV)	Energy[a] (keV)	Theory (keV)	Assignment[b] J^π	Energy (keV)	Energy[a] (keV)	Theory (keV)	Assignment[b] J^π
G S	G S	---	$3/2^+$	1120	---	1124	$7/2^{+\prime+}$
61	60.8	---	$5/2^+$	1207	---		---
144	143.8	---	$7/2^+$	1238	---	1241	$(9/2^{+\prime+})$
254	---	252	$9/2^+$	1276	---		---
325	---		---	1318	---		---
379	---	384	$11/2^+$	1352	---		---
527	---	539	$13/2^+$	1417	---		---
598	597.5	---	$1/2^{+\prime}$	1454	---		---
640	637.5	---	$3/2^{+\prime}$	1487	---		---
699	697.4	---	$5/2^{+\prime}$	1535	---		---
795	---	797	$7/2^{+\prime}$	1578	---		---
896	---	898	$9/2^{+\prime}$	1602	---		---
927	---	923	$17/2^+$	1631	---		---
947	---		---	1659	---		---
994	992.6	---	$3/2^{+\prime+}$	1695	---		---
1048	1044.5	---	$5/2^{+\prime+}$	1749	---		---
1080	---		---				

[a] F. H. Blichert-Toft, E. G. Funk, and J. W. Mihelich , Nucl. Phys. A100, (1967) 369-391.
[b] 1 = member of ground state rotational band; 1' = member of K=K_π-2 γ-vibrational band.
1'' = member of K=K_π ±-vibrational band.

Table 2. States Populated Through the $^{165}Ho(p,t)$ Reaction.

Energy (keV)	Theory (keV)	Assignment[a] J^π	Energy (keV)	Theory (keV)	Assignment[a] J^π
G S	---	$7/2^-$	1117		---
100	---	$9/2^-$	1156		---
224	222	$11/2^-$	1175		---
369	367	$13/2^-$	1194		---
533	533	$15/2^-$	1232		---
560	---	$3/2^{-\prime}$	1245		---
618	---	$5/2^{-\prime}$	1259	1256	$15/2^{+-}$
695	699	$7/2^{-\prime}$	1286		---
720	722	$17/2^-$	1308		---
755		---	1345		---
791		---	1373		---
807	804	$9/2^{-\prime}$	1419		---
826		---	1441		---
898		---	1457		---
912		---	1513		---
926	931	$11/2^{-\prime}$			
1060		---			
1075	1082	$13/2^{-\prime}$			

[a] 1 = member of ground state rotational band; 1' = member of K=K_π-2 γ-vibrational band

Table 3. States Populated Through the $^{169}Tm(p,t)$ Reaction.

Energy (keV)	Energy[a] (keV)	Assignment[b] J^π
10	G S	$1/2^+$
	10.4	$3/2^+$
117	116.6	$5/2^+$
142	142.4	$7/2^+$
329	326.5	$9/2^+$
374	371.0	$11/2^+$
470	---	---
604	---	---
624	---	---
663	---	---
682	---	---
706	---	---
1010	---	---
1092	---	---
1154	---	---
1192	---	---
1210	---	---
1283	---	---
1320	---	---
1380	---	$5/2^{+\prime+}$
1404	---	$7/2^{+\prime+}$
1434	1435[c]	$9/2^{+\prime+}$
1457	---	---
1486	---	---
1526	---	---
1574	---	---
1598	---	---
1625	---	---
1655	---	---

a) Ref. 3
b) 1 and 1''' are members of the ground and γ vibrational bands respectively.
c) Energy calculated from the first two members of this band.

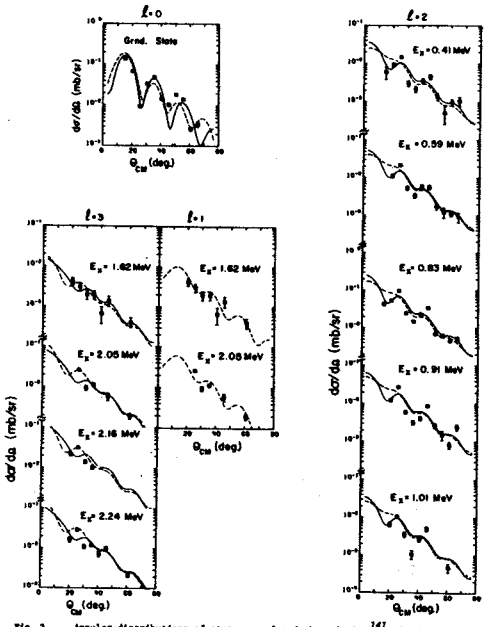

Fig. 2. Angular distributions of states populated through the $^{141}Pr(p,t)$ reaction. Theoretical two neutron pick-up and cluster transfer calculations are represented by continuous and broken curves respectively. Relative cross sections have been normalized to reflect measured absolute values.

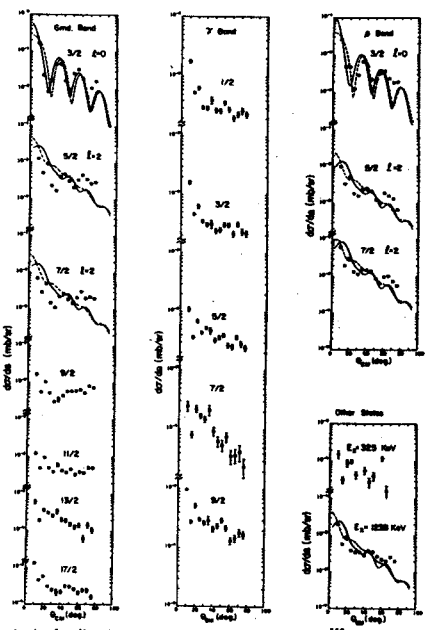

Fig. 4. Angular distributions of states populated through the $^{166}Tm(p,t)$ reaction. Theoretical two neutron pick-up and cluster transfer calculations are represented by continuous and broken curves respectively. Relative cross sections have been normalized to reflect measured absolute values.

The β^+/ε Decay of ^{143}Eu

Richard B. Firestone

The decay of ^{143}Eu was first studied by Kotajima and Malan,[1,2] who measured its half-life (2.6 min) and β-endpoint energy (4.0 MeV). No γ-ray decay schemes were reported, presumably because of the weak transitions and the interference of the short-lived ^{143}Sm daughter decay. ^{143}Sm has been part of a continuing study of N=81 isotones by the Nuclear Spectroscopy Group at Michigan State University, and the ^{143}Eu decay scheme is a welcome by-product of this study.

^{143}Eu was prepared by the reaction ^{144}Sm(p,2n)^{143}Eu on a separated isotope target (95.10% ^{144}Sm), using 28-MeV protons from the Michigan State University Sector Focused Cyclotron. As the ^{143}Sm daughter has a half-life of only 8.8 min, a series of 9 min spectra were taken so that the transitions arising from various decays could be separated by half-life. Figure 1 shows the first 9 min spectrum which was accumulated starting 2 min after bombardment to allow very short-lived activities to decay away. This spectrum was taken with a 10.4% Ge(Li) detector of 2.1-keV (FWHM) resolution at 1332 keV.

From the ^{144}Sm(p,d)^{143}Sm reaction data of Jolly and Kashy,[3] levels in ^{143}Sm were found at 0.110 MeV ($1/2^+$), 0.76 MeV ($11/2^-$), 1.11 MeV ($5/2^+$), 1.36 MeV ($7/2^+$), 1.53 MeV ($5/2^+$), 1.72 MeV ($5/2^+$), 1.95 MeV ($1/2^+$), 2.06 MeV ($5/2^+$), 2.06 MeV $5/2^+$), 2.16 MeV ($7/2^+$), and 2.29 MeV ($7/2^+$). Using this information, and energy sums and intensity balances for γ rays seen in the present study, a tentative decay scheme for ^{143}Eu has been prepared, and is shown in Fig. 2. None of the energies and intensities or log ft values given in this decay scheme are to be taken as well-established, as more definitive experiments are still in progress.

References

1. K. Kotajima, K.W. Brockman, and G. Wolzak, Nucl. Phys. 65, 109(1965).
2. H.P. Malan, H. Munzel, and G. Pfenning, Radiochem. Acta. 5, 24(1966).
3. R.K. Jolly and E. Kashy, MSUCL-28, 1970.

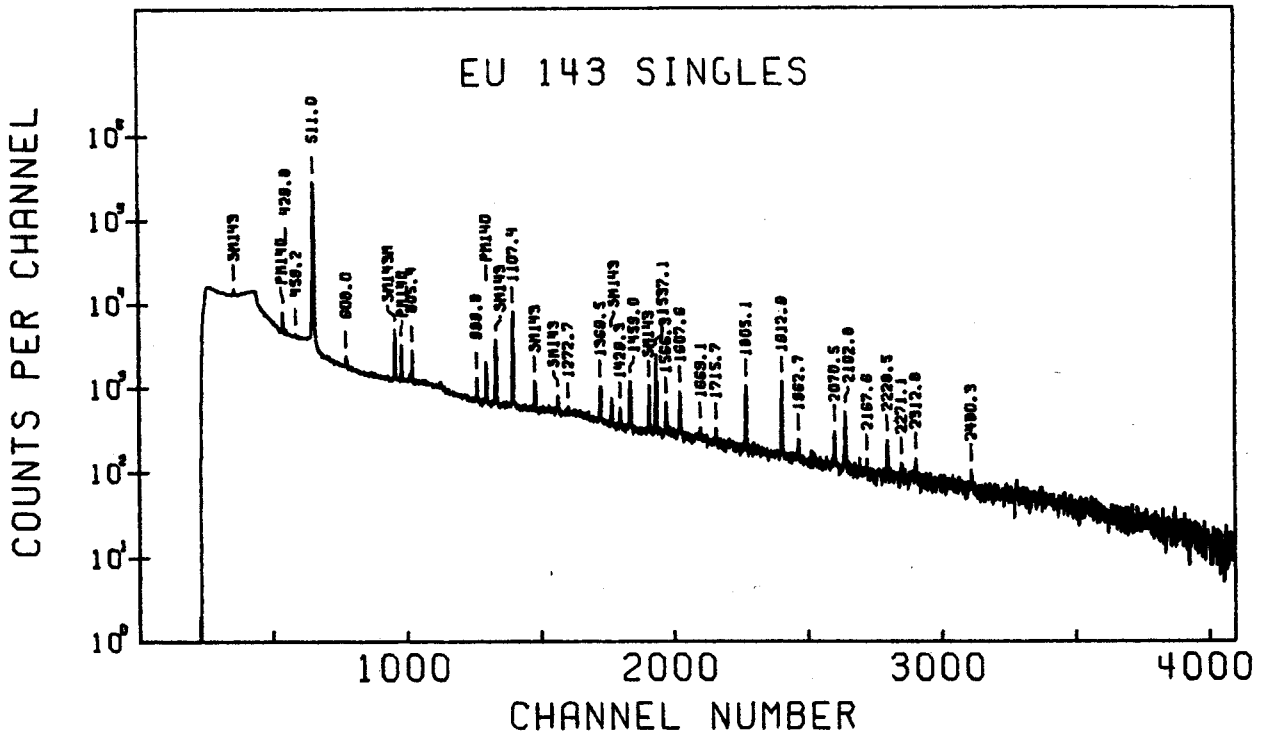

Fig. 1 γ-ray singles spectrum for ^{143}Eu.

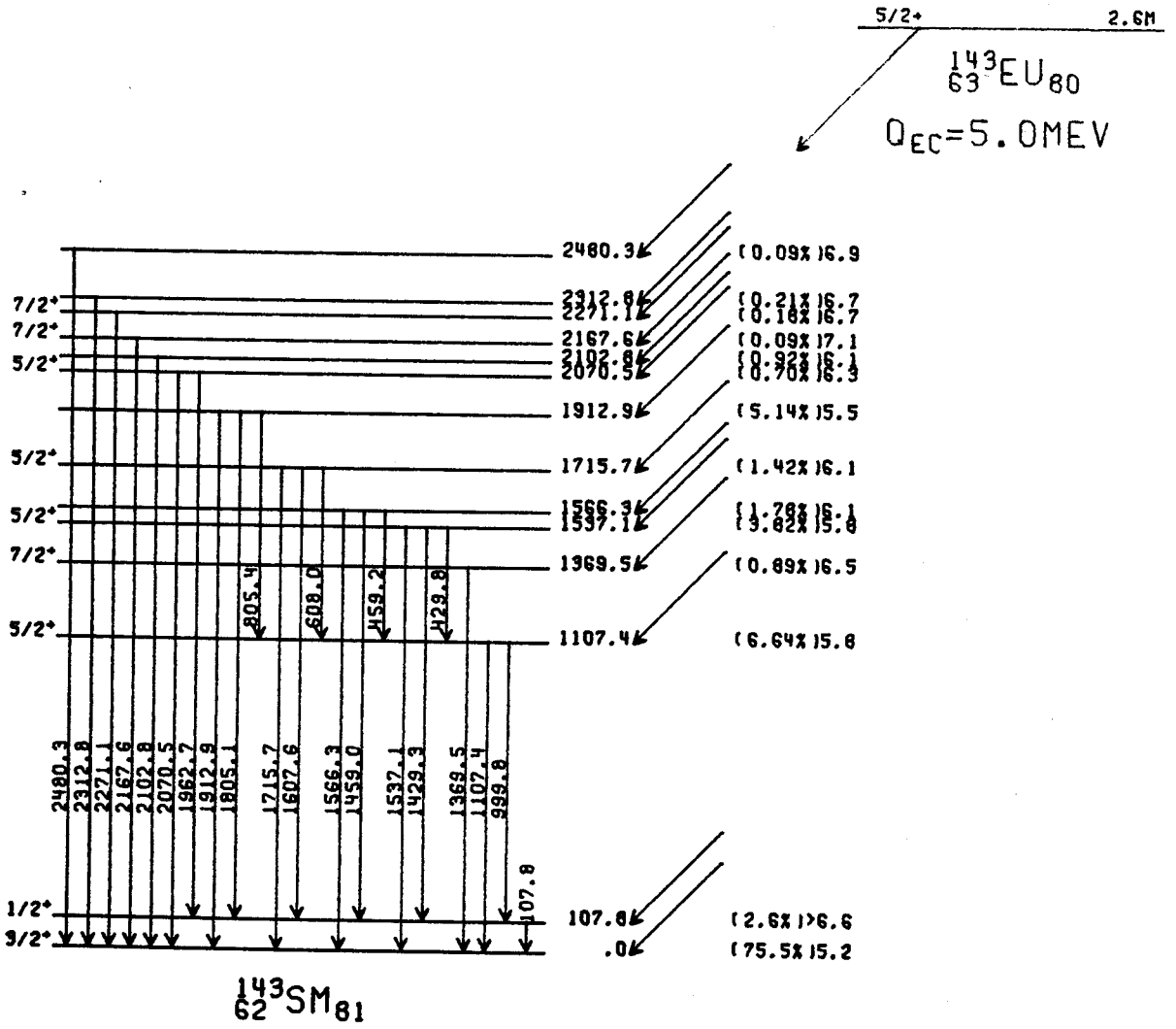

Fig. 2 Decay scheme for ^{143}Eu.

The β^+/ε Decay of ^{143}Sm

Richard B. Firestone

The decay of ^{143}Sm has been studied most thoroughly by Frenne, Heyde, et al.[1,2] They produced ^{143}Sm by the (γ,n) reaction on natural Sm_2O_3 (3.09% ^{143}Sm). A decay scheme was presented along with several log ft values.

The study of the ^{143}Sm decay is of considerable interest in the light of previous work[3,4] on the neighboring odd Z, N=81 isotones, ^{141}Nd and ^{145}Gd. All three isotones have $11/2^-$ metastable states at 720-756 keV with 60- to 85-sec half-lives. The ^{143}Sm and ^{145}Gd metastable states were found to have small β branches in their decays.

Of further interest are the $7/2^+$ first-excited states in the daughters of all three isobars. These appear to be the $1g_{7/2}$ quasiparticle states predicted for N=82 nuclei by Kisslinger and Sorenson.[6] These states occur at 145.4, 272.9, and 329.5 keV in ^{141}Pr, ^{143}Pm, and ^{145}Eu, respectively. The log ft values given for the $7/2^+$ states in ^{141}Pr and ^{145}Eu were 8.8 and 7.5. Prior to this study, no value was reported for the log ft of the corresponding state in ^{143}Pm, but since the transition to this state is from the $3/2^+$ ground state of ^{143}Sm, this second-forbidden transition might be expected to lie in the range $10 \leq \log ft \leq 14$. The transitions to the $7/2^+$ states in the other two nuclei are also second forbidden however, suggesting that the ^{143}Sm decay to the $7/2^+$ state may also show an abnormally low log ft value.

In an attempt to measure this log ft, and to determine more precisely other properties of the decay scheme for ^{143}Sm, the reaction ^{142}Nd(^{3}He,2n)^{143}Sm was first tried. This reaction proved unsatisfactory, as the rather loosely bound α particles in this region make the (^{3}He,^{4}He n) reaction more probable. The problem is compounded by the fact that ^{143}Sm decay goes overwhelmingly to the ground state of ^{143}Pm.

The reaction ^{144}Sm(p,2n)^{143}Eu, in which the 2.6-min ^{143}Eu quickly decays to its ^{143}Sm daughter, has been used with more success. The ^{143}Eu decay is discussed in another section. Singles spectra of ^{143}Sm have been taken using a 10.4% Ge(Li) detector with 2.1-keV (FWHM) resolution, and peak-to-Compton ratio of 38:1 at 1332 keV. To separate the ^{143}Eu and ^{143}Sm activities, a series of spectra at 9-min intervals were accumulated, starting 2 min after bombardment and continuing until all short-lived activity was unnoticeable. The fourth 9-min spectrum is shown in Fig. 1, and consists primarily of transitions originating from ^{143}Sm. A tentative decay scheme for ^{143}Sm is given in Fig. 2, based on the ^{142}Nd(^{3}He,d) results of Wildenthal as well as the current study.

The log ft value for the second forbidden decay to the 272.9-keV level is seen to be 8.1, much lower than usual, but similar to those for the corresponding decays of ^{145}Gd and ^{141}Nd.

References

1. D. De Frenne, K. Heyde, L. Dorikens-Vanpraet, M. Dorikens, and J. Demuynck, Nucl. Phys. A110, 273(1968).
2. D. De Frenne, E. Jocobs, and J. Demuynck, Z. Physik 237, 327(1970).
3. D.B. Beery, W.H. Kelly, and Wm.C. McHarris, Phys. Rev. 171, 1283(1968).
4. R.E. Eppley, Ph.D. Thesis, Michigan State Univ. (1970).
5. J. Felsteiner and B. Rosner, Phys. Letters 31B, 12(1970).
6. K.S. Kisllinger and R.A. Sorenson, Revs. Mod. Phys. 35, 853(1963).
7. H.J. Bleyl, H. Munzel, and G. Pfennig, Radiochem, Acta, 9, 173(1968).

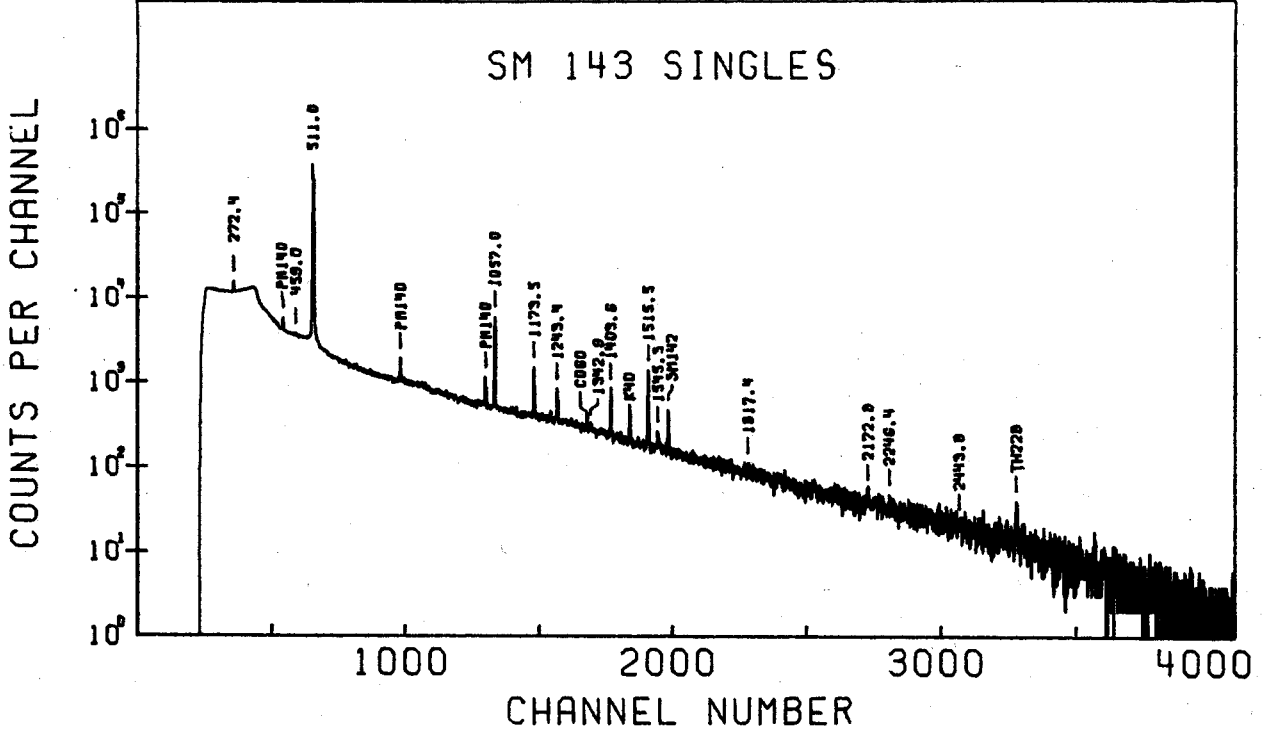

Fig. 1 γ-ray singles spectrum for ^{143}Sm.

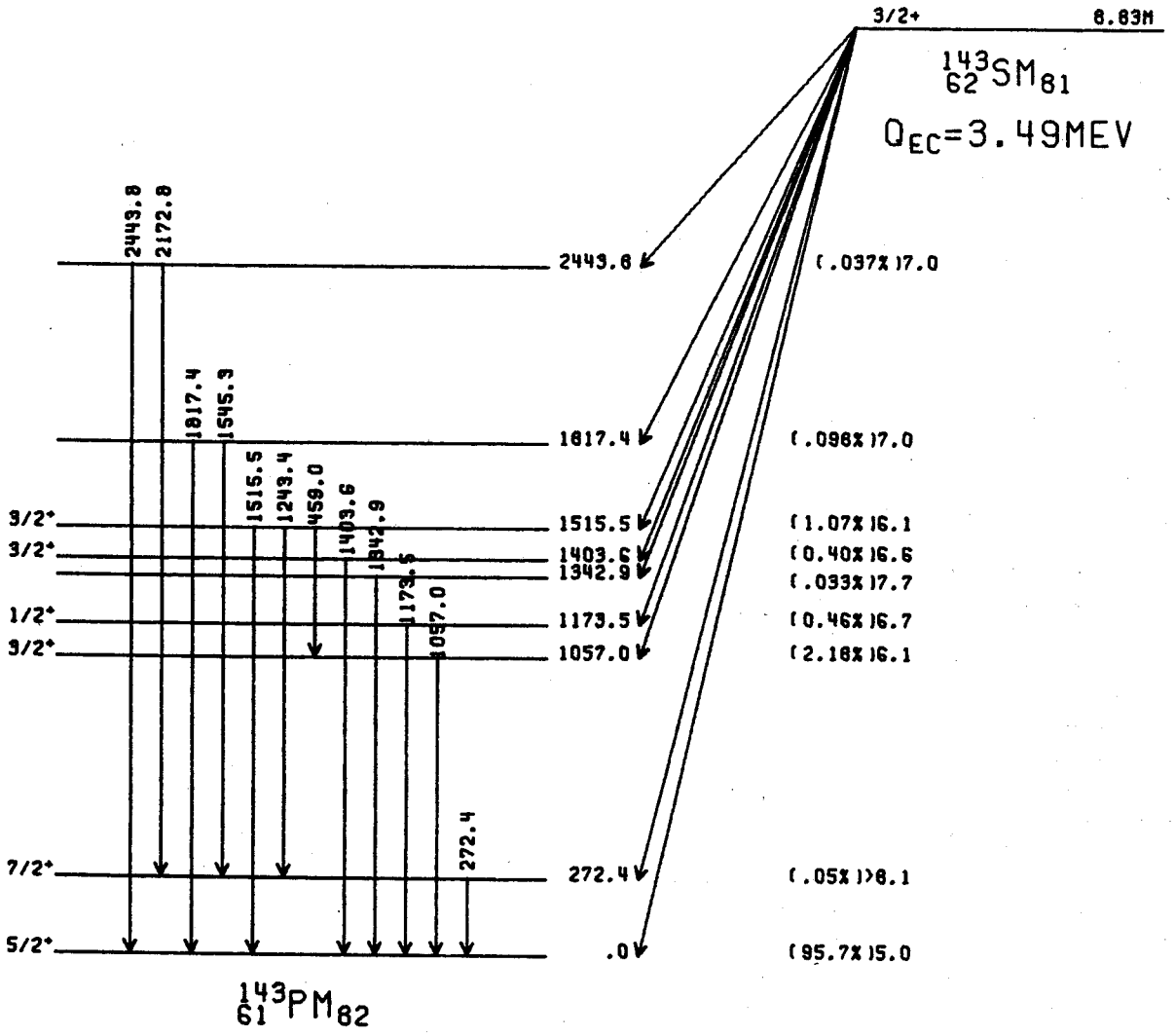

Fig. 2 Decay scheme for ^{143}Sm.

The Decay of $^{141}_{61}Pm_{80}$ to States in $^{141}_{60}Nd_{81}$

F.Y. Yap,* R.T. Todd, R. Warner, W.H. Kelly, and Wm.C. McHarris

$^{141}_{60}Nd_{81}$ is a link in the chain of nuclides near the N=82 closed shell, a region of the nuclidic chart which the nuclear γ-spectroscopy group is currently investigating. We have made measurements of the states of this isotope resulting from the β^+/ε decay of $^{141}_{61}Pm_{80}$.

Our samples were prepared via the $^{144}Nd(p,2n)^{141}Pm$ reaction. We bombarded the powdered oxide, Nd_2O_3, of the 99.9% pure separated isotope for typically 0.5-2 min with a 0.5-3 μA 25 MeV proton beam from the MSU cyclotron. Counting was usually started 5-10 min after bombardment after most of the suspected short-lived contaminants had decayed.

Unravelling the decay scheme required experiments of various configurations: γ-ray singles, two-dimensional "megachannel" γ-γ coincidence, anticoincidence, and γ-511-511 keV coincidence. For our main runs we used at various times four Ge(Li) detectors of 1.0%, 2.5%, 4.5%, and 10.4% efficiency to record the high resolution γ-ray spectra, with resolutions typically ranging from 2.0 to 3.5 keV at the 1.33 MeV γ-ray of ^{60}Co. An 8x8 inch NaI(Tl) split annulus was also used for the γ-511-511 keV coincidence and anticoincidence detection. Standard NIM electronics were employed for amplifying, gating, and timing, and the data were analyzed by one or more 4096-channel ADC's coupled to either the MSU Sigma-7 or the PDP-9 computer. Various in-house computer codes such as MOIRAE, EVENT RECOVERY, MOIRAE(EI) and SAMPO[1] were then used to help reduce the data to energies, intensities and log ft values necessary for the construction of the decay scheme.

Our results are presented in Table I, where we list the energies and relative intensities of the γ-rays observed in the various experiments. The γ-rays belonging to our decay scheme were identified on the basis of their half-lives. From the data we were able to deduce the decay scheme shown in Fig. 1. The transition and excited-state energies are given in keV, and the disintegration energy Q_ε is taken to be the value measured by Charvet et al.[2] All the transition intensities are expressed in percent of the total ^{141}Pm disintegrations, and the log ft values are calculated on the basis of a measured 20.6-min half-life for ^{141}Pm. The possible spin and parity assignments are listed in Table II and were made from an examination of the log ft values, as well as the electromagnetic transition rates to levels of known spins and parities. Those assignments which are less probable are enclosed in parentheses. For comparison, we also list in the same table the spins and parities obtained by Jolly and Kashy[3] for corresponding levels from their deuteron angular distribution studies of the $^{142}Nd(p,d)^{141}Nd$ reaction.

In the main our decay scheme is in good agreement with that proposed by Charvet et al.,[2] but we have greatly extended the number of γ-ray transitions and the range of levels. There are a few noteworthy differences. The amounts of β-feeding to the various levels in ^{141}Nd differ appreciably, especially in the ground state transition, where we obtain 88.6% feeding while they saw 95% feeding. We placed a new level at 1051.9 keV based on the existence of a γ-ray of that energy with the correct half-life, as well as its enhancement in the γ-511-511 keV coincidence experiment. The new level at 2066.4 keV rests on the observation of a γ-ray of that energy and another of 1872.6 keV in coincidence with the 193.8 keV γ-ray from the first excited state. The levels at 2246.6, 2303.4, 2354.4, 2388.4, 2620, and 2805 keV are supported by the results of our anticoincidence experiment. From the sums and differences of several observed γ-rays with the requisite half-life, as well as the anticoincidence results, we also place a level at 2506 keV. The remaining new levels are only tentative since they are based solely on their observed half-lives and relatively large energies.

Table I. Relative Intensities of γ-rays in the Decay of ^{141}Pm in Various Experiments.

Energy (keV)	Singles	Anti-Coinc.	Integral Coinc.	194 keV Gated Coinc.	γ-511-511 keV Coinc.
180.2	0.6				
193.8	34.9	26.4	574.1		7.5
289.4	3.6		39.6	1.9	
511.0	2385.	---a	----a	---a	65.5
538.2	1.7		7.4		
544.7	1.4				
597.2	1.2		4.7		
622.2	18.9	7.3	58.7		4.6
647.2	1.3				
706.0	1.0				
886.3	52.5	20.5	114.3	3.3	4.2
901.2	1.1				
958.7	1.3		2.1		
966.3	2.0		3.4		
1022.8	2.8		4.7		
1029.9	7.8	1.9	17.3	6.9	5.3
1051.9	2.0				12.6
1080.7	1.0				
1223.3	100.0	56.1	100.0		100.0
1282.1	0.9				3.3
1345.8	27.6	9.0	39.3		8.6
1371.0	2.2		2.7	2.8	
1403.2	16.0	5.8	17.5	16.0	6.6
1564.8	17.9	13.9	6.5		16.9
1596.8	16.1	16.1	3.2		19.4
1626.7	5.8		7.1	5.8	
1703.8	1.2		0.7	0.6	
1820.4	1.6	2.0	1.0		
1872.6	0.5		0.8	1.3	
1879.9	6.9	3.8	4.2	6.0	
1897.1	1.1				
1967.6	3.6	3.4			
2052.8	2.6			2.5	
2066.2	1.3				
2073.7	13.4	16.0			1.8
2109.6	1.8	2.5			

Energy (keV)	Singles	Anti-Coinc.	Integral Coinc.	194 keV Gated Coinc.	γ-511-511 keV Coinc.
2145.2	0.3				
2246.4	1.5	2.5			
2265.3	0.7				
2303.4	2.4	2.5			
2311.6	0.5				
2354.4	1.0	1.1			
2388.4	1.3	1.5			
2429.8	0.6	0.3			
2505.0	0.6	0.5			
2602.1	0.1				
2619.6	0.4	0.3			
2804.9	0.5	0.3			
2985.5	0.9				

[a]Not measured in total annihilation.

Table II. Spins and Parities of States in ^{141}Nd Obtained in this work and by Jolly and Kashy.

This Work		Jolly & Kashy	
E (keV)	J^π	E (MeV)	J^π
0	$3/2^+$	0	$3/2^+$
193.8	$1/2^+$	0.19	$1/2^+$
756.7	$11/2^-$	0.76	$11/2^-$
1051.9	$3/2^-,5/2^-,7/2^-$		
1223.3	$5/2^{+(-1)}3/2^{+(-)}$	1.20	$5/2^+$
1345.8	$7/2^{+(-)}$	1.33	$(7/2^+)$
1564.8	$5/2^+,(3/2^+)$	1.56	$(5/2^+)$
1596.8	$3/2^\pm,(5/2^\pm)$		
1820.4	$5/2^{+(-)},(3/2^\pm)$	1.80	$(5/2^+)$
1897.1	$3/2^\pm,(5/2^\pm)$	1.87	$1/2^+$
1968.0	$7/2^\pm,(5/2^\pm),(3/2^\pm)$		
2066.4	$3/2^\pm,(5/2^\pm)$	2.06	$(5/2^+)$
2073.7	$3/2^\pm,(5/2^\pm)$		
2109.6	$5/2^+,(3/2^+)$	2.19	$11/2^-$
2145.2	$3/2^-,5/2^-,7/2^-$		
2246.6	$3/2^+,5/2^+,7/2^+$		
2265.3	$3/2^\pm,5/2^\pm,7/2^\pm$		
2303.4	$5/2^+,7/2^+$	2.30	$(7/2^+)$
2354.4	$3/2^\pm,5/2^\pm,7/2^\pm$		
2388.4	$3/2^\pm,5/2^\pm,7/2^\pm$		
2430	$3/2^\pm,5/2^\pm,7/2^\pm$		
2506	$3/2^+,5/2^+,7/2^+$		
2620	$3/2^\pm,5/2^\pm,7/2^\pm$		
2805	$3/2^\pm,5/2^\pm,7/2^\pm$		
2986	$3/2^\pm,5/2^\pm,7/2^\pm$		

We are indebted to Dr. Henry Blosser and the clerical and computer staff of the MSU Cyclotron Laboratory for their assistance during various phases of this work. We also thank Dr. Dwight Beery and Messers Kenneth Kosanke, Clare Morgan, and William Chaffee for their helpful discussions and aid in data reduction.

References

1. J.T. Routti and S.G. Prussin, Nucl. Instr. and Methods 72, 125(1969).
2. A. Charvet, R. Duffait, A. Emsallem, and R. Chery, Journ. de Physique 31, 737(1970).
3. R.K. Jolly and E. Kashy, Phys. Rev. (to be published, 1971).

*NSF Summer Research Participant. Permanent address: Department of Physics, Wilson College, Chambersburg, Pa. 17201

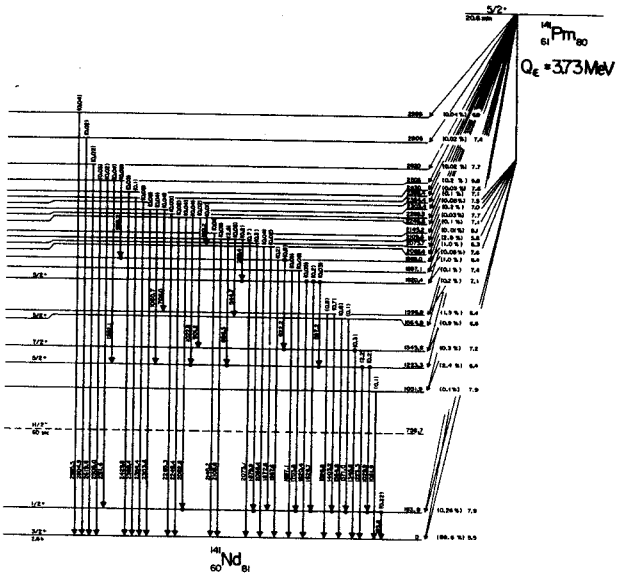

Fig. 1 The decay scheme of $^{141}_{61}Pm_{80}$ deduced from the present study. Energies are given in keV and transition intensities are given in percent of the total ^{141}Pm disintegrations.

The Electron Capture Decay of ^{56}Ni

L. Samuelson

The electron capture decay of ^{56}Ni was used as part of a study of the levels of ^{56}Co below 1.8 MeV of excitation. Singles γ-ray spectra and γ-γ coincidence spectra using a Ge(Li)-Ge(Li) spectrometer were taken of the ^{56}Ni electron capture decay. These two experiments yielded γ-ray energies and intensities and γ-ray placement in the ^{56}Ni decay scheme.

The 6.1-day ^{56}Ni activity was produced via the ^{56}Fe(^{3}He,3n)^{56}Ni reaction (Q = -16.3 MeV) by bombarding a 0.001 inch iron foil with 70 MeV ^{3}He particles (reduced to approximately 45 MeV with an aluminum absorber) from the M.S.U. cyclotron. After a 10-day wait to allow the 1.5-day ^{57}Ni contaminant activity to die down, and an appropriate chemical separation, the source was dissolved in 15N HCl and placed in a plastic vial for counting.

Singles spectra were taken at two different source to detector distances (for identification of sum peaks) with both a 2.5%-efficient Ge(Li) detector and a 10.4%-efficient Ge(Li) detector. Fig. 1 shows a typical ^{56}Ni singles spectrum. All singles spectra were analyzed using the peak-fitting computer code SAMPO.[1] After correcting the measured peak areas for the relative γ-ray detector efficiencies and averaging several runs, the ^{56}Ni γ-ray intensities were obtained and are listed in Table 1. The ^{56}Ni γ-ray energies were measured by counting several well-known γ-ray energy standards simultaneously with the ^{56}Ni activity. A quadratic least-squares fit was then made to the resulting peak centroids and calibration energies in two energy regions (100-800 keV and 700-2000 keV). The ^{56}Ni γ-ray energies obtained are listed in Table 1.

Table 1. Energies and relative intensities of γ-rays from the electron capture decay of ^{56}Ni.

Energy keV	Relative γ-ray intensity
158.4±0.1	100.
269.5±0.1	36.0±1.4
480.5±0.1	36.0±1.5
749.9±0.1	50.5±2.5
811.8±0.1	88.5±4.4
1562.0±0.2	14.3±1.4

The two parameter γ-γ prompt coincidence experiment was performed with a 4.5%-efficient Ge(Li) detector and a 10.4%-efficient Ge(Li) detector placed in a 150° geometry with a graded lead absorber placed between them to prevent Compton scattering from one detector into the other. Coincident events (resolving time 2t=100 nsec) from both sides were processed and their addresses listed in pairs on magnetic tape using the M.S.U. cyclotron Sigma-7 computer code EVENT.[2] This listing yielded a 4096x4096-channel array of prompt-coincidence events which were sorted off-line in gated slices including background subtraction, using the computer code EVENT RECOVERY.[3] The resulting any-coincidence and gated spectra are shown in Fig. 2 and the coincidence results are summarized in Table 2.

Table 2. Summary of γ-γ prompt coincidence results.

	Coincidence relations						
Gamma ray	158	269	480	511(β^+)	750	812	1562
158		yes	yes	no	yes	yes	yes
269	yes		yes	no	no	yes	no
480	yes	yes		no	no	yes	no
511(β^+)	no	no	no		no	no	no
750	yes	no	no	no		yes	no
812	yes	yes	yes	no	yes		no
1562	yes	no	no	no	no		

Finally the resulting ^{56}Ni electron capture decay scheme is presented in Fig. 3. Internal conversion corrections have been included using internal conversion coefficients measured by Jenkins and Meyerhof.[4] Decay intensities are normalized to 100 decays of the 158.4-keV first excited level. This decay scheme corroborates those presented elsewhere by Ohnuma,[5] et al., and Piluso,[6] et al.

References

1. J.T. Routti, S.G. Prussin, Nucl. Instr. and Meth., 72, 125(1969).
2. EVENT, computer code written by D. Bayer, unpublished.
3. EVENT RECOVERY, computer code written by D.B. Beery and G. Giesler, unpublished.
4. R.C. Jenkins, W.E. Meyerhof, Nucl. Phys. 58, 417(1964).
5. Hajime Ohnuma, Joshio Hashimoto, and Isao Tomita, Nucl. Phys. 66, 337(1965).
6. C.J. Piluso, D.O. Wells, and D.K. McDaniels, Nucl. Phys. 77, 193(1966).

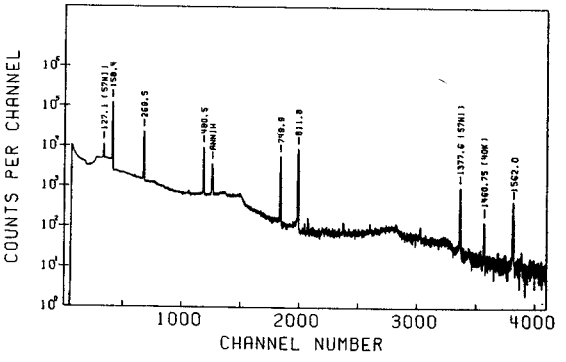

Fig. 1 Typical ^{56}Ni singles spectrum.

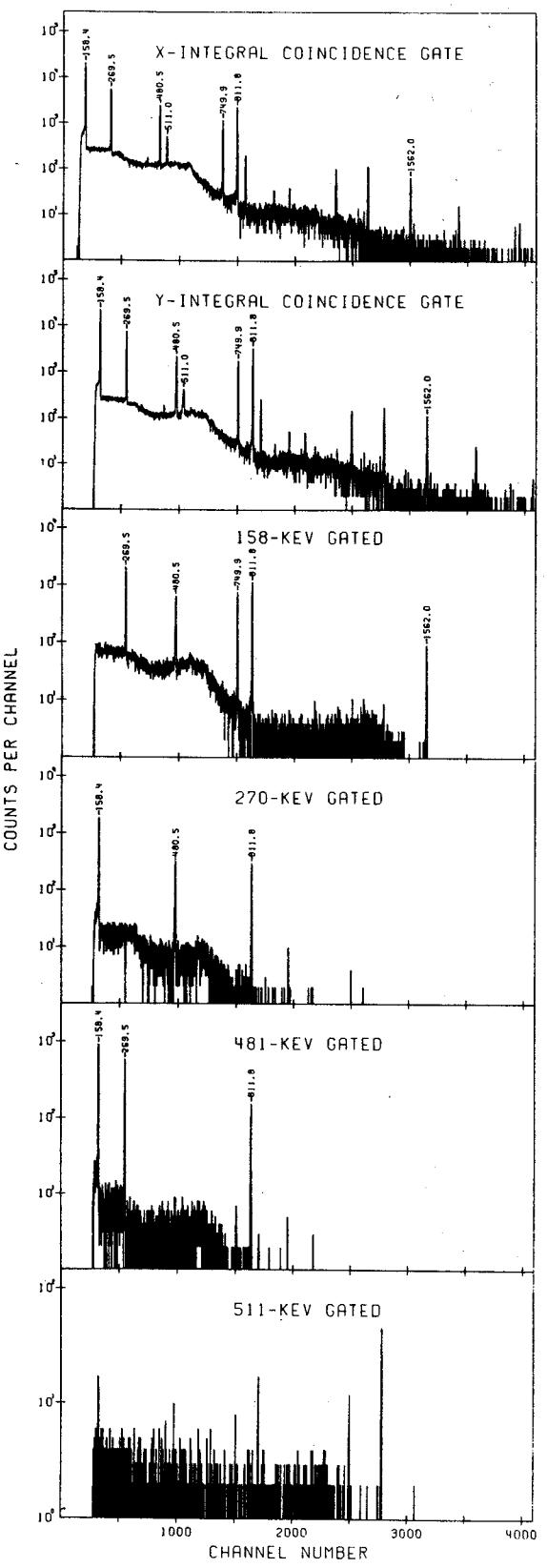

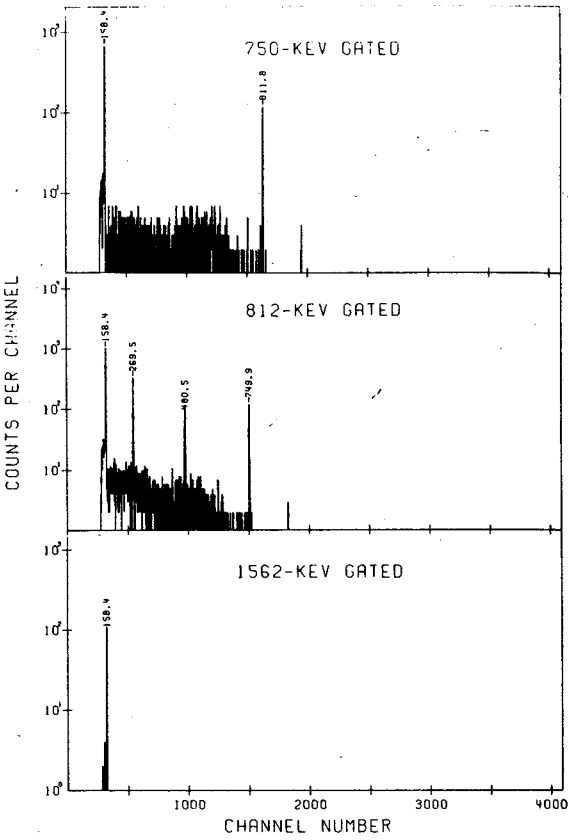

Fig. 2 Integral coincidence and gated spectra of the ^{56}Ni γ-γ coincidence experiment. Unlabelled weak peaks in the gated spectra are either triple coincidences where two of the γ rays have been summed in one detector or chance coincidences with intense peaks.

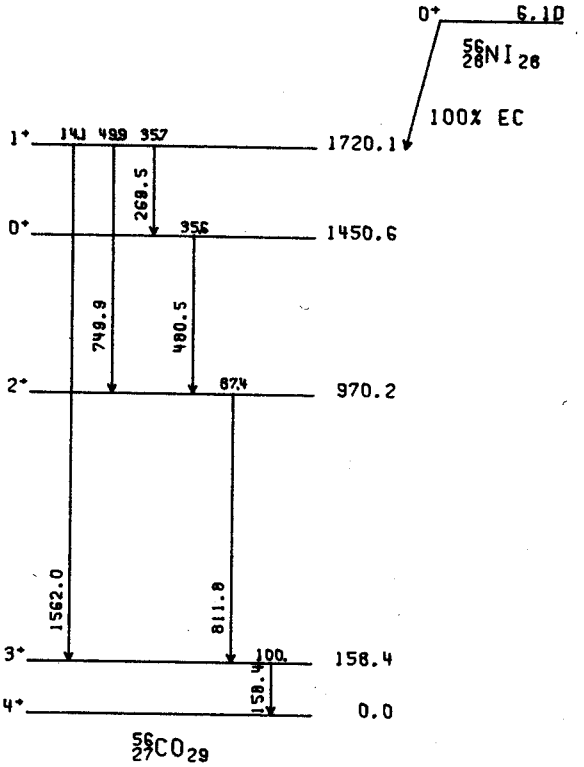

Fig. 3 Decay scheme of ^{56}Ni. The labelled intensities are normalized to 100 decays of the 158-keV level.

Low-Lying States of ^{56}Co from ^{56}Fe(p,nγ) Thresholds and γ-ray Angular Distributions

L. Samuelson

The ^{56}Fe(p,nγ)^{56}Co reaction was used to study the levels of ^{56}Co below 1.8 MeV of excitation. Excitation functions, γ-ray angular distributions, and absolute (p,n) cross-sections (at E_p=7.30 MeV) were measured by detecting de-exciting γ-rays in a 2.5%-efficient Ge(Li) detector. Proton beams of 5.55 to 7.45 MeV in 100-keV steps were furnished for the excitation functions measurements by the Western Michigan University Tanden Van de Graaff while proton beams of 5.77, 6.65, 7.05, and 7.30 MeV were furnished for the γ-ray angular distribution and absolute cross-section measurements by the Michigan State University Cyclotron. The target was a 99.4% isotopically enriched ^{56}Fe foil of 0.9 mg/cm^2 thickness (approximately 40 keV at the above beam energies). A least squares fit to the experimental γ-ray angular distributions using the computer code GADFIT[1] was made to the equation $W(\theta)=A_0[1+A_2^*P_2(\cos\theta)+A_4^*P_4(\cos\theta)]$. The absolute level feedings and the γ-ray mixing-ratio dependent parameters $A_2^*=A_2/A_0$ and $A_4^*=A_4/A_0$ (i.e. δ-ellipses) were calculated using the statistical CN computer code MANDY.[2] Energy-level spins and parities presented are those that are most consistent with the present experiment, with all previous work[3] done on ^{56}Co, and with shell-model calculations[3] done on ^{56}Co.

Table 1

Measured γ-ray Energies and Mixing Ratios

Energies keV	Mixing Ratio	Transition assumed
158.4	$-.04\leq\delta\leq-.01$	3+ → 4+
576.5	$.04\leq\delta\leq.07$	5+ → 4+
671.3	$.24\leq\delta\leq.27$	4+ → 3+
829.6	$.05\leq\delta\leq.85$	4+ → 4+
811.8	$.02\leq\delta\leq.04$	2+ → 3+
1009.2	$.07\leq\delta\leq.15$	5+ → 4+
284.8	$-.04\leq\delta\leq.08$	3+ → 4+
1114.5	$-.10\leq\delta\leq-.05$	3+ → 4+
480.5	0.0=δ	0+ → 2+
269.5	0.0=δ	1+ → 0+
749.9	$-.03\leq\delta\leq.23$	1+ → 2+
1561.9	---	1+ → 3+

Table 2

Experimental and Theoretical ^{56}Fe(p,nγ)^{56}Co Absolute and Relative (normalized to the 158 keV level) Cross-sections at E_p=7.30 MeV

Level keV	σ exp millibarns	σ rel exp	σ thy millibarns	σ rel thy	Spin & Parity assumed
158	88.1	1.000	28.2	1.000	3+
577	15.3	.177	5.2	.173	5+
830	24.6	.356	8.6	.279	4+
970	72.4	.895	23.2	.822	2+
1009	9.3	.112	3.3	.106	5+
1115	41.33	.424	13.4	.469	3+
1451	19.7	.458	4.5	.224	0+
1720	19.0	.273	3.8	.216	1+

References

1. GADFIT, computer code written by R. Warner, unpublished.
2. E. Sheldon and R.M. Stang, Computer Physics Communications 1, 35(1969).
3. M.J. Schneider and W.W. Daehnick, and Refs. cited therein, to be published.

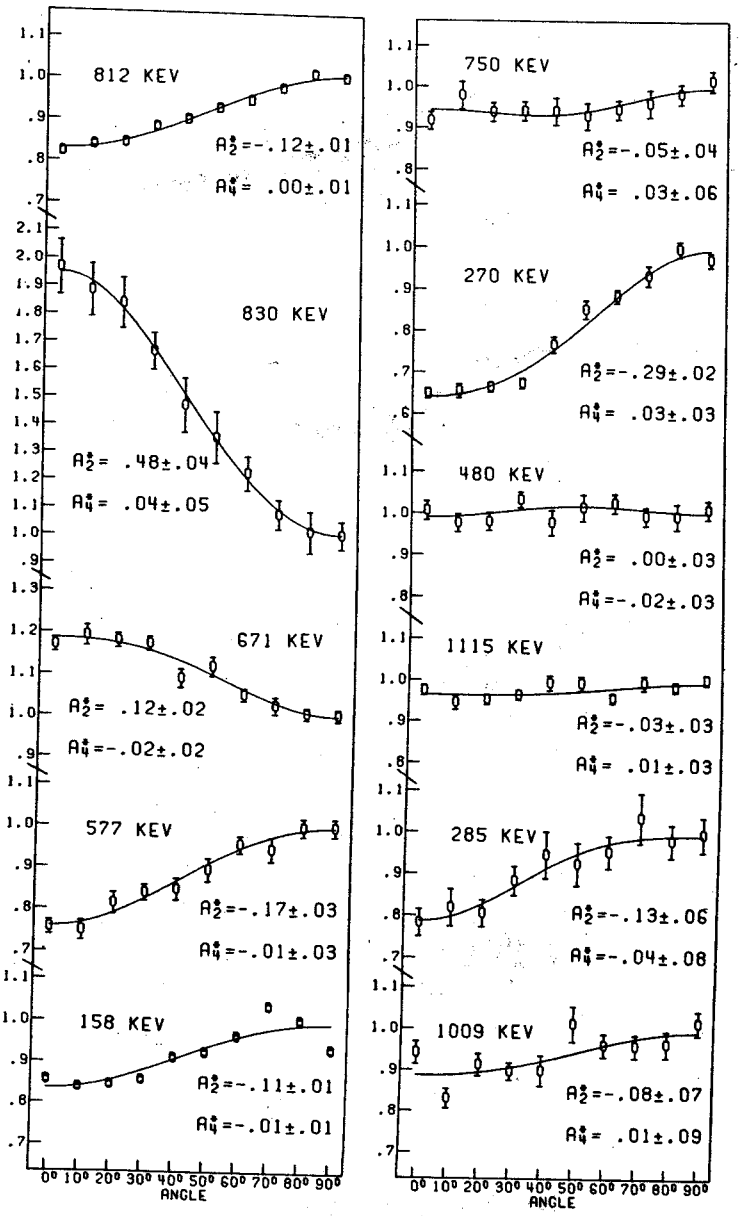

Fig. 1 Experimental γ-ray angular distributions. The solid lines represent least squares fits to the data using the equation for W(θ) given in the text.

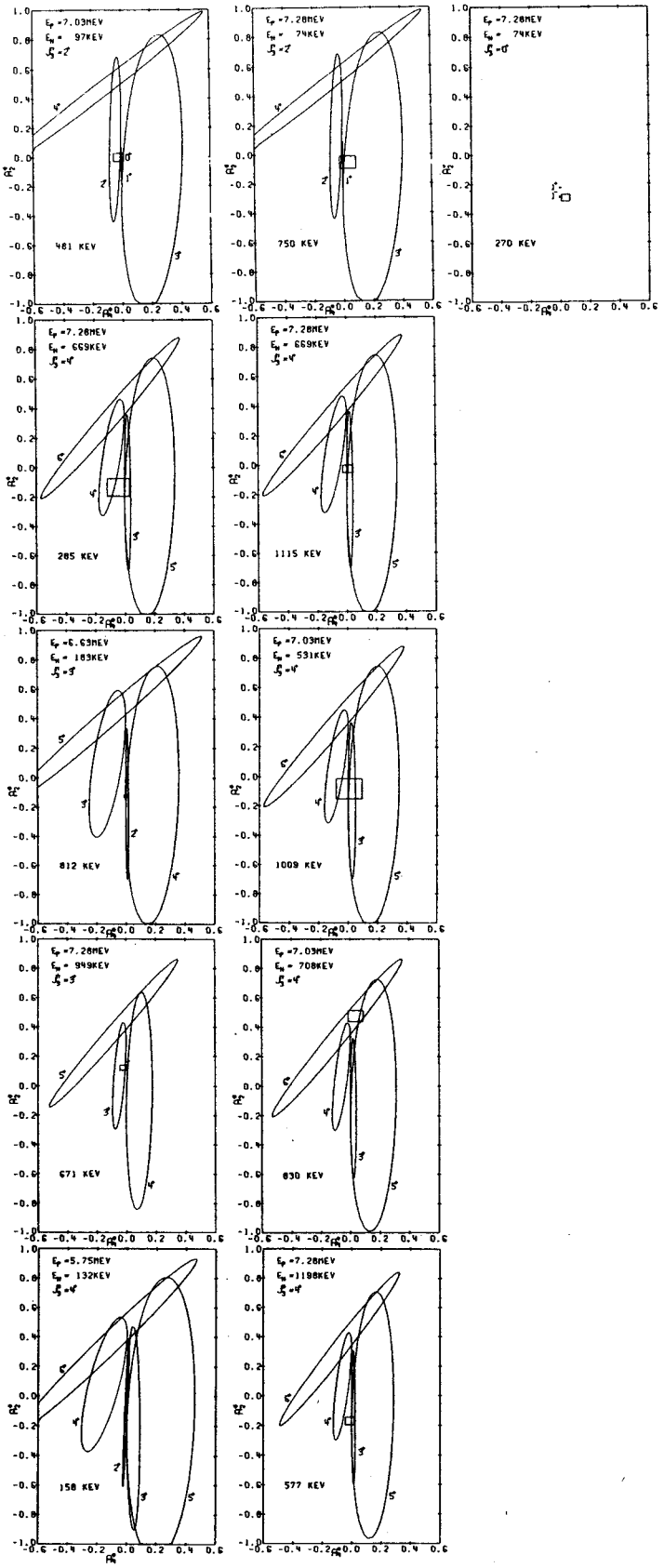

Fig. 2 Theoretical γ-ray δ-ellipses. The boxes represent the experimental values of A_2^* and A_4^* and their associated errors. The possible initial-state spins and parities label the ellipses while the J_3^π value represents the spin and parity assumed for the final state.

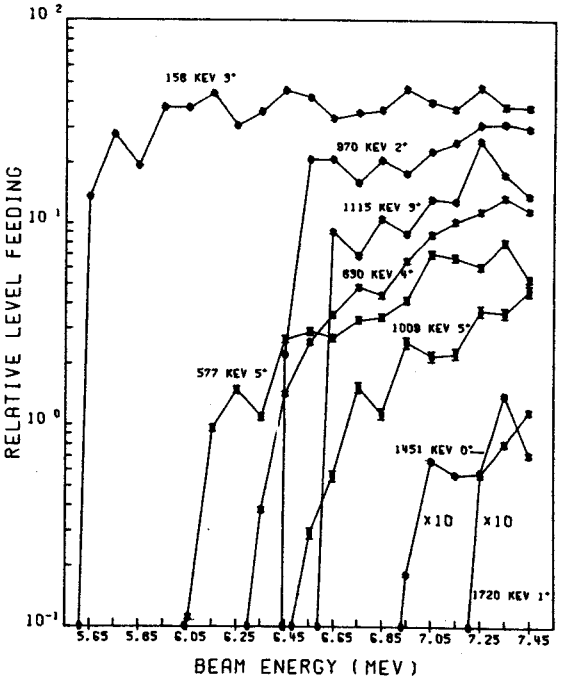

Fig. 3 Excitation functions for the eight energy levels of ^{56}Co lying below 1.8 MeV of excitation. The data were taken at θ=125°, a zero of $P_2(\cos\theta)$. The appropriate intensities of de-exciting and feeding γ-rays have been added and subtracted to obtain the relative level feedings. The thresholds were calculated using Q=-5.36 MeV.

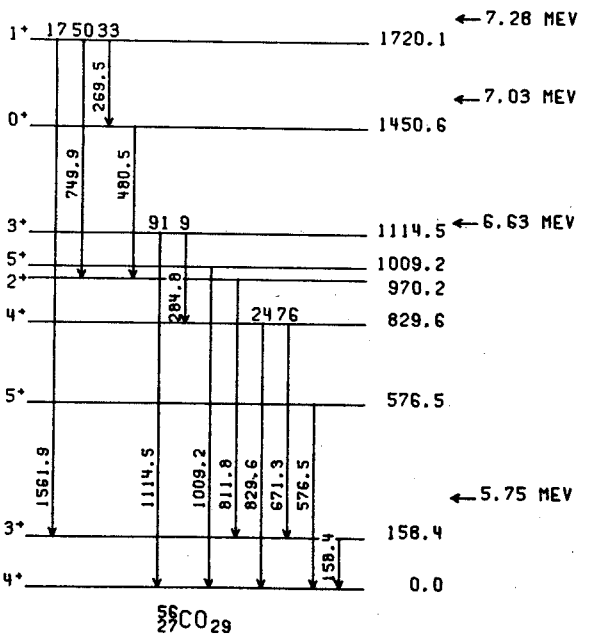

Fig. 4 γ-ray decay scheme for excitations of ^{56}Co. Where appropriate, γ-ray branching ratios are given. The arrows on the right indicate the maximum possible excitation for the labelled incident proton energy.

Decay of the Neutron Deficient A=63 Isotopes

G. Giesler

As part of a search for β-delayed α emission and an examination of the systematics of the light Zn and Cu isotopes, the β decays of ^{63}Ga and its daughter ^{63}Zn were examined. The possibility of β-delayed α emission in the light Ga isotopes was proposed by Tangepera and Nurmia[1] along with their predictions for all nuclei with Z=82 or less. A further discussion on these possibilities and the results of a search for β-delayed α emission are given in another section of this report.

Nurmia and Fink[2] reported the discovery of 33-second ^{63}Ga in 1965, but did not report any other information about the isotope. A further examination of this isotope was performed by Dulfer et al.[3] in which they reported the placement of nine γ rays with energies of 192.9, 247.8, 627.1, 637.1, 649.9, 768.2, 1065.1, 1395.5, and 1691.8 keV in a decay scheme containing levels at 0, 192.9, 247.8, 627.1, 637.1, 649.9, 1065.1, 1395.5, and 1691.8 keV. They also reported a half-life of 31.4 sec. Berstein et al.[4] reported the results of the ^{63}Cu(p,nγ) reaction used to examine the excited states of ^{63}Zn up through the 1065-keV state. There is good agreement between the two sets of results.

For our work, a 4.6% efficient Ge(Li) detector with a resolution of 1.9 keV was used in a Ge(Li) time coincidence system to examine the decay of ^{63}Ga. This system is used to obtain several successive, timed spectra from the decay of ^{63}Ga by adding together the successive, timed spectra from each of many separate samples. A further description of this system is found in Ref. 5. These timed spectra were used to determine which of the many γ rays present decayed with a half-life corresponding to that of ^{63}Ga. It was also used to measure the 32.4±0.5 sec half-life of ^{63}Ga. Sixteen γ rays were assigned to the decay of ^{63}Ga. A decay scheme summarizing our results is shown in Fig. 1. The total transition intensities, in percent of total ^{63}Ga decays, are given in the decay scheme. The total β feedings to the levels and the log ft's based on them are given to the right of the levels. The spin and parity assignments deduced from the β and γ transitions and the charged particle scattering results are given on the left of the decay scheme.

The decay of ^{63}Zn was first reported by Bothe et al.[6] in 1937. Since then many groups have studied the β decay of this isotope. Since the advent of Ge(Li) detectors, several authors have reported γ-ray results that are a great improvement over the earlier NaI(Tl) detector γ-ray results. Although numerous results from γ-ray studies are available, only one author[7] has reported any coincidence results, these being from a Ge(Li)-NaI(Tl) coincidence spectrometer. In addition to the β-decay results, many different charged-particle reactions have been used to examine the excited states in ^{63}Cu.

We studied the decay of ^{63}Zn by γ-γ mega-channel, anti-, and 511-keV-511-keV-γ coincidence experiments in addition to γ-ray singles experiments. In addition to Ge(Li) detectors our 20.3x20.3-cm NaI(Tl) split annulus and a 7.6x7.6-cm NaI(Tl) detector were utilized for the various coincidence experiments. Details of the various coincidence systems used are given in Ref. 5. The results of these various experiments were combined to place the forty-three γ transitions, including nine not reported by other authors, in a decay scheme containing twenty-four levels, shown in Fig. 2. The β^+ feedings were obtained from the 511-511-γ triple coincidence results while the total feedings to each level were obtained from the relative transition intensities and the feeding to the ground state. The percent β feedings and the log ft's based on them are given on the right. The spins and parities given on the left are based on our γ-ray results and the charged particle reactions results.

We observed several very interesting results during this study. One interesting result was the resolving of the 1392-keV γ-ray peak into a doublet of the 1389.5- and 1392.3-keV γ rays. All previous authors report it as a single γ ray. Since the 1389.5-keV γ ray is only about one-third the intensity of the 1392.3-keV γ ray, it appears only as a slight broadening on the low energy side of the 1392-keV peak. Using the computer program SAMPO,[8] we were able to reproduceably strip this peak into the doublet. Both γ transitions fit well into the decay scheme with the placement of the 1392.3-keV γ ray substantiated by the γ-γ mega-channel coincidence results.

Another interesting result is the placing of two levels in the 1965-keV region. All previous results including charged-particle scattering results, have reported only one level in this region. The γ-ray singles experiments show two resolved peaks at 1860.9 and 1865.7 keV. The relative intensities of the two have remained rather constant even though several different Ge(Li) detectors have been used and both chemically separated and unseparated sources have been used.

In the anticoincidence experiment results, these two have the same relative intensities as in the singles. Although they were not enhanced over their singles intensities, several other weak ground-state transitions in this region were also not enhanced. The possibility of either one being a double escape peak is removed since their intensities remain constant relative to each other while using several different detectors and, the

strongest known double-escape peak in the spectrum is several times weaker in intensity. Since both transitions appear to be of the same type, cascade or ground-state, we place them both as ground-state transitions based on the relative singles and anti-coincidence results.

Although the states in the neutron deficient A=63 isotopes are known, both from γ-ray decay studies and charged particle reaction results, their interpretation has been somewhat neglected. Only the ground state and first three excited states of ^{63}Cu have had any significant characterization. Since the systematics of this region just beyond the doubly closed shell at ^{56}Ni are not well known, we are endeavoring to characterize these states and improve the systematics in this region.

References

1. R. Taagepera and M. Nurmia, Ann. Acad. Sci. Fenn. AVI, 78(1961).
2. M. Nurmia and R.W. Fink, Phys. Letters 14, 136(1965).
3. G. Dulfer, H. Beertema, and H. Berheul, Nucl. Phys. A149, 518(1970).
4. L. Birstein, M. Harchol, A. Jaffe, and A. Tsuksoritz, Nucl. Phys. 84, 81(1966).
5. G.C. Giesler, Ph.D. Thesis, Michigan State University, COO-1779-55, 1971.
6. W. Bothe and W. Gentner, Z. Physik 106, 236(1937).
7. I. Borchert, Z. Physik 223, 473(1969).
8. J.T. Routi and S.G. Prussin, Nucl. Instr. and Methods 72, 125(1969).

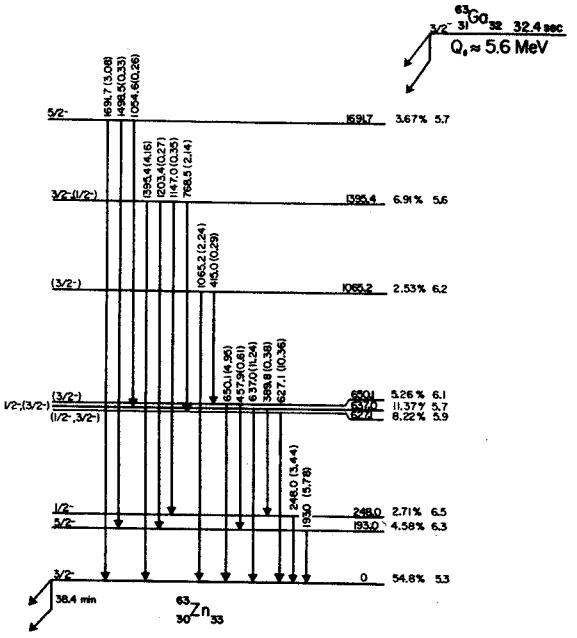

Fig. 1 The decay of ^{63}Ga.

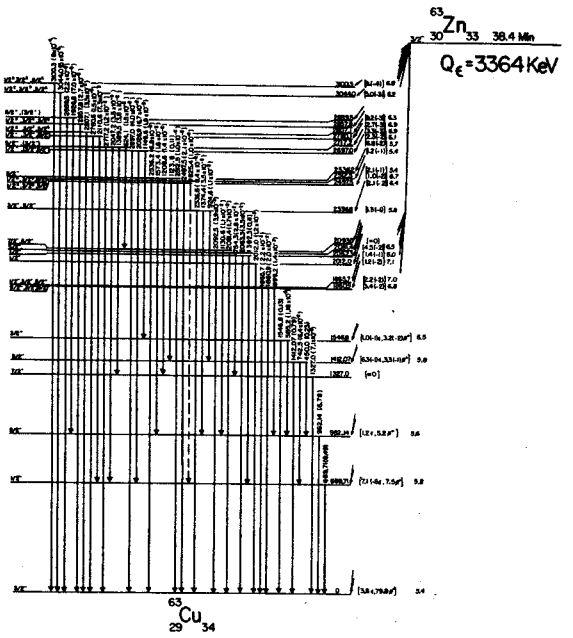

Fig. 2 The decay of ^{63}Zn.

Decay of the Neutron Deficient A=62 Nuclei and the Possibility of β-Delayed α Emission

G. Giesler and K. Kosanke

The examination of these nuclei was prompted by the possibility of β-delayed α emission in the light Ga isotopes. In order to be able to identify γ transitions from the parent, the γ transitions of the daughter must be well known. Although there has been a flurry of activity in this region, with several authors studying the decay of ^{62}Zn with Ge(Li) detectors, no γ transition was observed above 650 keV even though it has a $Q_\varepsilon \approx 1620$ keV. Davidson et al.[1] used the results from the ^{62}Ni(p,nγ) reaction to study the excited states in ^{62}Cu. They reported γ transitions from levels through 916 keV.

For our examination, we used the largest Ge(Li) detectors we have available with relative efficiencies as large as 10.4%. All samples used were chemically separated to remove any possible contaminants. Six γ transitions above 650 keV were observed that had not been previously reported in β decay studies. Figure 1 shows these transitions placed in a decay scheme. The percent β feedings to the levels and the log ft's obtained from them, are shown on the right of the levels, and the spins and parities are given on the left. The placement of the transitions and the spins and parities of the levels below 920 keV are from Davidson et al.[1] and are consistent with the β-decay results. The remaining levels indicated on the right are from the ^{61}Ni(τ,d) reaction.[2]

The possibility of these γ rays being from the ^{62}Cu daughter is ruled out based on the β-decay studies of Jongoma et al.[3] and the ^{61}Ni(n,γ) results of Farger, et al.[4]

The possibility of β-delayed α emission in the light Ga isotopes was first proposed by Taagepera and Nurmia.[5] Further calculations were performed by Fenges and Rupp[6] in which the predictions were given for all nuclei with Z<85 using the mass tables of Myers and Swiatecki.[7] Their results indicated ^{64}Ga would be the heaviest possible β-delayed α emitter for Ga. The heaviest know β-delayed emitter is 297-msec ^{32}Cl.

In their reports of the discovery of ^{63}Ga, Nurmia and Fink[8] reported their purpose was to look for delayed α's from ^{62}Ga, but they did not observe any. We have extended their study and looked for delayed α emission from isotopes as light as ^{60}Ga. We bombarded natural Cu foils with 70 MeV τ and examined the activitated nuclei with both Si(Li) α detectors and Ge(Li) γ detectors. Lower beam energies were obtained by using appropriate Al absorbers. The beam energies were chosen to maximize the production of ^{60}Ga, ^{61}Ga, and ^{62}Ga. The activated nuclei were removed from the activation area to a distant counting area by using the He-jet thermalizer described elsewhere in this report.

Figure 2, the α spectra obtained are shown. The results of the experiments indicate the possibility of delayed α emission from ^{60}Ga although an upper limit of ten parts per million delayed α branching has been placed on it by comparison of the γ-ray results with the α spectra. Any delayed α emission from the heavier Ga isotopes appears to have a smaller upper limit. The presence of the light Ga isotopes was determined by the observation of the decay of their Zn daughters. The Ga isotopes were not observed directly since their half-lives are expected to be seconds or less.

The non-observance of delayed α emission could be from several different sources. The α binding energies for the Zn isotopes are about 3 MeV, so in order to produce β-delayed α emission from these isotopes, the Ga parents must decay to states in Zn above the α binding energy. Even though the Ga ground states are calculated to be 10 MeV or more above their Zn daughters, the probability of their decaying to the higher lying states in the Zn daughters is small.

Several anomalies in these systematics are also noted. The ^{61}Ga and ^{61}Zn are mirror nuclei, and as such would permit super-allowed β decay from the ^{61}Ga ground state to the ^{61}Zn ground state. As a result the possibility of β feeding to the higher-lying excited states would be almost zero. A completely different case is presented by the ^{60}Zn since it may be considered as a doubly magic ^{56}Ni core with an α particle bound to it. This would lead to a much lower binding energy for the α particle and greatly increase the possbility of β-delayed α emission. Experimental results indicate that there may be β-delayed α emission from ^{60}Ga.

Even if the α binding energies are low enough to permit β feeding to levels above them, another problem enters. This problem is the Coulomb barrier which is about 7 MeV in this region. If the α particles are to go over the barrier, they would have to come from states that are more than 8 MeV above the ground state if the α binding were only 1 MeV. Obviously, the β feeding to these levels would be extremely small. If the α particles with lower energy were to tunnel through the barrier, the β feeding to the states producing α emission would be greater but the probability of the particle escaping the nucleus would be small. In either case the probability of β-delayed α emission is very small.

Even with all these obstacles, β-delayed emission is possible but only to a very small extent. Further work is in progress, both to better define the limitations on β-delayed α emission

and to determine the decay schemes of these light Ga isotopes.

References

1. W.F. Davidson, M.R. Najam, P.J. Dallimore, J. Hellström, and D.L. Powell, Nucl. Phys. A154, 539(1970).
2. G.C.Morrison, private communication.
3. H. W. Jonjsma, B. Bengtsson, G.H. Dulfer, and H. Verheal, Phys. 42, 303(1969).
4. U. Fanger, D. Heck, W. Michaelis, H. Ottmar, H. Schmidt, and R. Gaeta, Nucl. Phys. A146, 549(1970).
5. R. Taagepera and M. Nurmia, Ann. Acad. Sci. Fenn. AVI, 78(1961).
6. T. Fengés and B. Rupp, ATOMKI Koylem. 10, 116(1968).
7. W. Myers and W. Sweatecki, UCRL-11980(1965).
8. M. Nurmia and R.W. Fink. Phys. Letters 14, 136(1965).

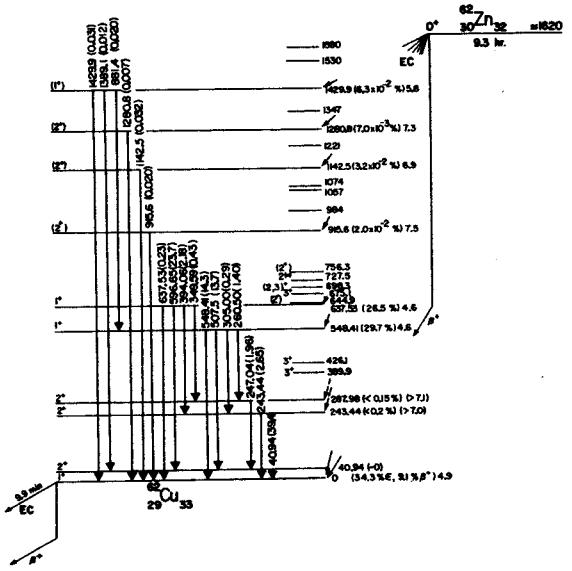

Fig. 1 ^{62}Zn decay scheme.

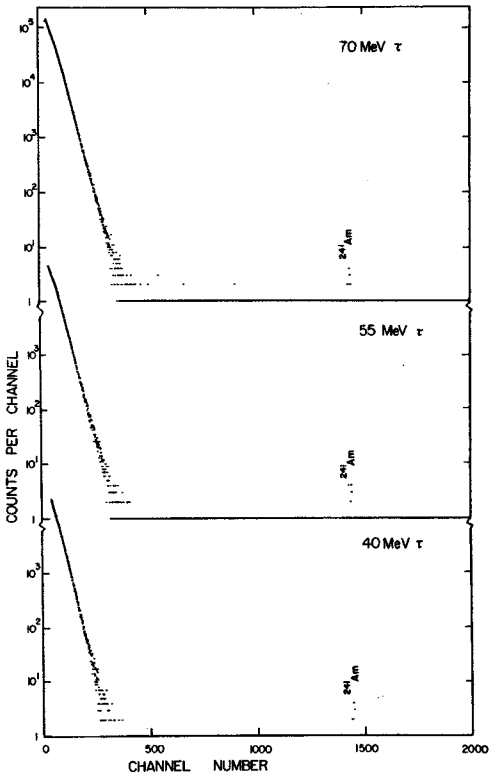

Fig. 2 A search for β-delayed α emission in eight Ga isotopes.

The Search for Three-Particle Isomeric States in ^{43}Ti and ^{43}Sc

J. Black

High-spin, three-particle states analogous to that discovered in ^{53}Fe may exist in ^{43}Ti and ^{43}Sc. Preliminary experiments have been performed on these isotopes, but were limited to activities with half-lives greater than 15 sec.[1] From these experiments, no evidence was found to support the existence of such three-particle isomeric states in these isotopes. However, the large decay energy of ^{43}Ti and the possibility of the decay of its $19/2^-$ state by a super-aolowed β^+ transition to the $19/2^-$ state of ^{43}Sc implies that the half-life of the state is shorter than 1 sec. On the other hand, it is thought that the $19/2^-$ state of ^{43}Sc is very similar to the ^{53}Fe case.

Thus far in the present investigation, we have attempted a number of different experiments in the search for these high-spin isomers. Due to the availability of target material, most of these experiments have utilized the ^{45}Sc(p,3n)^{43}Ti reaction, using 35 MeV protons from the MSU Cyclotron. This reaction affords both the possibility of observing γ rays from the de-excitation of ^{43m}Ti directly or from the de-excitation resulting after a super-allowed β^+ transition to the analogous level in ^{43m}Sc.

The first experiments performed made use of the "slow-pulsing" technique to look for half-lives in the 10-1000 msec range. In these experiments, the cyclotron beam was pulsed by RF modulation, such that the activity was produced by beam bursts of about 2-sec duration; and then counted in 4 successive, routed, beam-off spectra of about 600 ns each. A spectrum of the beam-on period was also obtained.

Experiments were also conducted to look for half-lives in the nsec region. These were achieved by routing γ spectra in the time intervals between the microscopic structure of the cyclotron beam.

Direct examination of half-lives in the μsec range is normally available by the so-called, fast-pulsing technique—in which only one of a selected number of microscopic beam bursts is allowed to be accelerated. However, this method is temporarily unavailable to us, due to thermal stability problems with the deflection plate mechanism. Therefore, examination of this crucial half-life region, is confined to setting limits on levels as observed in the msec and nsec regions—e.g. a peak in this region would appear long-lived in the nsec experiments and short-lived in the msec ones.

Another type of experiment was performed in which a helium-jet thermalizer was used to look for ^{43m}Sc. A thin ($\sim$0.5 mg/cm^2) layer of isotopically separated ^{44}Ca was evaporated onto a tantalum backing and mounted in the thermalizer chamber. A beam of 24 MeV protons was used to produce the ^{43}Sc by the $^{44}_{20}Ca_{24}(p,2n)^{43}_{21}Sc_{22}$ reaction. The resulting recoils were thermalized in helium and transported through a polyethylene capillary to a collector and counting facility on the roof of the cyclotron vault. Due to the transit time in the capillary, this method was limited to half-lives greater than a few tens of msec.

All of the above experiments employed large high-resolution, Ge(Li) detectors having efficiencies of 2.5-10.4% compared with 3x3-NaI crystal at 25 cm.

While the analysis of our data is not complete, the results of preliminary experiments show the existence of many unidentified γ rays, some of which may belong in the ^{43m}Sc or ^{43m}Ti decay scheme. The positive assignment of a γ ray to one of these unknown schemes is rather tedious, due to the large number of side products from unwanted reactions and contaminants. It is hoped that improved half-life discrimination may be used to identify γ rays from these high-spin isomers.

The isomeric level in ^{43}Sc has been tentatively identified by other workers. Iordachescu[2] reported the existence of two short-lived species in this region when performing a survey of α particles of 17.2-20.0 MeV on a number of thick natural targets. With a potassium target, a γ activity with an energy of 154 keV and a half-life of 456 μsec was reported. With a calcium target, a γ ray with an energy of 163 keV and half-life of 450 μsec was found.

More recently Sawa and Bergström[3] have reported a decay scheme for ^{43m}Sc (Fig. 1). The isomeric transition they report is an E2 with an energy of 136 keV and half-life of 0.5 μsec. Here it appears that the $15/2^-$ state has crossed below the $19/2^-$ level, resulting in a much shorter half-life than one would expect from comparison with the ^{53m}Fe conjugate configuration.

In our present study, we have observed all the γ rays reported by these workers, including the 136-keV transition. However, the assignment of these γ rays to a decay scheme for ^{43m}Sc has not been attempted, since a number of problems exist which are difficult to reconcile with our data. If the isomeric transition decays with a half-life of about 0.5 μsec, then one would expect the γ rays in the resultant cascade to follow a similar half-life. However, our pulsed-beam measurements indicate a much longer (>>2 sec) half-life for the 1157-keV, (15/2+11/2) transition. Indeed, the assignment of this γ ray to the ^{43m}Sc decay scheme is difficult, since the reactions used to produce the ^{43}Sc also produce ^{44}Sc—whose decay contains a strong γ ray at almost the same energy (1156-keV). Using our method of bracketing

the half-life range, we have found several γ rays which follow the expected half-life—including the 135- and 1830-keV transitions. Because of the lack of energy sums and crossovers, it is not obvious that one can construct a completely unambiguous decay scheme for ^{43m}Sc. The rather extensive study of the low-lying states in ^{43}Sc by Ball, et al.[4] provides a few states which could belong to the isomer decay cascade (the 1157-keV problem also exists in this scheme). Nevertheless, it is quite difficult to assign γ rays to these and higher levels without very good half-life measurements.

References

1. K. Eskola, Phys. Letters 23, 471(1966); K. Eskola, Ann. Acad. Sci. Fenn. 261, 8(1967); I. Dernedde, Zeit. Für Physik 216, 103(1968).
2. A Iordachescu, Rev. Roum. Phys. 13, 911(1968).
3. Z.P. Sawa and I. Bergström, Annual Report, Research Institute for Physics, 10405 Stockholm, Sweden (1970) p. 102.
4. G.C. Ball, J.S. Forster, F. Ingebretsen, and C.F. Monahan, Canadian Journal of Physics 48, 2735(1970).

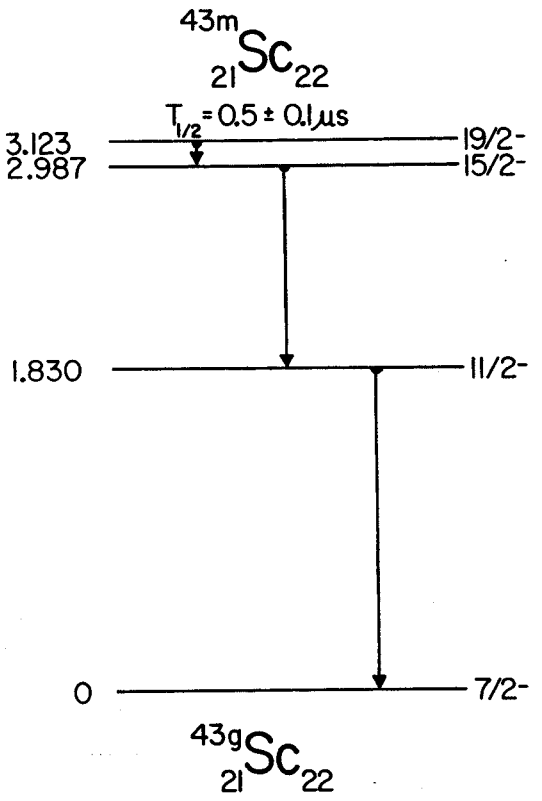

Fig. 1 The proposed decay scheme for ^{43m}Sc from Ref. 3.

The γ Decay of ^{53m}Co

J. Black

The discovery of a high-spin, three-particle isomer in the ^{53}Fe nucleus has prompted the search for analogous isomers in nuclei having a similar configuration.[1] An early search for such isomers by Eskola yielded negative results for isomers having half-lives greater than 15 sec.

The isomer ^{53m}Co is especially interesting, since its $19/2^-$ state can decay by a super-allowed β^+ transition to the isobaric analogue state in ^{53m}Fe—an isotope being studied in this laboratory. A search is continuing for a γ-decay branch of ^{53m}Co. We are attempting to produce the ^{53m}Co by a ^{54}Fe(p,2n)^{53m}Co reaction using 35-MeV protons from the MSU cyclotron. Although various oxide targets have been tried, we are presently using a self-supporting, isotopically-separated ^{54}Fe foil. Two types of experiments have been carried out thus far. A series of experiments have been performed in which the beam was pulsed, with the beam on for about 1 sec and off for 1 sec. During the beam-off period, four 4096-channel spectra were routed in 0.25-sec intervals. A 2.5%-efficient Ge(Li) detector was used to observe the resulting γ-rays. The second type of experiment utilized a helium-jet thermalizer. The ^{54}Fe foil was bombarded with 35-MeV protons, and the resulting recoils were thermalized in helium and piped up to a fixed collector on the roof of the cyclotron vault.

A 10.4%-efficient Ge(Li) detector was then used to observe the γ rays associated with the recoils. Since the mechanism for moving the collecting surface was not operational when these spectra were taken, they contain many peaks due to the buildup of longer-lived species on the fixed collector. Both of these series of experiments provided a relatively large number of unidentified γ rays. The presence of ^{53m}Fe γ rays was noted in all of these experiments. However, since the 13.6-MeV threshold for the ^{54}Fe(p,pn)$^{53m+g}$Fe reaction is lower than the threshold for the ^{54}Fe(p,2n)$^{53g(+m)}$Co reaction (22.8 MeV), one cannot conclude merely from the observation of ^{53m}Fe gamma-rays that he has produced its ^{53m}Co analogue.

There exist unidentified γ rays in the helium-jet data which can be fitted to a decay scheme very much like that of ^{53m}Fe. However, half-life determinations from the on-line experiments are still somewhat ambiguous. Thus, at this time, our data cannot attribute them positively to that nucleus.

Meanwhile, Cerny, et al.[2,3] have shown the existence of proton radioactivity from the ^{53m}Co nucleus. Using ^{40}Ca(^{16}O,2n p) and ^{54}Fe(p,2n) reactions to produce the isomer, they have observed a 1.57±0.03 MeV proton activity with a 242±15-msec half-life. This half-life implies that the dominant mode of decay is by positron emission to ^{53m}Fe. The partial half-life for the Fermi component of the super allowed β^+ decay was calculated to be 350 msec.[4] If one then uses the pure $(f_{7/2})^{-3}$ configuration and includes the Gamow-Teller matrix element, the calculation yields a predicted β^+ half-life of 200 msec— which agrees reasonably well with the experimental half-life.[5] The observed proton activity thus represents only a weak branch in the ^{53m}Co decay. Using statistical model calculations, an order of magnitude estimate of 50 sec. was obtained for the proton partial lifetime.[2]

The facts currently known about the modes of decay of ^{53m}Co are illustrated in Fig. 1. The search for a gamma branch in this decay is now in progress. Transitions in existing spectra are being examined, and an attempt is being made to assign them more concretely to levels in ^{53m}Co. It is hoped that this study will establish the existence of γ rays corresponding to transitions from the $19/2^-$ state of ^{53m}Co, and thus extend the present knowledge of these three-particle isomer systematics.

References

1. K. Eskola, Phys. Letters 23, 471(1966); K. Eskola, Ann. Acad. Sci. Fenn. 261, 8(1967); I. Dernedde, Zeit, für Physik 216, 103(1968).
2. K. Jackson, C. Cardinal, H. Evans, N. Jelley and J. Cerny, UCRL-19963, preprint (1970).
3. J. Cerny, J. Esterl, R. Gough, and R. Sextro, UCRL-19973, preprint (1970).
4. J. Freeman, J. Jenkin, G. Murray, and W. Burcham, Phys. Rev. Letters 16, 959(1966).
5. A. de-Shalit and I. Talmi, Nuclear Shell Theory, Academic Press, 1963.

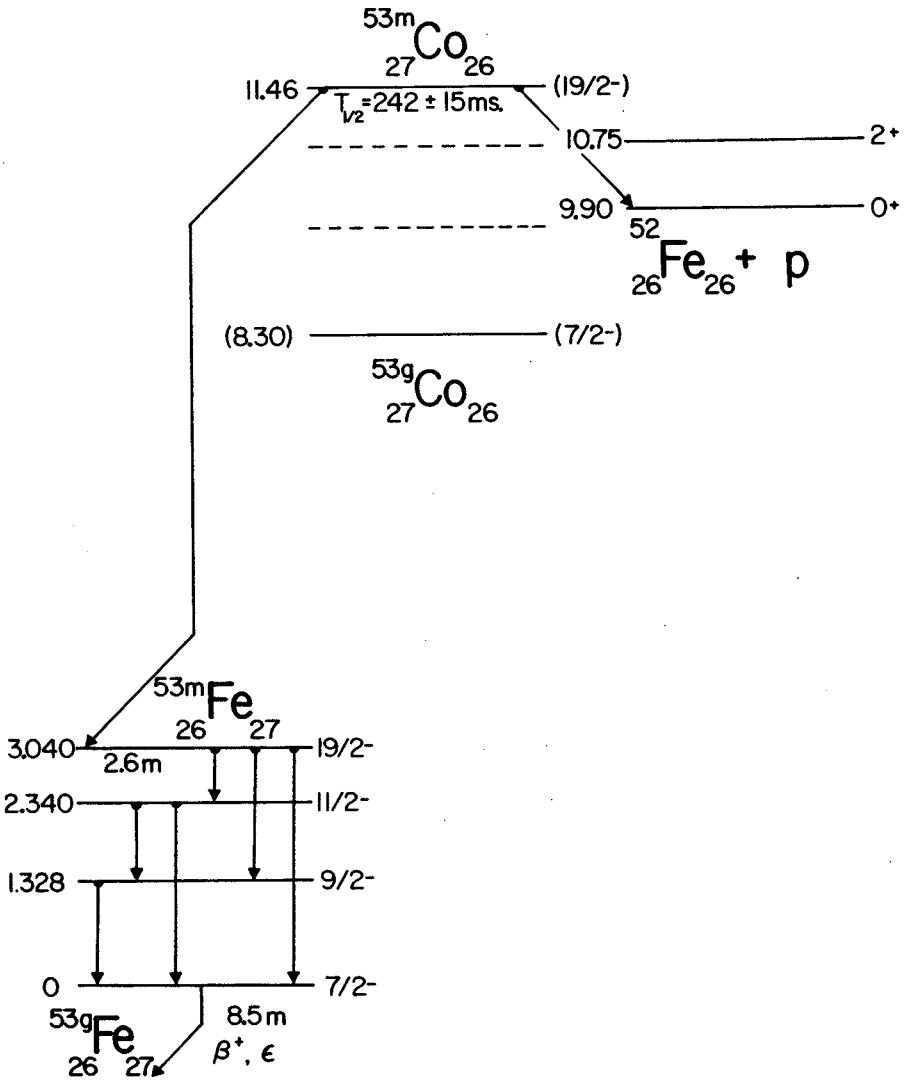

Fig. 1 The known modes of decay for ^{53m}Co. (The dashed lines indicate levels that could be populated by a γ-decay branch.)

Nitrogen Fixation

C.P. Wolk,* S.M. Austin, J. Bortins, and A. Galonsky

The remarkable process of cell differentiation in the human embryo was learned by most of us in our high-school years if not earlier. The process occurs in all the higher plants and animals and is responsible for their great diversity. Lacking, however, is an understanding of the mechanisms involved in the development of organisms and of the influence of environmental factors. Blue-green algae exhibit phenomena analogous to basic developmental processes encountered in the higher forms of life. In filamentous forms of blue-green algae, Fig. 1, special cells called heterocysts arise from the vegetative cells not at random but at rather regular intervals. Such algae may be to cell differentiation what p-p scattering is to nuclear physics. The function of the heterocysts was for many years considered a "botanical enigma". It has recently been suggested that the heterocyst is the sole site of nitrogen fixation in these algae. [On the practical side we note that rice agriculture depends upon atomspheric nitrogen fixed by various blue-green algae.] Evidence on this proposition is inconclusive in spite of great interest and much work on the subject. Destructive biochemical techniques such as centrifugation and sonication have not led to definitive experimental results.

Our approach is to obtain pictorial, in vivo, evidence from ^{13}N autoradiography. Because of the short half-life (10 minutes) of ^{13}N, it must be used where it is produced, and a cyclotron or similar accelerator is required for its production.

We use the $^{16}O(p,\alpha)^{13}N$ reaction with 20 MeV protons incident on a 15 MeV thick target of Li_2CO_3. The chemical separation following production requires a small sample. We use 50 mg packed into a cylinder less than 4 mm in diameter. When the beam is properly focussed and aligned it penetrates the target to a Faraday cup where it is monitored throughout the bombardment. The target holder is shown in Fig. 2.

The production cross-section is energy dependent but averages around 20 mb. Hence, bombardment with a 1 μamp beam produces ^{13}N at the rate of 10^9/sec. At the end of a saturation bombardment there are $\sim 10^{12}$ ^{13}N atoms. This is 2×10^{-11} of the target atoms and equivalent to $\sim 3\times10^{-8}$ atmospheric cc of N_2 gas. To within our factor-of-two accuracy all of the calculated ^{13}N activity is collected in gaseous form after chemical treatment with a commercial (Coleman) nitrogen analyzer utilizing mainly hot copper and hot copper oxide, a liquid nitrogen trap, and an alkaline permanganate wash to remove oxides of nitrogen. Further development of our chemical processing is underway to reduce below 0.01% nitrogen gases more rapidly fixed than N_2.

The activity collected in one run was counted until it had decayed by a factor of 10^4. The decay curve was a single exponential with half-life 9.84 minutes. There was no trace of ^{11}C (half-life 20 minutes). This is important because the algae assimilate CO_2 more readily than N_2.

We have seen some tracks originating in algae and are presently working to improve our autoradiographic techniques. In comparison to ^{14}C autoradiography, which has become routine, ^{13}N autoradiography should be more difficult because of the paucity of low-energy, highly-ionizing positrons. Most of the positrons are near minimum ionizing. A reasonable solid angle for seeing minimum-ionizing tracks requires thick emulsions, which are more difficult to develop quickly and without distortion. ^{32}P, which is more readily available than ^{13}N and whose electron spectrum is similar to that of ^{13}N, is being used as we improve our autoradiography. A track from ^{32}P decay originating in a vegetative cell of an algae is visible in Fig. 3.

In addition to the present project, development of ^{13}N autoradiography should be of value for future biological research.

*MSU-AEC Plant Research Laboratory.

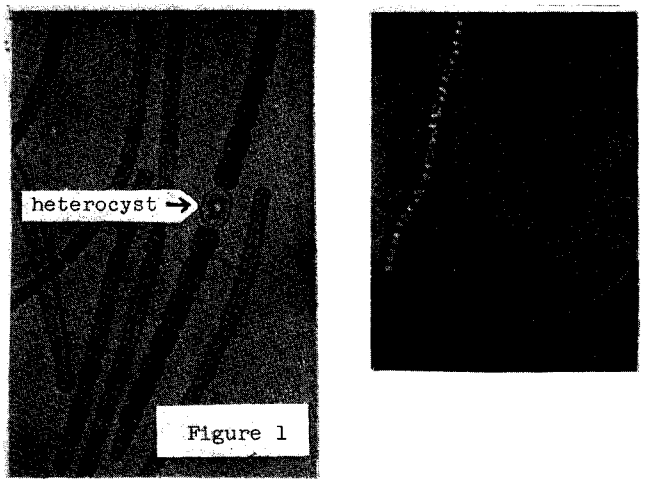

Figure 1

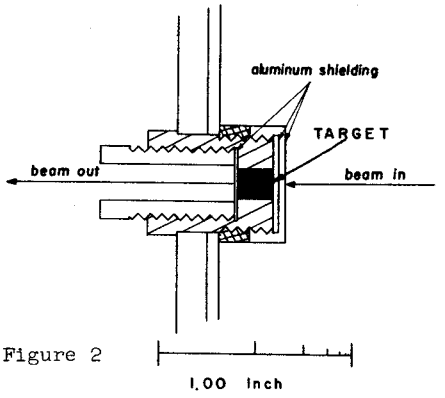

Figure 2

Neutron Yields From Proton Bombardment of Thick Targets

T. Amos, A. Galonsky and R.K. Jolly

Stopping targets of natural C,Al, Cu, Ag, Ta and Pb have been bombarded by 22, 30 and 40 MeV protons. The resultant yield spectra of neutrons above 0.5 MeV were measured by the time-of-flight (TOF) technique at laboratory angles of 1, 30, 60, 90, 120, and 150 degrees.

The targets used were selected because they represent a reasonably wide mass sample of the known nuclides, and because they are commonly used in scientific instruments and applications where there are high energy protons present.

For each energy the targets were disc 2.54 cm in diameter with a thickness equal to the range plus range straggling of the incident protons. The TOF detector was a cylindrical glass encapsulated NE213 plastic scintillator 4.4 cm in diameter x 1.9 cm thick optically coupled to an RCA 8575 photomultiplier.

The dynamic range of neutron energies covered in the experiment was from 0.5 MeV to a maximum of about 40 MeV, or 80/1. Due to the non-linearity of the scintillator response as a function of neutron energy, this energy range corresponds to a range in pulse height in the photomultiplier output of approximately 600/1. The experimental electronics are incapable of handling such a large range of pulse heights with adequate resolution. Therefore the TOF spectra were taken in two parts: one spectrum gives accurately only neutrons between 0.5 and 4.5 MeV with a range in pulse height of approximately 35/1 and flight path of 0.5 meter; the second spectrum corresponds to neutrons between 3.5 and 40 MeV with a range in pulse height of 25/1 and a flight path of 1.5 meter.

The time of flight resolution as measured by the full width at half maximum of the target gamma peak was typically 0.5 nsec..

The high ambient flux of gamma rays from neutron capture events in the experimental room, plus the extremely large number of gamma rays from nuclear events inside the targets themselves required the use of pulse shape discrimination to separate neutrons from gamma rays. With the relatively small dynamic ranges noted above, gamma rejection ratios of better than 200/1 were easily achieved.

Typical gamma and neutron TOF spectra are shown in Fig. 1. The neutron TOF spectra were converted to energy spectra, corrected for dead time losses and detection efficiency, and plotted with no other normalizetion factors as absolute yield spectra, two of which are shown in Fig. 2.

The data are currently being analyzed and will be treated to give yield spectra, angular distributions and angle- and energy- integrated total yields for all targets as a function of mass number and bombarding energy.

By subtracting corresponding thick target spectra taken at two different energies, "thin" target spectra may be obtained. These spectra will be compared with predictions of the statistical model to obtain nuclear temperature and level density parameters. In addition, such spectra will be used in an attempt to determine the individual yields of neutrons produced by direct and compound processes.

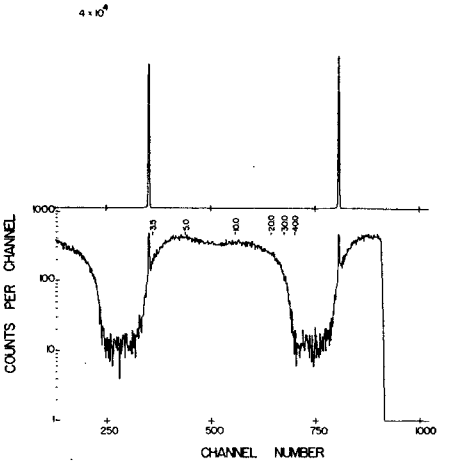

Fig. 1 Gamma-ray and neutron TOF spectra from bombardment of a thick lead target by 40 MeV protons, measured at 30° lab angle. The lower spectrum is that of neutrons above 3.5 MeV, with the energy scale of MeV at the top of the spectrum.

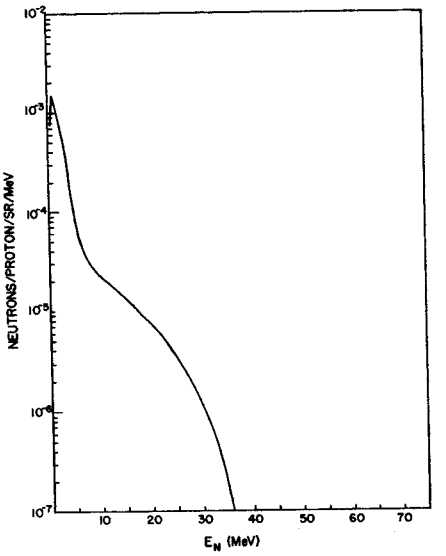

Fig. 2 The neutron yield spectrum corresponding to the TOF spectrum in Fig. 1, with the yield for neutrons between 0.5 and 3.5 MeV included to give the entire spectrum above 0.5 MeV.

Elemental Analysis by Elastic Scattering

R.K. Jolly and H.B. White

The object of the present study is to examine the nuclear scattering process, with a view to understanding the conditions that enable one to achieve maximum sensitivity and efficiency in its application to elemental analysis. In the following paragraphs it is shown that the chief value of the elastic scattering technique lies in the fact that, unlike conventional techniques, one can get information about all the elements in the sample in one good energy resolution measurement.

In the nuclear scattering technique, the sample to be analysed is bombarded by projectiles of mass m and energy E_{inc}. The energy loss $\Delta E=E_{scatt}-E_{inc}$ which can be shown to be given by

$$\Delta E=\frac{2E_{inc}}{(1+A/m)} \qquad (1)$$

for a scattering angle of 90° (chosen for simplicity).

Thus, for a given E_{inc} and m one can measure A, the mass of the target nucleus by measuring ΔE, the energy lost in the scattering process. An element is identified by its characteristic isotopic abundance which serves as its signature (both in terms of the average atomic mass of the element and the relative abundance of its isotopes).

A plot of $\frac{E_{scatt}}{E_{inc}}$ vs scattering angle both for protons (m=1) and α-particles (m=4) is shown in Fig. 1 for various atomic masses. The rate of change of E_{scatt} with A and for scattering at 90° can be written as

$$\frac{\Delta E_{scatt}}{E_{inc}} = \frac{2m}{(A+m)^2} \qquad (2)$$

Here ΔE_{scatt} is the energy difference between particle scattered from two nuclei that differ by $\Delta A=1$ mass unit. ΔE_{scatt} is, therefore, the energy resolution required to separate two nuclei that differ by 1 mass unit. Table I gives some values of ΔE_{scatt} for both protons and α-particles of E_{inc}=20 MeV. It is apparent that the energy resolution requirements for protons are three to four times as stringent as those for α-particles of the same energy.

However, for α-particles the specific energy loss, $\frac{dE}{dx}$, in all materials is ∿10 times that for protons of the same energy (20 MeV). This means that the thickness of the sample and, therefore, the yield will be lower by a factor of ten for α-particles to maintain the same energy loss as in the case of protons. The yield, however, also depends on the scattering cross-sections which have been compared for 20 MeV α-particles and protons in Table II for nuclei of masses A=60, 120, and 208. It is highly unlikely that a typical sample will contain all the elements in the periodic table in equal abundance. Table III shows a more probable list of elements of comparable abundance in a given sample (only the most abundant isotopes in these elements have been tabulated). All the elements in such a sample can be easily resolved from one another at 40° with an energy resolution much poorer than that routinely achieved (10-15 keV) in several low energy nuclear physics laboratories. If several neighboring, very heavy, elements are present then the measurements have to be made at a larger angle like 80° to resolve these elements. At both of these angles the α-particle scattering cross-sections for the heavy elements (Pb-Sn) are at least an order of magnitude greater (Table II) than the proton scattering cross-sections, so that the loss in yield due to a smaller target thickness is cancelled by the increase in yield due to the larger α-scattering cross-sections. However, the advantages of greater mass resolution and the low inelastic scattering background due to the higher Coulomb barrier for α-particles still remain.

For large solid angles, compensation of the larger kinematic broadening for α-particles necessitates the use of magnetic spectrograph.[1]

Table 1

	PROTONS			α-PARTICLES		
	120°	80°	40°	120°	80°	40°
A= 25	83	48	14	236	160	54
A= 50	23	12	3.7	75	46	14
A=100	6	3.5	0.9	21	12	3.7
A=200	1.5	0.9	0.23	5.7	3.2	0.9

Table II

Differential Scattering Cross-sections (mb/sr) for 20 MeV α-particles and Protons for ^{60}Ni, ^{120}Sn, and ^{208}Pb

	Θ=40°		Θ=80°	
	α-particles	Protons	α-particles	Protons
^{60}Ni	366	130	5.9	20
^{120}Sn	2920	100	117	5.0
^{208}Pb	5800	500	470	40

Table III

Target Nucleus	E_{scatt}(MeV) at 40°	ΔE(keV) at 40°
^{207}Pb	19.8193	89.8
^{138}Ba	19.7295	23.3
^{127}I	19.7062	19.6
^{119}Sn	19.6866	109.4
^{88}Sr	19.5772	72.4
^{75}As	19.5048	93.1
^{63}Cu	19.4117	72.4
^{56}Fe	19.3393	258.3
^{40}Ca	19.0810	23.1
^{39}K	19.0579	105.0

Table III con't.

^{35}Cl	18.9529	105.0
^{32}S	18.8573	95.6
^{31}P	18.8215	35.8
^{23}Na	18.4265	395.0
^{16}O	17.7705	656.0
^{14}N	17.[illegible]	301.2
^{12}C	17.0705	398.8

Table V shows the number of counts/hr. for an organic target of thickness 100 μgm/cm and an impurity of mass=A and fractional atomic abundance 10^{-6} for a 20 MeV, 1 μA α beam and $d\Omega=4\times10^{-3}$sr

Table V

	$\theta_{LAB}=40°$	80°
A= 60	2.5×10^{2}	5
A=120	2×10^{3}	10^{2}
A=208	5×10^{3}	5×10^{2}

It is apparent that for samples typified by Table III, atomic concentrations of various elements to the levels of 10^{-6} to 10^{-8} can be measured within an hour with 1 μA. of beam intensity.

The first two spectra presented below were measured with a counter telescope while the last two measurements were made with a magnetic spectrograph.

i) Human Blood: A spectrum from human blood is shown in Fig. 2. Some of the carbon and oxygen in the spectrum is from the backing. Quite a few elements heavier than A=16 are seen. Most prominent are ^{23}Na, Cl, ^{31}P, Ca, Fe, and Pb.

A comparison between the relative abundance of the various elemenets seen in the blood of an average human (Ref. 2) and those observed in the present work in a single human blood specimen is shown in Fig. 3. The two sets of data are normalized to have equal abundance of K. Agreement is reasonably good in view of the large variance of the relative elemental abundance from one blood sample to another. The abundance measured in the present work is that of the prepared thin film sample used in the α-scattering measurement and, therefore, has several possible sources of error.

ii) Milk: An α-particle spectrum from a deposit of milk on Formvar is shown in Fig. 4. The most prominent peaks are those of C, N, O (an appreciable fraction of the C and O peaks are from Formvar) P, Cl and (K+Ca). But, in addition, there are also traces of F, Si, S, As and Pb(?). Both K and Ca are probably present in the spectrum in Fig. 5 as the (Ca+K) peak is broader than the Cl peak. The relative abundances of most elements in Fig. 4 qualitatively agree with those listed in Ref. 2.

iii) Whole Fish and the Composite (Au, Zn, and Mg) Sample:

The focal plane orientation was adjusted as far as possible for simultaneous kinematic compensation for all elements from C to Pb. To obtain an "in situ" mass and/or energy calibration for the fish sample measurement, an exposure was also made with a composite thin target (∿20 μgm/cm² each of Au, Zn, and Mg on Formvar) in place of the fish sample. The spectrum from the composite target is shown in Fig. 5 indicating the peaks from Au, Zn, and Mg in addition to those from the Formvar backing. The energy resolution for the heavy mass peaks is 11 keV (1/2 mm for 22 MeV α-particles). Of particular interest is the elastic scattering from Zn where the elastically scattered α-particles from the three even isotopes of Zn (^{64}Zn 49%, ^{66}Zn 28%, ^{68}Zn 19%) are clearly separated.

The fish spectrum (Fig. 6) shows a fairly strong Hg peak in addition to those from K, Cl, P, Na, O, N, and C. There are also small peaks from Br, Sr, and Ba. The atomic concentration of Hg is estimated to be 0.2 ppm in the original fish specimen. The concentrations for Br and Sr are probably even greater because their scattering cross sections at 70° are 1% of the cross-section for Hg.[3] The light mass peaks are broad because complete kinematic compensation for these peaks could not be achieved because of the physical limitation of orienting the focal plane at the unusual angle required for the above purpose.

The main conclusions of the present work about the elastic scattering technique are as follows:

i) The chief value of this technique lies in its ability to provide infomation on all the elements in a sample in one measurement at a suitably chosen angle.

ii) The technique is particularly well suited for elemental analysis of biological samples (particularly in the areas of microbiology, pollution studies, and the role of heavy elements in the Biosphere).

iii) Low energy α-particle scattering offers better kinematic separation and possibly lower inelastic scattering background as compared to protons of the same energy without any loss of efficiency.

iv) The sensitivity for detecting heavy elements in the presence of a bulk of light elements (e.g. Hg pollution of fish) is very high because of the practically non-existent background for the heavy elements. With the currently available intensities, concentrations of a few isolated heavy elements ∿10^{-7}-10^{-8} can be measured in a few tens of minuets. In favorable cases much higher sensitivities are achievable.

References

1. H.A. Enge, Nuclear Instr. and Methods 49, 181(1967).

3. R.K. Jolly and H.B. White (Elemental Analysis by Elastic Scattering, Nucl. Instr. and Methods (to be published).

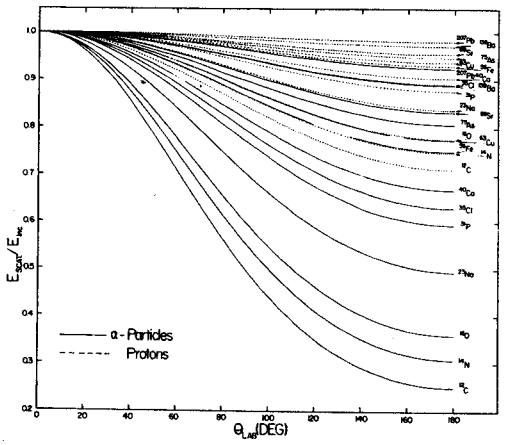

Figure 1

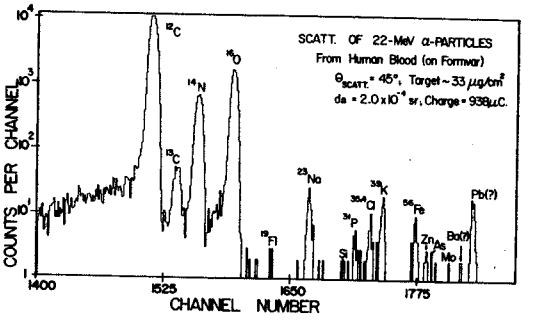

Figure 2

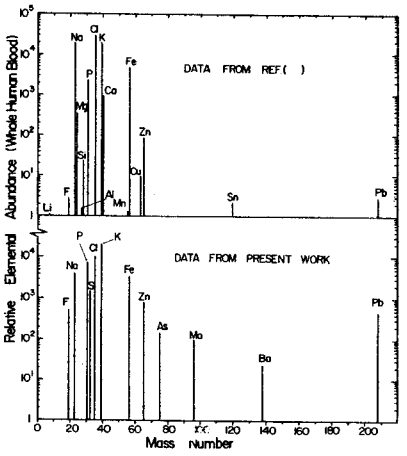

Figure 3

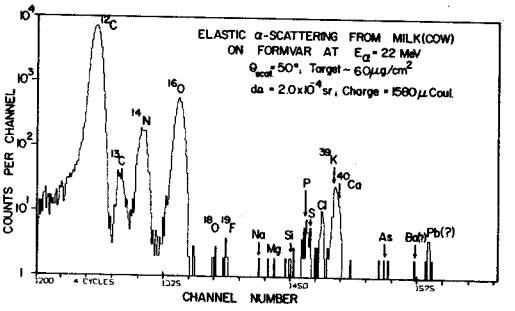

Figure 4

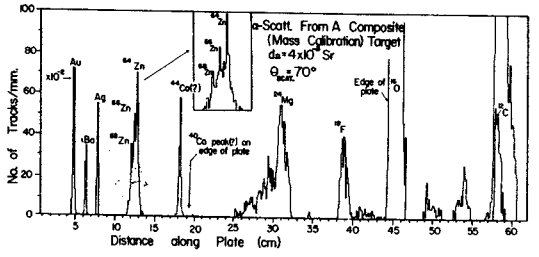

Figure 5

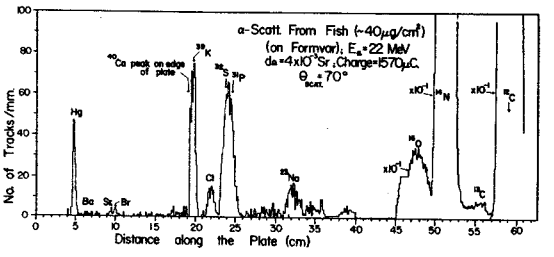

Figure 6

New Computer Program for Field Trimming Calculations

M.M. Gordon and D.A. Johnson

A sector-focused cyclotron requires an efficient system for determining the multitude of "knob settings" necessary to produce a specific ion beam with a given energy. The MSU Cyclotron has been operating quite successfully for a long time with the use of a computer program "Set-Op" which provides these knob settings as output.[1] In order to achieve certain operational improvements, it was recently decided to rewrite the main part of this program which calculates the eight trim coil currents and the rf frequency. As a result, we have developed a completely new field trimming program "Fielder" which can determine the optimum values of these parameters under a wide variety of conditions.

Instead of trying to match the measured trim coil fields to a predetermined "ideal field", the Fielder program adjusts the parameters so as to obtain a least-square fit to a prescribed phase-energy curve $\phi(E)$ for the central ray trajectory. Since $\phi(E)\equiv 0$ corresponds to perfect isochronism, this prescription is usually employed, although the program is not limited to this choice. The program will accept as input any reasonable value for the initial phase $\phi_o = \phi(E=0)$, and will automatically incorporate this choice into the fitting process. In the Set-Op program this quantity has the fixed value $\phi_o = 20°$, and while this choice has proved generally satisfactory, there is some recent evidence which indicates that a larger value may obtain in certain cases.

The least-square fitting routine in the new program contains a provision for imposing a set of linear constaints on the adjusted parameters within the fitting process. Several different types of constraints are available, some of which are always imposed, while others are optional. One optional constraint, for example, requires the $\phi(E)$ curve to pass through a specified point. The number and type of constraints which are employed will differ from case to case depending on the circumstances.

For a separated turn cyclotron such as ours, a spread in initial phase $\Delta\phi_o$ within the beam will produce a spread in final energy values ΔE_f, and this energy spread must be minimized for optimum performance. The Fielder program carries out this minimization simply by imposing a suitable constraint within the fitting process. In the Set-Op program, however, this minimization was accomplished by an adjustment of the rf frequency after the completion of the field fitting, and this procedure sometimes yields an undesirable overall slope in the $\phi(E)$ curve. The method used in the new program eliminates this difficulty entirely.

Small fluctuations in the magnetic field level (or rf frequency) will produce corresponding fluctuations in the final energy of the beam. By imposing another type of constraint on the fitting process, the Fielder program can also minimize this effect. (This capability is not available in the Set-Op program.) As a result of this minimization, and the one described above, the new program will produce a non-isochronous field with a resultant $\phi(E)$ curve which possesses two very important properties of a perfectly isochronous field operating with $\phi_o = 0$.

It is sometimes desirable to use the trim coils to produce a small change in the axial or radial focusing frequency, ν_z or ν_r, at certain energies. For example, if an isochronous field were to be employed for proton energies above 40 MeV, then the value of ν_z would be too low (or even imaginary) in the energy region from 0.8 to 0.9 of the final energy. This difficulty was circumvented in the Set-Op program by use of a non-isochronous "ideal field" which provides adequate focusing together with tolerable phase excursions, but which required a rather tedious empirical process for its determination. The Fielder program handles this problem by providing an appropriate constaint within the fitting process whereby the value of ν_z can be fixed to a specified value for a particular energy. This type of constraint can also be used to adjust the value of ν_r. The cyclotron makes use of the $\nu_r = 1$ resonance to facilitate beam extraction, and a small ν_r adjustment is sometimes needed in order to properly position this resonance.

The Fielder program operates in a cycle. In order to check the set of trim coil currents and rf frequency derived from the fitting process, the program calculates equilibrium orbit data (including focusing frequencies) for the resultant magnetic field, and then integrates the longitudinal motion equations to obtain the actual $\phi(E)$ curve for this field and the given frequency. The program then uses these data to improve the fitting process. The entire cycle can be repeated as often as necessary to achieve convergence, although a single iteration has so far proved satisfactory. After examining the final data, the program user can alter the constraints as he sees fit and then extend the iteration process still further. In this way, the user can determine empirically the specific set of constraints which yield the optimum results under given operational conditions.

---

[1] R.E. Berg, MSUCP-24 (MSU, East Lansing, 1966).

Studies of Orbit Centering

L. Learn and M. Gordon

Successful third harmonic operation (where the rf frequency is three times the orbital frequency) is essential for producing the most important heavy ion beams, as well as low energy protons and deuterons. Previous studies have clearly shown that third harmonic operation will be hampered by difficulties in obtaining well centered orbits. Since interest in heavy ion beams has increased substantially, it was decided that an intensive effort should be made to overcome these difficulties.

Well centered orbits are highly desirable since they avoid possible troubles with certain resonances, and since they generally improve the performance of the cyclotron. Accelerated orbits are driven off center by the electric gap crossing resonance which results from the interaction of the three sector magnet geometry with the two sector electric gap geometry. Moreover, when the orbits are off center, the resultant phase deviations produce an asymmetry in the gap voltages which tends to drive the orbits still further off center. Since this latter effect increases with harmonic number, the orbit centering problem will be most severe under third harmonic operational conditions.

Orbit centering problems can be studied most easily with the use of a computer program "Disport" which calculates the displacement of the instantaneous equilibrium orbit resulting from the acceleration process.[1] Comparing the results obtained under typical first, second, and third harmonic operational conditions with our present dee geometry, we find that the third harmonic orbit center displacements are much larger in magnitude at all energies. In addition, these displacements make rather rapid changes in direction, which are quite contrary to the slow variations found for the lower harmonics. These studies verify that well centered orbits will be difficult to achieve under third harmonic operational conditions, at least for the present dee geometry.

In searching for a means to overcome this difficulty, it was decided to investigate the effect of reducing the dee angle from its present 138° down to 90°. When this change is simulated within the Disport program, the output reveals remarkably small center displacements for the accelerated orbits at all energies. This quite beneficial result can be attributed to the fact that when the electric gaps are all 90° apart, the resultant electric field then possesses fourfold rather than twofold symmetry.

In order to confirm this solution to the orbit centering problem, results were obtained from the Disport program for all dee angles from 60° to 180°. Part of these results are shown in the figure below where the magnitude of the orbit center displacement (in mils.) is plotted against dee angle (in degrees) for one particular energy. The first harmonic curve (h=1) corresponds to 18 MeV protons, the second harmonic curve (h=2) to 9 MeV deuterons, and the third harmonic curve (h=3) to 24 MeV C^{4+} ions; in each case, this energy is just one-half the final energy of the ions at extraction. All three curves represent an energy gain per turn $\Delta E=E/60$ at the given energy E, and the dee voltage is adjusted to make ΔE constant independent of dee angle. Under these conditions, the dee voltage would become infinite for h=3 when the dee angle approaches 120°, and also for h=2 when the dee angle approaches 180°; consequently, the corresponding two curves misbehave at these angles. Similar sets of curves obtained for different values of ΔE or of E indicate that the displacements are roughly proportional to $(\Delta E)/E$ at most energies. From the results of these studies it can be concluded that for three sector cyclotrons such as ours, the use of 90° dees will effectively eliminate orbit centering problems.

[1] M.M. Gordon, IEEE. Trans. Nuc. Sci. NS-13(4), 48(1966).

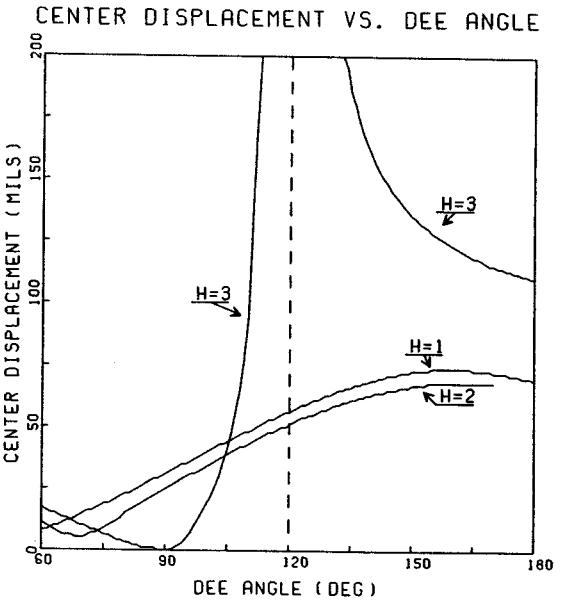

Stabilization of Cyclotron Main Field with Beam Phase Sensing

H.G. Blosser, J. Collins, and R.A. deForest

The phase of a beam packet ϕ relative to the RF phase of a cyclotron is adequately described by the equation

$$V(\sin\phi-\sin\phi_o)=2\pi\left[w_{rf}\int_o^E \frac{m(E)dE}{qB(r(E))} - E\right]$$

where V = Peak RF voltage;

w_{rf} = RF frequency (radians/sec);

m(E) = Particle mass at energy E;

q = Particle charge;

B = Magnetic field at particle radius r, which is in turn a function of E;

ϕ_o = Initial phase of beam packet.

Note that V appears as a gain factor when ($\sin\phi-\sin\phi_o$) makes small excursions about zero, and may, therefore, be considered unimportant if beam phase is to be stablizied by a device which holds ($\sin\phi-\sin\phi_o$) close to zero. Note that a small change in B the magnetic field is the only term on the right hand side which could cause a small phase change in a given mode of operation, since w_{rf} is orders of magnitude more stable than B. With this in mind, two devices for sensing beam phase are being tested. One device uses a photomultiplier to observe protons elastically scattered from a 100 $\mu g/cm^2$ carbon target which is mounted in the beam line external to the cyclotron. Timing pulses from the photomultiplier are compared in a time-to-amplitude converter (TAC) with the zero crossings of the RF. Thus far timing resolutions of 150 ps have been achieved. The significance of this number is revealed by noting that for 30 MeV protons a 100 ps change in phase represents a 5 ppm change in the Magnetic Field. The second device is a capacitive non-interfering probe. This probe has not yet been made insensitive to RF signals in the beam pipe, but if it can be made so, it would supply a simpler device than the photomultipler.

Stabliziation has been successfully achieved by electronic equipment which senses the beam phase indicated by the TAC output and generates an analog signal which can be fed into the Main Magnet regulator.

The stabliziation scheme is illustrated in Fig. 1. The up/down counter together with the digital-to-analog converter insure a phase error signal

$$E_\phi = K \sum_{t=0}^{t} (W_1-W_2),$$

that is the error signal is proportional to the difference between the number of TAC pulses which fall in window number 1 and those which fill in window number 2.

Figure 2 shows a typical spectrum measured by applying the TAC output to a multichannel analyzer.

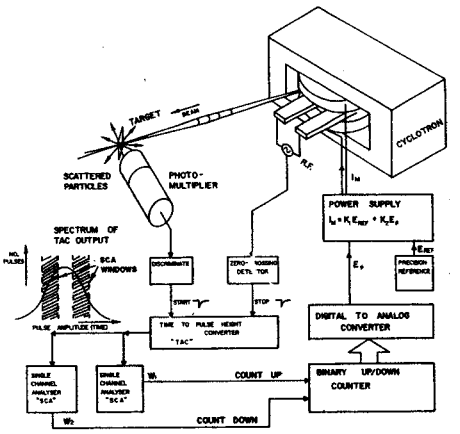

Figure 1

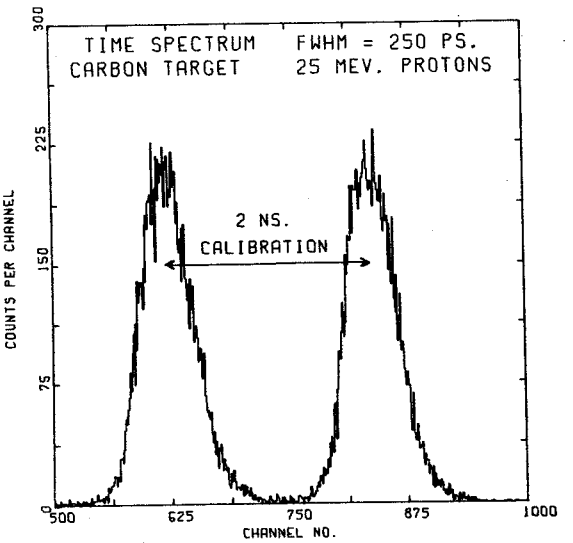

Figure 2

Computer Compatible Servo-System for Cyclotron RF

P. Sigg

Abstract

A new servo control system, which allows computer as well as manual setup of the RF-system of the MSU Cyclotron has been built and tested. It features automatic switching to phase detectors when the desired positions are reached, in order to fine-tune the system if the RF drive goes on.

I. Introduction

The new RF-servo system allows simultaneous setup , either from thumbweelswitches on the console of the Cyclotron or from a computer.

Since the system contains seven tunable elements, this saves a considerable amount of time, since the old system required te operator to set each element to the desired position by a manual control switch. The operator no longer is required to pay any attention to the tuning process, though it still could be done manual if so desired. Separate two-speed clocks for each servo allow a high setting speed and a matched low speed for tuning from phase detectors or position indicators. The RF system has been described previously.[1,2]

The entire design of the control electronics is modular; the basic units are printed circuit boards which can be used in all servo loops. Since all threshold and speed adjustments are on front panels, modules of the same type can be exchanged without requiring recalibration. The basic units (PC-boards) are compatible with commerically available modules which allows us to use some XDS T-series modules and directly interface into our XDS Sigma-7 computer. Integrated circuits in dual in line packages are used throughout, diode-transistor-micrologic (DTμL) for logical functions and microamplifiers (μA), for operational amplifiers and fast discriminators. For analog and signal switching, DTμL-compatible minature relays are used.

II. Description of the System

Figure 1 shows the seven different servo control loops. Some loops are in the same circuit, hence not operating independent. The DC stepping motors are controlled the following way:

Automatic setup (computer setup)

The program for setup checks whether the RF voltage is off and the servos operable, then five positions (12 bits BCD) are transferred into Digital-to-Analog Converters and strobed. Input buffers allow parallel setting, and when the devices have reached their appropriate positions, the system automatically switches over to phase detectors for fine tuning and flags this to the computer as well as to the operator.

Manual Setup

Thumbweelswitches on the main console allow setting of three decimal digits according to a run-sheet. Pushing a "manual set" button then sets up the same way as the automatic setup, however, this does not require an operable computer.

Furthermore, using a manual control switch which overrides all other signals (except limits) one can position the devices by hand and read their positions on a Digitial Voltmeter (DVM).

III. Description of a Typical Servo Loop

Figure 2 shows a block diagram of a typical servo loop. As mentioned above, setting can be done three different ways:

1) Computer
2) Thumbweelswitches on Console
3) Manual direction control switch on Console

The method to implement this is described now.

The manually controllable multiplexer switches inputs between computer and thumbweelswitch. The output of the multiplexer is fed into a Digital-to-Analog Converter (DAC) which has an output accuracy of $\sim$0.01% F.S., $\pm\frac{1}{2}$LSB. Strobing (transfer of input register into output) of the DAC can only be done while RF voltage is off. This prevents erroreous detuning while the Cyclotron is operating.

The output of the DAC is the reference voltage in an analog feedback loop and is compared with a voltage proportional to the position of the tuning element.

An absolute value of the amplified error-signal is then used to determine "how far away" the real position is from the desired position and, if sufficiently small, switches the clock to low speed for fine tuning. An even smaller threshold is used to determine when the error signal is approximately zero and the input source control then switches on the phase detector and indicates this to the computer.

As soon as the computer has the confirmation that all servos are properly set, it can initiate the RF voltage control program, which turns on the RF drive and brings the RF voltage up to the desired value. Two voltage comparators (Zero Detector) then are used to determine the required sense of rotation of the stepping motor. The subsequent encoder and control unit transforms this information into pulse trains suitable for stepping motors. The encoder and control unit also contains lamp drivers for motion and limit indication lights on the main console. Furthermore, there are move and limit indication outputs available, as well as compatible inputs. With these, one system can be interconnected in a way as to inhibit another one while it is tuning. Or there occurs another case; if one servo (with a narrow tuning range) reaches a limit it starts another sero (with a wide tuning range) to move such that the first servo gets back within it's tuning range. (Course and fine tuning, for example).

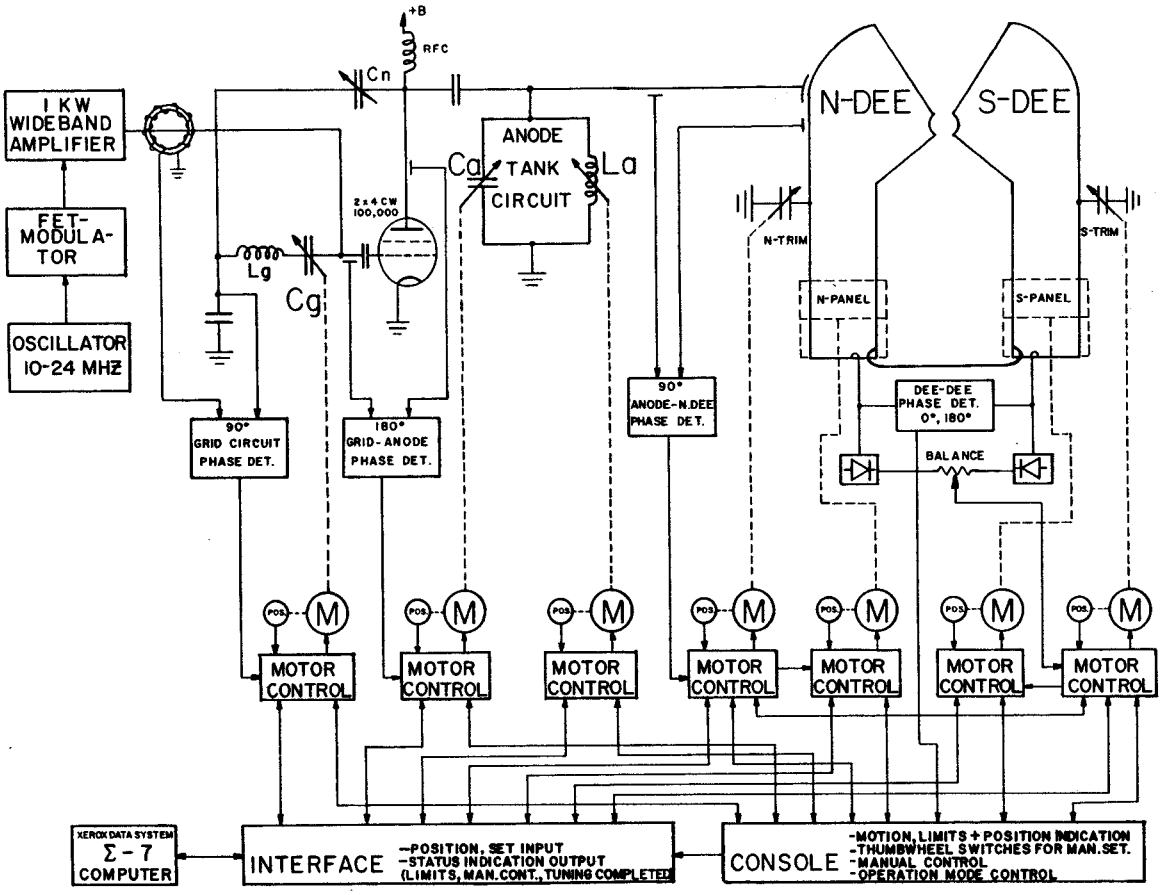

Figure 1

This shows why adjustable, independent tuning speeds are essential, because the two tuning speeds of two servo loops have to be adjusted such that the system always stays tuned during such a process.

References

1. W.P. Johnson, CERN Report 63-19, 279-285(1963).
2. W.P. Johnson, P. Sigg, IEEE Trans. on Nucl. Science, Vol. NS-16 #3 (1969).

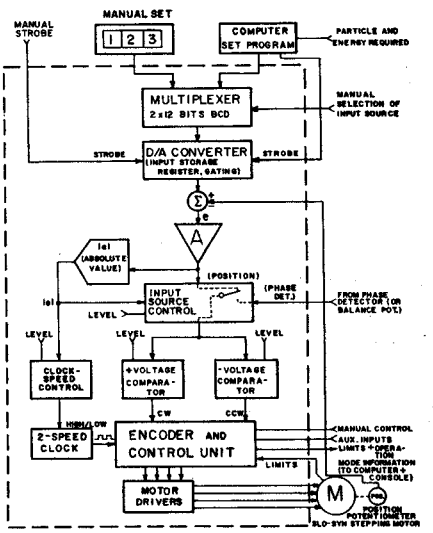

Figure 2

Additions and Improvements to Laboratory Computer

Richard Au

The computer system is a unified data acquisition, analysis and control service unit. To improve and extend these services four major hardwave and three software additions have been made, giving a marked improvement in the data analysis and acquisition areas. Each addition produced multiple improvements and, therefore, will be discussed in that context.

The addition of 16 words of CPU main core storage produced two results:

(1) The data acquisition area was increased to double the number of data collection routines running concurrently.

(2) The calculation overhead for large data analysis routines was reduced by a factor of ten and an increase in the number of concurrent routines was obtained.

A large (30"), high accuracy (.005") plotter was added to the computer system to reduce the backlog of plots and the resulting data analysis, acquisition conflicts caused by a single slow device. This produced the additional benefit of producing publication quality plots directly and thereby reducing the drafting load.

A small peripheral computer was acquired to perform four functions:

(1) To releave the main computer of the real-time scope display function and thereby gain about 10-20% in computational speed.

(2) Provide for multi-low-cost remote interactive terminate stations for on-line data analysis via user FORTRAN routines. One of these terminals is to be used at the cyclotron console for machine control.

(3) As a backup system to provide essential data acquisition and control functions (complex data analysis being lost) in the event of main computer failure.

The addition of a 25 mega-character diskpack storage unit was done for the following system improvements.

(1) To provide user program storage for use during remote operation.

(2) As data storage for faster analysis.

(3) For raw data storage of multi-dimensional mega-channel analysers.

(4) As a backup device to hold output for any device termporally overloaded or inoperative.

(5) To extend user file storage during stepwise computational runs.

(6) And as a high speed "tape" unit to increase data search speed by about ten times.

The new software routines include a task for close-loop stablization of the spectragraph and a task for high speed sequencially ordered data acquisition. A library of 500 FORTRAN scientific and numerical routines has been tested and are available on-line. A number of new compilers have been added for users which include:

(1) An extended FORTRAN to optimize code generation for increased execution efficiency.

(2) A fast FORTRAN for quick compile and execution during the debugging process.

(3) And additional compilers of SNOBOL, LISP, and BASIC to provide the remote user editing function, literature searches and report writing.

In summary the computer system has increased its data analysis service capacity by an order of magnitude by the addition of devices and software. The data acquisition service was doubled by the addition of core storage and extended into mega-channel analysers with the device additions. The sytem has proved it is capable of closed-loop control upon cyclotron equipment via the spectragraph.

An Ultra-Thin-Window Gas Cell

H. Laumer

In our program to measure proton induced spallation of the elements ^{12}C, ^{14}N, ^{16}O, and ^{20}Ne[1] we were lead to consider gas targets for all except ^{12}C. Usually the gas is confined in a gas cell which employs a foil or "window" through which the beam enters and reaction products leave to be detected outside the cell. A common foil used for gas cells is 1/2 mil thick Kapton. For the relatively heavy, low energy, reaction products to be detected in the spallation experiments this still implies a large and unacceptable energy loss. The gas cell described here permits exit particle areal densities in the range of 50-130 $\mu g/cm^2$. The gas cell is shown in Fig. 1. The cell body is made of brass. The unique aspect of the cell is the shell sliding in the keyway. The shell end closest to the beam serves as defining slit and exit beam window support. The front end is tapered to allow close approach to the beam at forward angles. The geometry of the shell and its vacuum seal determine the minimum detection angle.

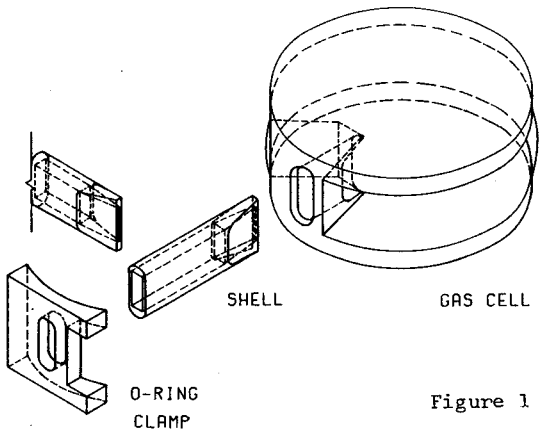

Figure 1

The angular range accessible with the cell is 10° to 170° provided the rotating table has a range of 360°.

The entrance beam window is 1/2 mil Kapton bonded to the cell structure with epoxy Ciba Araldite 502. For the exit beam window we selected formvar. The slit end of the shell is buffed so the lips of the slit are rounded and no sharp edges remain. A 2% solution of formvar in 1,2 Dichloroethane is prepared and films are produced by casting on water.[2] The film is picked up with a wire loop and transferred immediately to the shell. This is repeated until a formvar window of the desired thickness is build up. A 30 $\mu g/cm^2$ formvar windown over a 40 mil slit sustains a pressure of 25 torr for many hours.

Reaction products lose energy not only in the formvar window but also in the gas they have to traverse. Depending on the detection angle the shell is positioned to minimize the gas traversed. For example for the nitrogen pressure, slit width, and formvar window mentioned above the average total exit areal density can be $\sim$50 $\mu g/cm^2$ at 90° and $\sim$130 $\mu g/cm^2$ at 15° detection angle.

In our application we wanted to avoid repeated mechanical adjustments of the shell, but still wanted to minimize energy loss in the gas. We simply mounted the gas cell and slit system slightly off center on the scattering chamber table. As shown in Fig. 2 table rotations between 15° (or 165°) and 90° can be carried out with one shell setting. The distance between the beam and the closest point of the shell is about constant and as a result a minimum in gas flight distance is achieved at all angles in this range.

In the present design the gas cell stays fixed with respect to the detector. This limits the incident beam intensity to about 1 μa for protons since the cell cannot be vibrated to spread the beam over an effectively larger area of Kapton.

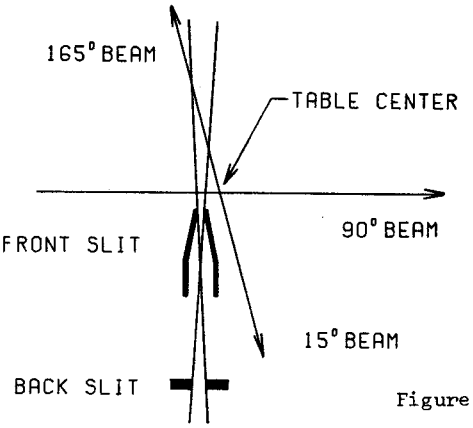

Figure 2

While in our experiment we where only interested in minimizing energy loss, the cell should be well adapted to yield good resolution energy spectra for heavier particles. The data in Table 1 was taken at 15° detection angle. The resolution of the detector for a 5.48 MeV calibration α peak was $\sim$35 keV FWHM.

Table 1. Energy Resolution for Various Particles

Peak Energy in MeV	Particle	Resolution FWHM in keV
	$^{16}O+p$ E_p=42 MeV	
18.0	^{6}Li	50
14.9	^{7}Be	80
11.8	^{14}N	140
8.9	^{16}O	380

References

1. Cary N. Davids, Helmut Laumer, and Sam M. Austin, Phys. Rev. C1, 270(1970). Also see topics on spallation in this report.
2. L. Yaffe, Ann. Rev. of Nucl. Sci., Vol. 12, 153(1962).

The cross-sections obtained by integrating the angular distributions are summarized in Fig. 3. The point at 17 MeV was obtained by degrading the 22 MeV beam with a thin aluminum plate.

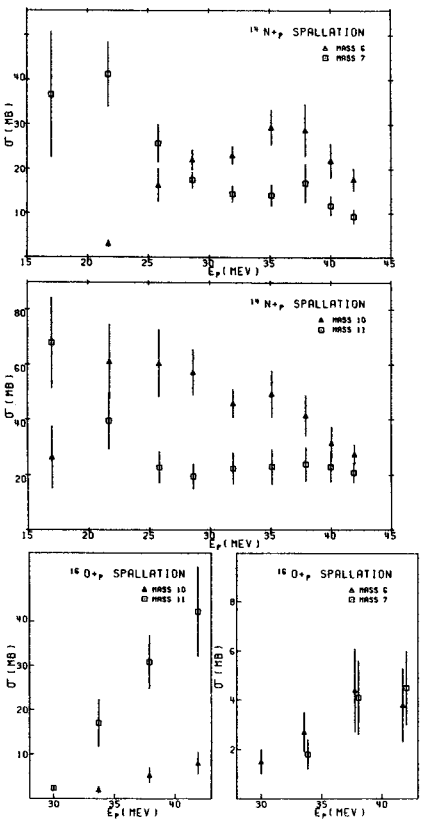

Figure 3

At 21.9 MeV the only mass-11 produced from ^{14}N+p is ^{11}C and the only mass-7 produced is ^{7}Be. To check the reliability of our time-of-flight technique we performed an activation experiment to measure ^{11}C and ^{7}Be production. We counted .511 MeV γ rays from the β^+ annihilation from ^{11}C decay (half-life 20.5 min) and .4796 MeV γ rays (from the state in ^{7}Li fed 10% of the time by the ^{7}Be decay) with a Ge(Li) detector. Absolute detector efficiency was determined with a National Bureau of Standards 5% standard ^{22}Na source. The ^{11}C cross-section found is 36±4 mb; the Be cross-section is 49±3.5 mb. These numbers compare favorably with our other values 39.5±10 mb for ^{11}C and 41.2±7.2 for ^{7}Be. They also agree with recently published cross sections by Epherre et al.[4]

Various theories for the origin of the light elements have been developed. None of them are entirely satisfactory. A reliable calculation of the net contribution of various light element production mechanisms is at present not possible. A very interesting type of calculation with a better chance of yielding information is concerned with the precise and constant isotopic ratios ^{7}Li/^{6}Li=12.5 and ^{11}B/^{10}B=4 for earth and meteorite samples. We assume a source of protons with an energy spectrum of the form $E^{-\gamma}$ irradiating an isotopic mixture in the proportion C:N:O=3:1:5. Using all available cross-section data we perform the integration $I_{ij} = \int_{E_{threshold}}^{\infty} E^{-\gamma}\sigma_{ij}(E)dE$; where $\sigma_{ij}(E)$ is the production cross-section of mass i from target nucleus j at proton energy E. Hence ^{7}Li/^{6}Li= $\Sigma_j I_{7j}n_j / \Sigma_j I_{6j}n_j$; where n_j is the relative abundance of the jth target nucleus quoted above.

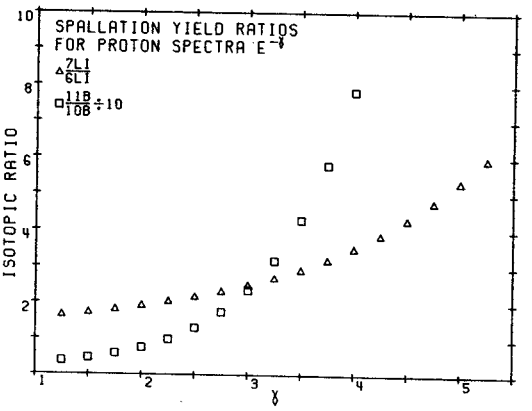

Figure 4

In Fig. 4 isotopic ratios are plotted as a function of γ for the region applicable to solar flare spectra. The ^{7}Li/^{6}Li ratio is far below 12.5 over the range of γ considered. ^{11}B/^{10}B=4 only near γ=1.5; and the ratio rises sharply for higher values of γ. This last result puts in doubt a theory by Fowler et al.[5] where the ^{11}B/^{10}B ratio was assumed to be 1; and ^{10}B depletion by a neutron flux was considered. From the low ^{7}Li/^{6}Li ratio one may suspect that either there is a source of ^{7}Li not due to proton spallation (big bang nucleosynthesis,[6] or $\alpha+\alpha$ in galactic cosmic rays[7]) or a ^{6}Li preferential depletion mechanism is involved. The fact that ^{11}B/^{10}B is only 4 may indicate a proton spectrum cutoff as inferred by Fowler[7] in his new theory of light element production by galactic cosmic rays. A mechanism to deplete ^{11}B and ^{6}Li simultaneously is not known.

References

1. Cary N. Davids, Helmut Laumer, and Sam M. Austin, Phys. Rev. C1, 270(1970).
2. Douglas L. Bayer, MSUCL-34 (MSU, East Lansing, Michigan, 1971).
3. R.M. Sternheimer, Methods of Experimental Physics, 5 Part B, Appendix 2.
4. E. Epherre and C. Seide, Phys. Rev. C3, 2167(1971).
5. W.A. Fowler, J.L. Greenstein, F. Hoyle, Geophys. JRAS 6, 148(1962).
6. R.V. Wagoner, W.A. Fowler, F.Hoyle, Ap. J. 148, 3(1967).
7. H. Reeves, W.A. Fowler, F. Hoyle, Nat. 226, 727(1970).

Preparation of Thin Film Deposits From Biological, Environmental and Other Matter

R.K. Jolly and H.B. White

In the elemental analysis of materials employing nuclear reaction and scattering techniques,[1,2,3] it is necessary to prepare the sample in the form of a thin film (10-1000 μgm/cm²). Below we describe a technique that enables one to prepare thin film deposits from such diverse materials as mineral and rock samples, animal tissue, blood and soluble salts using relatively inexpensive equipment. In certain materials like a whole fish, the uniformity of the deposit depends on the uniformity and size of the particles in the colloidal suspension that is prepared.

Any material to be deposited must be first reduced to a solution or a suspension of microscopic particles (∿1-10 μ) in an inert solvent. Table I gives a listing of the techniques used by the authors towards accomplishing this objective. The suspended or the dissolved material is placed in the container shown in the apparatus (called a Nebulizer[5]) in Fig. 1. The compressed gas (preferably inert) forces the liquid through a small hole in the form of a high speed spray which in turn impinges on an obstruction and thus breaks up into droplets of various sizes. The finest of these droplets are swept along by the gas escaping out of the nozzle. These droplets are so fine that they are not visible to the unaided eye. Illuminating the mouth of the nozzle reveals a cloudy mist but the individual droplets are still not seen. The nebulized mist is then allowed to deposit on a rotating substrate. By mounting the nebulizer bottle on a stand that performs a slow up and down (or sideways) oscillatory motion such that all parts of the substrate receive the mist for the same length of time, a very uniform deposit can be obtained. The microscopic size of these droplets is important for two reasons: i) The droplets evaporate immediately so that one does not get any streams of running fluid on the substrate and ii) Any one droplet brings such a small quantity of the suspended or dissolved matter with it that with a reasonably prolonged (30 minutes) period of deposition, a uniform layer of the dissolved or suspended matter is obtained. The heating coil in the figure is to inhibit condensation of the mist in the nozzle thus ensuring an unobstructed flow of the mist.

A microphotograph of the deposit from a sonicated whole fish (some skin removed) prepared in accordance with the procedure outlined in Table I is shown in Fig. 2. Particles of all sizes up to 5 are seen with the majority in the range of 0.2-2 μ. The larger particles are probably bone fragments and can perhaps be further broken down by using ultrasound of higher frequency and intensity or else eliminated by using a microfilter.

Examples of the use of thin (30-60 μg/cm²) whole fish, blood and milk deposits on formvar in 22 MeV α-particle scattering measurements are presented in another section by the authors.

REFERENCES

1. B.L. Cohen and R.A. Moyer,Analytical Chem. 43, 123(1971).
2. R.K. Jolly, C.R. Gruhn, and C. Maggiore, IEEE, Vol. NS-18, No.1 p. 91(1971).
3. R.K. Jolly and H.B. White (Nuclear Inst. and Methods. To be published).
4. For example one marketed by McCrone Research Associates Ltd. 2 McCone Mews, LONDON NW3.
5. For example Nebulizer 180 commercially marketed by DeVilbiss Company of Somerset Pa

TABLE I

Reduction of Biological, Environmental and Other Matter to a Solution or Colloidal Suspension

Class of Materials	Technique for Reduction
I. Animal Tissue, Plants etc.	Slow freezing to rupture the cells followed by i) reduction to a liquidized form by a high speed blender (e.g. Waring Scientific Blender. 15,000 rpm model.) and ii) immersion of an ultrasonic probe in the liquidized sample for several minutes (length depending on the quantity and type of material).
II. Blood, Milk etc.	Sonication with an ultrasonic probe if necessary to break up the indivual cells (25-50μ). In some applications (proton scattering, x-ray florescence) these substances may be deposited without any sonication.
III. Rock, Dry Wood etc.	Grinding in a tungsten carbide mortar and presle or a micronising mill[4] and subjecting a paste of the material to sonication (with an ultrasonic source) if necessary.
IV. Beverages and Soluble Materials, etc.	May be simply dissolved or diluted in pure water before deposition.

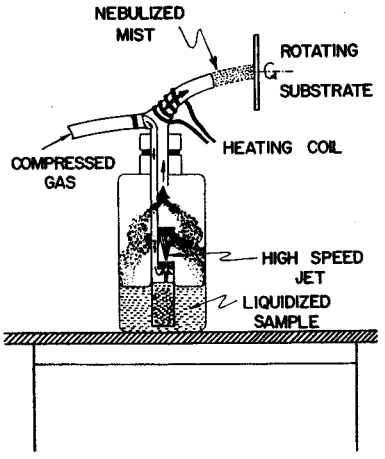

Figure 1

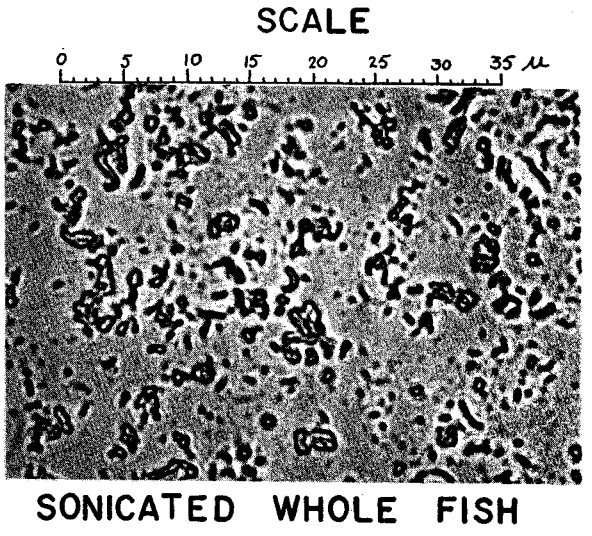

Figure 2